May 6, 1974

To the Graduate Council:

I am submitting herewith a thesis written by Joseph F. Roman entitled "Die Swell in Molten Polymers." I recommend that it be accepted for 12 quarter hours of credit in partial fulfillment of the requirements for the degree of Master of Science, with a major in Chemical Engineering.

James J. White
Major Professor

We have read this thesis and recommend its acceptance:

Joseph J. Perona

John F. Fellers

Accepted for the Council:

Hilton A. Smith
Vice Chancellor for Graduate Studies and Research

S

DIE SWELL IN MOLTEN POLYMERS

A Thesis

Presented to

the Graduate Council of

The University of Tennessee

In Partial Fulfillment

of the Requirements for the Degree

Master of Science

---

by

Joseph F. Roman

June 1974

ACKNOWLEDGEMENTS

The author wishes to express his appreciation to Dr. James L. White, his advisor, for his thorough guidance and assistance throughout this investigation.

The author would like to thank Bette Leonard, Woody Troy, Art Freeborg, Tom Ayres and Bob Goga for their assistance in this project.

Thanks are also extended to the faculty and staff of the Department of Chemical and Metallurgical Engineering for their efforts.

1147230

ABSTRACT

The die swell of six polymer melts was measured and the melts were rheologically characterized. The materials studied were high density polyethylene of melt indices 5, 0.1 and 0.02, low density polyethylene, polystyrene and polypropylene.

The die swell was measured in four different ways: (1) from frozen extrudates; (2) from annealed extrudates; (3) from photographs of extrudates emerging from the capillary; (4) isothermally, from photographs of extrusion into a hot oil bath.

The die swell was correlated as a function of shear rate, shear stress, L/D ratio, and a normal stress-shear stress ratio. The die swell observed experimentally was compared with literature values and behavior of families of polymers was considered.

The experimental die swell was compared to predictions based on various theories in the literature and it was shown how the choice of strain tensor in the constitutive equation affects the prediction of die swell. The behavior of families was also compared to predictions of die swell.

Die swell was measured under tension and the effect of increasing tension on the diameter of the emerging extrudate was observed. The results were interpreted as a response similar to that of unconstrained recovery from shear and an expression for the swell was developed.

TABLE OF CONTENTS

CHAPTER		PAGE
I.	INTRODUCTION	1
II.	LITERATURE SURVEY	3
	A. Jet Expansion for Newtonian Fluids	3
	B. Studies of Polymer Fluids	5
	C. Viscoelastic Fluid Theory	12
	D. Theoretical Studies of Die Swell	17
III.	RHEOLOGICAL PROPERTIES	25
	A. Materials	25
	B. Measurements	25
IV.	DIE SWELL--QUALITATIVE STUDIES	43
	A. Procedure	43
	B. Appearance	44
	C. Solidified Extrudate Swelling	48
	D. Annealed Extrudates	65
	E. Photographs	74
	F. Isothermal Extrusion	77
V.	INTERPRETATION	80
	A. Interpretation of Die Swell	80
	B. Correlation of Die Swell and Flow Rate	86
	C. Comparison of Experimental Data with Rheological Properties	91

CHAPTER PAGE

D. Behavior of "Families" and Comparison with Literature 104

E. Comparison with Various Theories 123

VI. DIE SWELL UNDER APPLIED TENSION. 133

A. Introduction 133

B. Equipment. 133

C. Procedure. 134

D. Results. 134

E. Interpretation 138

VII. CONCLUSIONS. 143

BIBLIOGRAPHY 145

APPENDIX 151

Appendix A 152

VITA 160

LIST OF FIGURES

FIGURE		PAGE
1.	Non-Newtonian Shear Viscosity as a Function of Shear Rate	30
2.	First Normal Stress Difference as a Function of Shear Rate	31
3.	First Normal Stress Difference as a Function of Shear Stress	33
4.	Shear Viscosity as a Function of Shear Rate for HDPE's and Literature Data.	34
5.	Relaxation Time ($\dot{\gamma} \rightarrow 0$) as a Function of Viscosity ($\dot{\gamma} \rightarrow 0$) for the PS, LDPE and HDPE's and Literature Data	38
6.	Relaxation Time as a Function of Shear Rate.	40
7.	Diagram of Isothermal Extrusion Apparatus.	45
8.	Die Swell of PP as a Function of Shear Rate.	49
9.	Die Swell of PP as a Function of L/D Ratio	50
10.	Die Swell of PS as a Function of Shear Rate.	52
11.	Die Swell of PS as a Function of L/D Ratio	53
12.	Die Swell of HDPE MI = 0.1 as a Function of Shear Rate . .	54
13.	Die Swell of HDPE MI = 01 as a Function of L/D Ratio . . .	55
14.	Die Swell of HDPE MI = 5 as a Function of Shear Rate . . .	56
15.	Die Swell of HDPE MI = 5 as a Function of L/D Ratio . . .	57
16.	Die Swell of HDPE MI = 0.02 as a Function of Shear Rate. .	58

FIGURE PAGE

17. Die Swell of HDPE MI = 0.02 as a Function of L/D Ratio . . . 59
18. Die Swell of LDPE as a Function of Shear Rate 61
19. Die Swell of LDPE as a Function of L/D Ratio 62
20. Comparison of Die Swell of Polymer Melts as a Function of Shear Rate, L/D = 48. 63
21. Comparison of Die Swell as a Function of L/D Ratio for Six Polymer Melts. 64
22. Comparison of Die Swell from Frozen, Annealed, Photographic and Isothermal Measurements as a Function of Shear Rate for PP 66
23. Comparison of Die Swell from Frozen, Annealed, Photographic and Isothermal Measurements as a Function of Shear Rate for PS, L/D = 48 67
24. Comparison of Die Swell from Frozen, Annealed, Photographic and Isothermal Measurements as a Function of Shear Rate for LDPE, L/D = 48 68
25. Comparison of Die Swell from Frozen, Annealed, Photographic and Isothermal Measurements as a Function of Shear Rate for HDPE MI = 5, L/D = 48. 70
26. Comparison of Die Swell from Frozen, Annealed, Photographic and Isothermal Measurements as a Function of Shear Rate for HDPE MI = 0.1, L/D = 48. 71
27. Comparison of Die Swell from Frozen, Annealed, Photographic and Isothermal Measurements as a Function of Shear Rate for HDPE MI = 0.02, L/D = 48 72

FIGURE PAGE

28. Comparison of Die Swell Measured from Photographs for Six Polymer Melts as a Function of Shear Rate, L/D = 48 73

29. Comparison of Die Swell Measured from Photographs for Six Polymer Melts as a Function of Shear Rate, L/D = 48 76

30. Comparison of Die Swell Measured Isothermally for Six Polymer Melts as a Function of Shear Rate, L/D = 48. . . . 79

31. Die Swell as Predicted for a Lodge Fluid and a Cauchy Fluid as a Function of $\frac{N_1 w}{(\tau_{12})_w}$ 87

32. Die Swell as a Function of Flow Rate for HDPE MI = 5 88

33. Die Swell as a Function of Shear Rate for HDPE MI = 5. . . . 90

34. Die Swell as a Function of Shear Stress for Frozen Extrudates of Six Polymer Melts, L/D = 48. 92

35. Die Swell Measured from Photographs as a Function of Shear Stress for Six Polymer Melts, L/D = 48 94

36. Die Swell of Annealed Extrudates as a Function of Shear Stress for Six Polymer Melts, L/D = 48 95

37. Isothermal Die Swell as a Function of Shear Stress for Six Polymer Melts, L/D = 48. 97

38. Die Swell of Frozen Extrudates as a Function of $\frac{N_1 w}{(\tau_{12})_w}$ for Six Polymer Melts, L/D = 48 99

FIGURE PAGE

39. Die Swell Measured Photographically as a Function of $\frac{N_1 w}{(\tau_{12})_w}$ for Six Polymer Melts, L/D = 48 100

40. Die Swell of Annealed Extrudates as a Function of $\frac{N_1 w}{(\tau_{12})_w}$ for Six Polymer Melts, L/D = 48 102

41. Isothermal Die Swell as a Function of $\frac{N_1 w}{(\tau_{12})_w}$ for Six Polymer Melts, L/D = 48 , ... 103

42. Comparison of Experimental and Literature Data Values of Die Swell for Frozen Commercial PS Extrudates as a Function of Shear Rate 106

43. Comparison of Experimental and Literature Values of Frozen Commercial PS Die Swell as a Function of Shear Stress. 107

44. Comparison of Experimental and Literature Values of Annealed Commercial PS Die Swell as a Function of Shear Stress. 109

45. Comparison of Experimental and Literature Values of Frozen Commercial PS Die Swell as a Function of $\frac{N_1 w}{(\tau_{12})_w}$ 110

46. Literature Values of Frozen Die Swell as a Function of Shear Rate for Narrow Molecular Weight Distribution PS. 111

FIGURE PAGE

47. Literature Values of Frozen Die Swell as a Function of Shear Stress for Narrow Molecular Weight Distribution PS 113

48. Comparison of Experimental and Literature Values of Frozen Die Swell as a Function of Shear Rate for HDPE. 115

49. Comparison of Experimental and Literature Values of Annealed Die Swell for HDPE's as a Function of Shear Rate. 116

50. Comparison of Experimental and Literature Values of Frozen Die Swell as a Function of Shear Stress for HDPE. 117

51. Comparison of Experimental and Literature Values of Frozen Die Swell as a Function of $\frac{N_1 w}{(\tau_{12})_w}$ for HDPE 119

52. Comparison of Experimental and Literature Values of Frozen Die Swell as a Function of Shear Rate for HDPE and LDPE 120

53. Comparison of Experimental and Literature Values of Annealed Die Swell as a Function of Shear Rate for HDPE and LDPE 121

54. Comparison of Experimental and Literature Values of Frozen Die Swell as a Function of Shear Stress for HDPE and LDPE 122

FIGURE PAGE

55. Comparison of Experimental and Literature Values of Frozen Die Swell as a Function of $\frac{N_1 w}{(\tau_{12})_w}$ for HDPE and LDPE 124

56. Comparison of Experimental Frozen Die Swell Measurements with Predictions. 125

57. Comparison of Experimental Die Swell Measured from Photographs with Predictions. 126

58. Comparison of Experimental Die Swell of Annealed Extrudates with Predictions 128

59. Comparison of Experimental Isothermal Die Swell with Predictions 129

60. Comparison of Experimental and Literature Values of Frozen HDPE and LDPE Die Swell with Predictions. 130

61. Comparison of Experimental and Literature Values of Frozen Die Swell of PS and PP with Predictions. 132

62. Die Swell as a Function of Tension. 136

63. Die Swell as a Function of Take-up Velocity 137

64. Die Swell as a Function of Stress 139

65. $[\frac{D_{\tau_{zz}}}{D_o}]^6$ as a Function of $[\frac{D^2}{D_o^6}\frac{D^4}{\tau_{zz}}\ \tau_{zz}]$ 142

CHAPTER I

INTRODUCTION

In the extrusion of molten polymers through a cylindrical die, the diameter of the extrudate is often found to be larger than the diameter of the die and at high extrusion rates, the extrudate becomes distorted. Since the market for extruded products is very large and continually growing, the problem of "die swell" is important in the field of extrusion.

Extruded products can generally be divided into eight areas of applications: (1) pipe, used industrially because of the light weight, toughness and resistance to corrosion; (2) sheet, used in food packaging and as liners and housings; (3) film, used in packaging; (4) melt spun fibers, used in textile manufacture; (5) extrusion coating, generally a polymer coating on a material such as paper, cellophane, aluminum foil or oriented polyester, usually used in packaging; (6) wire and cable covering, used as insulation; (7) monofilaments, used in rope, textiles and automobile industry; and (8) miscellaneous contours, including gaskets and weatherstripping.

The technology in these areas differ and the products are not necessarily similar, but the problem of post-extrusion swelling is a common one, whether it be in the spinning of single fibers of the extrusion of whole sheets. All these products must be produced according to specifications, pipes must have a certain inside diameter

and wall thickness, fibers must be a certain radius and sheets a certain thickness. Post-extrusion swelling causes an increase in extrudate dimensions which must be estimated or planned for in the final product. A working relationship between the rheological properties of the melt and the die swell would be of value in the plastics and fiber industry. The purpose of this thesis is to examine the variables affecting die swell and relate the die swell to the rheological properties of the melt.

CHAPTER II

LITERATURE SURVEY

A. JET EXPANSION FOR NEWTONIAN FLUIDS

Harmon (36) analyzed the behavior of Newtonian liquid jets by means of a mass and momentum balance between the exit and a position downstream where the velocity profile has become flat. This analysis predicted a value of 0.866 for the ratio of the jet diameter to the capillary diameter and accounted only for contraction of the jet. Middleman and Gavis (52) later examined the expansion and contraction of capillary jets of Newtonian fluids. Using hydrodynamic and dimensional analysis arguments, they predicted the ratio of the jet diameter to the capillary diameter to be a function of the Reynolds Number and the Weber Number, the ratio of the inertia force to surface tension force. They observed that the swell was independent of Reynolds numbers less than six and was limited to 1.06 times the capillary diameter. At high Reynolds numbers, the ratio of the jet diameter to the capillary diameter was observed to approach 0.866.

Gavis and Modan (28) later observed swelling as high as 1.20 for Newtonian fluids at low Reynolds numbers. They observed that the diameter of the jets were noticeably affected by viscous dissipation for Reynolds numbers less than 16. At higher viscosities, higher viscous normal stresses and greater jet diameters were observed. Gavis and Modan also observed dependence of the swelling on the L/D ratio

of the capillaries. As the L/D ratio increased, there appeared a sharp decrease in the magnitude of the swell.

Middleman (50) applied a boundary layer type analysis to three distinct axial regions of the jet in an attempt to calculate the velocity profile and jet diameter as functions of the distance from the exit. This calculation was limited to high Reynolds numbers. Goren and Wronski (31) approached the problem as a perturbation analysis about the final state of the jet and also as a boundary-layer treatment valid for short axial distances and the large Reynolds numbers which predict the surface velocity and change in jet radius both increase as the cube root of the axial distance. Goren and Wronski observed that for Reynolds numbers below 12 the jet diameter increased monotonically with axial distance, but the magnitude of the increase diminishes as the Reynolds number is increased. Above a Reynolds number of approximately 17 the jet diameter monotonically decreases with axial distance and the magnitude of the change increases as the Reynolds number increases. Between Reynolds numbers of 12 and 17 the jet diameter first decreases and then increases as the axial distance is increased. This behavior at Reynolds numbers less than 16 also manifested itself in unexpectedly peculiar behavior of the eigenvalues in the perturbation analysis.

Duda and Vrentas (25) developed a coordinate system whose coordinate lines change shape in a manner determined by a change in jet dimensions. They defined the jet fluid mechanics in terms of a Weber number and the Reynolds number divided by the Froude number,

the ratio of inertia forces to gravity forces. Contraction of the jets was greater with increasing Weber number, surface tension opposing contraction by producing an adverse pressure gradient. This method can accurately predict the behavior of jets discharging into inviscid media for Reynolds numbers greater than 200.

Tanner (67) used finite element methods to compute the swell of a Newtonian jet at very low Reynolds numbers. Using the Navier-Stokes equations, with a computer model, Tanner performed successive iterations about the capillary exit and determined the swell to be 1.128. This agrees well with experimental values. Tanner indicates present die swell theories are inadequate because of complexity of non-viscometric flow at the exit.

There is another analysis that has been widely discussed but never published. One can conclude that for Reynolds numbers approaching zero, the Navier-Stokes equations take on the form of a biharmonic equation $\psi = 0$, where ψ is the stream function. This is true for $+\psi$ or $-\psi$ and one can conclude that the flow patterns out of the capillary will be the same as the flow patterns into the capillary. Thus the efflux diameter should approach infinity.

B. STUDIES OF POLYMER FLUIDS

Barus (7) studied the changes in shape of viscous marine glue on its emergence from a duct. Extrudates were cut into short cylinders and the subsequent distortion of these was followed over a period of about a day. The chief modes of deformation observed by Barus were axial, with his short cylinders deforming to produce conoids. The

residual contents of the duct were observed to recoil axially into the duct after the driving force was removed. If any radial expansion occurred, Barus failed to observe it. Both the axial deformation noted by Barus and the increase in diameter have their origin in the same stress relaxation process (46).

The first specific discussion of the nature of polymer extrudates emerging from dies that the author has found was published in 1930's. This was the work of J. H. Dillon and Johnston (24) and was primarily concerned with the extrusion of commercial natural rubber-carbon black compounds at high shear rates. They noticed that the highly compounded stocks appeared to have more regular flow patterns than lightly compounded stocks of natural rubber. The swell of the extrudates was observed to increase with the rate of efflux and decrease with increasing extrusion temperature.

We first turn to a survey of the general extrusion characteristics of polymers. Spencer and R. E. Dillon (62, 63) studied the character of extruded polystyrene. As the shearing stress increased, the appearance of the extrudate changed. Three regions of shearing stress were defined:

(1) At low shearing stresses, the filament was smooth and the diameter increased with the shear stress.

(2) Intermediate region, spirals were observed in the extrudates with some roughening of the surface.

(3) At high shear stresses, the surface again became smooth and appeared as small segments joined together haphazardly.

They observed that the shearing stress at the wall at the spiral point was independent of the diameter of the die and varied inversely with molecular weight and was relatively independent of temperature. They thoerized that the skin was more oriented than the core and on its emergence from the capillary, it cannot cool fast enough to prevent recovery of orientation due to the shearing stress at the wall. The outside of the extrudate would like to contract axially more than the less oriented core and compresses it. The core buckles into a spiral.

Tordella (68, 69, 70) observed that in the extrusion of various molten amorphous polymers, the free surface and cross section became irregular as the pressure gradient increased. Again the distortion progressed from spiral grooves on the surface of the extrudate to a point where the stream is discontinuous. The irregularity of extruded samples increased with decreasing extrusion temperature. The samples vibrated violently and the rate of extrusion appeared irregular. The irregularity was affected by the shear stress and the die geometry. The flow in the capillary was not axially symmetric and tended to be from one side of the charge. The instability or fracture as Tordella termed it appeared to result from the large amount of deformation imposed in the approach to the capillary. Tordella later used tracer particles to observe flow of polyethylene. He observed that irregular shaped extrudates were accompanied by irregular flow. Shear fracture occurred in the capillary inlets above a critical shear rate. Using high density polyethylene and

copolymers of tetrafluroethylene and hexafluroethylene, Tordella observed transition from smooth extrudate to fine surface roughness similar to a close pitch screw thread and finally recurrence of smooth surfaces as the shear rate was increased. The irregularity was associated with flow instabilities initiating at the capillary inlet in some cases and instabilities initiating within the capillary in others.

Ballenger and White (6) observed the development of the velocity field in polymer melts approaching a capillary die. They observed that for melts of polystyrene, polypropylene and low-density polyethylene at low flow rates, approximately radially inward flow to the capillary. At higher flow rates, circulating secondary flows develop in the corners for polystyrene and low density polyethylene. The flow inward resembled a wine glass. At high extrusion rates, a spiralling in the inlet became apparent and the extrudate took on a helical appearance. Increasing L/D ratio at constant shear rate, decreased the approach angle and damped out disturbances in the melt, leading to a smoother extrudate. Oyanagi (57) also reports that for high density polyethylene, the occurrence of spiralling in the die entry resulting in extrudates showing a transition from a smooth surface to a helical screw thread appearance which evolves to one of gross distortion. This distortion is accompanied by large oscillations in pressure. For elastomers the extrudate character develops from a mesh matte surface to a quasi screw thread to gross distortion (79). Surveying the literature, White (76) concludes that at low flow rates the polymer melts behave as Newtonian fluids and the

flow patterns resemble creeping flow. At higher flow rates vortices develop near the die inlet, interpreted as being caused by stress fields in the fluid. Large vortices and small entrance angles seem to be due to high elastic memory. Three types of extrudate distortion are observed: (1) a dull surface or matte appearance at low flow rates, due to interaction of cooling and stress relaxation in the melt; (2) a spiral or screw thread, due to spiralling flow into the die, occurring at a critical shear stress; (3) gross distortion, due to a grossly disrupted flow field in the die entry.

There have been many observations of the phenomena of post extrusion swelling, but the various workers have shown little uniformity in characterizing the extrudates. Researchers have measured (1) the diameter of the solidified extrudate after cooling at room temperature, (2) after being allowed to relax in an oven, (3) by photographing the jets and measuring the swell from enlargements, (4) after being extruded into various types of oil baths and various other methods.

Bagley, Storey and West (3) examined post extrusion swelling of polyethylene melts. They measured the diameters of the frozen extrudates one-fourth inch from the initially extruded end. They observed that the swell properties of polyethylene decreased with increasing capillary length, at a constant shear stress, although the viscosity remained constant. This work, however, was more concerned with extrudate appearance than die swell. Nakajima and Shida (53) studied the swelling behavior of a butene-1 ethylene

copolymer which was allowed to cool at room temperature and then annealed in an oven containing a nitrogen atmosphere. The extrudate swelling was measured from photographs, measurements made about one-eighth inch from the end. They observed swelling as the shear rate was increased and an increase in swelling as annealing time increased until recovery became complete and further annealing had no effect on the swelling ratio. At higher annealing temperature, recovery occurred at a more rapid rate. Rogers (59) used polyethylene melts and ethylene-butene copolymers to study die swell. The extrudates were measured one-fourth inch from the initially extruded end and annealed in an air oven at 100°C. Little difference was observed between the annealed and frozen extrudates. This lack of recovery was a result of the annealing temperature. Had an annealing temperature above the melting point been used, an effect of annealing would have been observed. Rogers did observe increased swell as shear rate increased and increased swell as L/D ratio decreased. Rogers also showed that swelling increases linearly with increasing molecular weight. There is so much scatter in this data, however, that its usefulness is limited.

Han and Charles (33) used photographs to measure the die swell as a function of shear rate and also as a function of relaxation time as the melts are extruded into an isothermal chamber. They observed increased die swell as relaxation time increased until complete relaxation was reached. The complete relaxation took place in a period of two to three minutes compared with about twenty minutes for

annealing in an oven by Nakajima and Shida. They also observed a difference in the die swell of frozen extrudate and photographs. This appeared to be a constant different, approximately ten percent and was attributed to crystallization of the polymer extrudates.

Graessley, Glasscock and Crawley (29) used two commercial and three narrow distribution polystyrene melts to study die swell. Here, measurements were made one centimeter from the initially extruded end, as compared with previous measurements at one-eighth inch and one-fourth inch. Air annealing at 120°C and annealing in silicone oil at 165°C were performed on the samples. Air annealing produced no change in the diameter of the extrudates, but annealing in silicone oil did result in increased swell ratio. The annealed samples were only slightly larger at low shear rates, but as the shear rate increased, the difference between annealed and unannealed became larger. Experiments extruding directly into oil bathes resulted in the same affect as annealing frozen extrudate. Graessley tries to show a correspondence between swelling and viscosity behavior. The die swell is also presented as a function of the shear stress, as shear stress increased, die swell increased. The narrow distribution samples displayed similar behavior, but displayed a constant swelling ratio over a wide range of low shear stresses, All swelling ratios approached a lower limit of 1.1 at low shear stresses. This work is limited to one type of polymer and there is no comparison between polystyrene and other polymers.

Mendelson and Finger (44, 45) did work similar to Graessley

using polyethylenes. They annealed in silicone oil at temperatures from 125°C to 150°C and measured the diameter one-eighth inch from the initially extruded end. For high density polyethylene only slight increase in die swell was observed at increasing shear rates and the annealed samples were much larger than unannealed samples. For low density polyethylene a similar effect of die swell versus shear rate was observed, but the annealed samples differed from frozen samples by less than ten percent. This work is limited to shear rates above five sec^{-1}.

Vlachopoulos, Horie and Lidorikis (73) have examined the die swell of narrow molecular weight polystyrenes and polystyrene blends and compared these values with theoretical predictions. This work concerned only cooled extrudates. For polystyrene, the die swell approached a limiting value of 1.1. The swelling ratio was observed to depend on the molecular weight distribution. The broader the distribution, the larger the swelling ratio. Vlachopoulos correlates the die swell as a function of the recoverable shear and compares it with Graessley's and Tanner's theoretical expressions which we will discuss in a later section.

C. VISCOELASTIC FLUID THEORY

Polymeric melts show a wide variety of responses in flow conditions, such as non-Newtonian viscosity, recoil, die swell and Weissenberg effect. They exhibit combined behavior of the properties of solids and liquids and show elastic as well as viscous responses to applied stresses. Before attempting a study of die swell in molten

polymers. it is necessary to choose a rheological equation which will express the stress-deformation relationship within the fluid to describe the flow behavior of the fluid. Two types of theories of viscoelastic materials have been developed. These are: (1) the rate theories based upon the differential equations relating stress to deformation and (2) integral theories in which the stress is written as an integral over the strain history.

Rate Theories

The rate theory derives from Maxwell's equation as:

$$\tau + \lambda \frac{d\tau}{dt} = G\lambda\dot{\gamma}, \quad G\lambda = u \qquad (1)$$

where τ is the stress, $\dot{\gamma}$ is the strain rate, G is the elastic modulus and λ denotes the relaxation time (42).

This theory does not predict normal stresses or non-Newtonian viscosity. Maxwell's theory was generalized to large deformation and a three-dimensional form by Zaremba in 1903 (85). Zaremba's theory predicts both normal stresses and non-Newtonian viscosity. Hencky (37) and de Witt (22) repeated the generalization of Maxwell's theory using a convected coordinate system. Other forms of non-linear Maxwell fluids which correlate linear viscoelastic data have been proposed by Oldroyd (55, 56), Williams and Bird (83) and Spriggs and Bird (64, 65). The simplest of the differential theories, which does a good job of data fitting, is the White and Metzner form (80). These differential rate theories are not as useful as integral theories. First, discontinuous relaxation spectra are predicted. Second, the

use of differential equations for constitutive equations makes it impossible to compute the stress tensor for all but the simplest kinematics except by perturbation or numerical solutions (12).

Integral Theories

Linear Theory. The integral theories are based upon the Boltzmann superposition principle (13). This constitutive equation contains a fading memory function. In one-dimensional form this is:

$$\tau(t) = \int_{-\infty}^{t} G(t - s) \left(\frac{d\varepsilon}{ds}\right) ds \qquad (2)$$

where, G(t) is a fading memory function of t, known as the relaxation modulus, ε is the strain and s is the time. The stress is presumed dependent not only on the instantaneous values, but also on its previous deformation. Integration of Equation 2 by parts yields

$$\tau(t) = [G(t - s)\, \varepsilon(s)]_{s=-\infty}^{s=t} - \int_{-\infty}^{t} \varepsilon(s)\, dG(t - s)$$

$$= G(o)\, \varepsilon(o) - \int_{-\infty}^{t} \Phi(t - s)\, \varepsilon(s)\, ds \qquad (3)$$

where $\Phi(t) = -dG(t)/dt$. Generally, one takes the instantaneous state as the standard state making $\varepsilon(o)$ equal to zero. This makes $(-\varepsilon(s))$ positive and

$$\tau(t) = \int_{-\infty}^{t} \Phi(t - s)\, [-\varepsilon(s)]\, ds \qquad (4)$$

The Maxwell equation can be shown to be a special case of the Boltzmann equation for

$$G(t) = G_o e^{-t/\lambda} \quad \text{and} \quad \Phi(t) = \frac{G_o}{\lambda} e^{-t/\lambda} \tag{5}$$

The relaxation spectrum $H(\lambda)$ is introduced to represent $G(t)$ as a generalized Maxwell fluid as follows:

$$G(t) = \int_{-\infty}^{\infty} H(\lambda) e^{-t/\lambda} \, d(\ln\lambda) \quad \text{and}$$

$$\Phi(t) = \int_{-\infty}^{\infty} \frac{H(\lambda)}{\lambda} e^{-t/\lambda} \, d(\ln\lambda) \tag{6}$$

Non-linear Theory. The Boltzmann equation is limited to infinitesimal deformations. To describe non-linear viscoelastic behavior observed in polymer fluid response it was necessary to extend the Boltzmann theory to large deformations. Lodge (41) was the first to develop and apply non-linear integral theories for viscoelastic fluids. In 1957, Green and Rivlin first developed a general constitutive theory accounting for non-linear effects, assuming the stress is a hereditary functional of the deformation history (30). Coleman and Noll (18, 54) expressed an equivalent formulation as

$$\underset{\sim}{\tau}(t) = -p\underset{\sim}{I} + F\left[\underset{\sim}{e}_{s=-\infty}^{s=t} \; (t-s)\right] \tag{7}$$

Here $e(s)$ is a Finger type strain tensor which measures deformation

from the instantaneous state to a past time s and is expressed

$$e_{ij} = \frac{1}{2}\left[C^{-1}_{ij} - \delta_{ij}\right] \quad \text{and} \quad C^{-1}_{ij} = \sum_m \frac{\partial x_i}{\partial x_m}\frac{\partial x_j}{\partial x_m} \tag{8}$$

This is known as Coleman and Noll's simple fluid (18). This may be expressed by a Frechet expansion of the functional yielding

$$\tau = -pI + \int_{-\infty}^{t} \Phi(t-s)\, e(s)\, ds \tag{9}$$

$$+ \int_{-\infty}^{t}\int_{-\infty}^{t} \{\psi(t-s_1, t-s_2)\, e(s_1)\, e(s_2)$$

$$+ \Sigma\,[(t-s_1)(t-s_2)]\,[\mathrm{tr}\, e]\, e\}\, ds_1\, ds_2$$

$$+ \ldots$$

where $\Phi(s)$, $\psi(s_1, s_2)$, $\Sigma(s_1, s_2)$, . . . are relaxation moduli dependent on time only. The multi-integral theory can be simplified using the Cayley-Hamilton theorem, as suggested by multistep stress relaxation experiments of Zapas and Craft (84) to

$$\underset{\sim}{\tau} = -p\underset{\sim}{I} + 2\int_{-\infty}^{t} [a_1(t-s, I_e, II_e)\, \underset{\sim}{e}(s)$$

$$+ a_2(t-s, I_e, II_e)\, e^2(s)]\, ds \tag{10}$$

Relaxation moduli $a_1(t-s, I_e, II_e)$ and $a_2(t-s, I_e, II_e)$ depend on time and deformation invarients $I_e = \mathrm{tr}\, e$ and $II_e = \mathrm{tr}\, e^2$. This equation is similar to, but more general than, the single integral

theories of Bernstein, Kersley, and Zapas (8), Bird and coworkers (11, 64, 65), Bogue and White (12), and Lodge (41). Lodge's equation is the special case of Equation 10 in which a_2 is zero and $a_1(t)$ is independent of the invarient.

D. THEORETICAL STUDIES OF DIE SWELL

Metzner and coworkers (47, 48, 49, 80) attempted to relate the normal stresses within the fluid to the expansion of an extrudate jet emerging from a capillary tube. In the absence of viscous drag of the air on the fluid jet, the only forces acting on it are the elastic and inertial forces of the fluid itself and gravity. Neglecting gravity, the total forces acting on the jet in the flow direction are constant. The forces acting on the fluid before it emerges from the capillary are the momentum flux and the tensile elastic stress, which is opposite in sign to the momentum flux. As the fluid recovers from the elastic stresses, its total momentum decreases and the jet diameter expands. This yields:

$$\int_0^R 2\pi r\rho\, U^2\, dr - \pi R_j^2\, \rho\, V_j^2 = \int_0^R 2\pi\, r\, \tau_{11}\, dr \qquad (11)$$

Solving for the die swell yields:

$$\left(\frac{D}{D_j}\right)^2 = 2\int_0^1 (U/V)^2 \left(\frac{r}{R}\right) d\left(\frac{r}{R}\right) - \left(\frac{2}{\rho V^2}\right) \int_0^1 \left(\frac{r}{R}\right) \tau_{11}\, d\left(\frac{r}{R}\right) \qquad (12)$$

Metzner, Houghton, Sailor and White (49) proposed a momentum-force balance on the fluid leaving the capillary to a point downstream

where the velocity distribution is flat as a method of determining normal stresses. They assumed steady, simple shear flow, incompressible fluid and negligible interfacial and gravitational effects, took $\tau_{22} = \tau_{33}$ and p at r = 0 at the end of the tube to be zero. Taking $(\tau_{11} - \tau_{22})$ as a function of τ_{12} only and solving for the normal stress difference:

$$[\tau_{11} - \tau_{22}]_R = \frac{\rho V^2}{n'} \{(n' + 1) \int_0^1 2\left(\frac{U}{V}\right)^2 \left(\frac{r}{R}\right) d\left(\frac{r}{R}\right)$$

$$- \left(\frac{D}{D_j}\right)^2 \left[n' + 1 + \frac{d\left[\ln \left(\frac{D}{D_j}\right)\right]}{d\left[\ln \frac{8V}{D}\right]}\right] \qquad (13)$$

For water and alcohol, Equation 13 reduces to Harmon's analysis and experimental values and calculated values were essentially the same. Concentrated syrups and glycerine solutions exhibited greater jet diameters than would be predicted for fluids exhibiting no normal stresses. This was certainly Middleman and Gavis' low Reynolds number effect on Newtonian fluid jet expansion. For polymer solutions at high Reynolds numbers, predicted values of normal stresses are consistent with rheogoniometer data.

Graessley (29) has shown that at low Reynolds numbers, the momentum balance predicts nonsense. Predicted values of $\tau_{11} - \tau_{22}$ differed from rheogoniometer measurements by a factor of approximately 10^7. Graessley indicates that the assumption of fully developed flow up to the exit unaffected by downstream events and the assumption

that the second normal stress difference $\tau_{22} - \tau_{33}$ is small or questionable. This is related to the very small values of momentum thrust. For melts, one must have

$$\int_0^R 2\pi r \, \tau_{zz} \, dr = 0 \qquad (14)$$

Theoretical analyses of die swell have been carried out by Graessley, Glasscock, and Crawley (29), Nakajima and Shida (53), and Bagley and Duffey (2), imagining the polymer melt as an elastic solid within the capillary. The die swell can be analyzed as two steps, flow as a viscoelastic liquid in a capillary reaching steady state in the extra stress components upstream from the exit and as a solid-like response to the release of imposed stress in the exit region, attaining in a short time the final extrudate dimensions. Flow in the capillary develops a preferred configuration for each fluid element relative to its configuration at the current time. The transition to the final diameter, if it takes place before the memory of the fluid has faded appreciably reflects the attainment of this preferred configuration of all elements consistent with the absence of external stresses and continuity of the fluids. The solid-like response is assumed to exist due to an entanglement network similar to crosslinked elastomers over moderate time scales.

Nakajima and Shida (53) used the concepts of rubber elasticity [reviewed by Treloar (71)] to calculate the tensile stress for elastic

deformation of the extrudate until its diameter becomes that of the capillary. They arrived at the equation:

$$\sigma = \left(\frac{D_j}{D}\right)^2 - \left(\frac{D_j}{D}\right)^{-4} \qquad (15)$$

where σ is the recoverable shear averaged over the cross-sectional area. Nakajima and Shida, however, consider the deformation to be that of uniaxial extension. This is not the case, it must be recovery from shear. Nakajima and Shida also find little correlation between theory and experimental results.

Bagley and Duffey (2) followed the analysis of Nakajima and Shida using a two-constant stored energy function, w, expressed as

$$w = C_1 (I_1 - 3) + C_2 (I_2 - 3) \qquad (16)$$

where I_1 and I_2 are the strain invariants expressed in terms of the principal extension ratios λ_1, λ_2, λ_3 as

$$I_1 = \lambda_1^2 + \lambda_2^2 + \lambda_3^3 \qquad (17)$$

$$I_2 = \lambda_1^2 \lambda_2^2 + \lambda_2^2 \lambda_3^2 + \lambda_3^2 \lambda_1^2 \qquad (18)$$

I_3 is assumed to be unity. Bagley and Duffey arrived at the equation:

$$\sigma^2 = \left(\frac{D_j}{D}\right)^4 - \left(\frac{D_j}{D}\right)^{-2} \qquad (19)$$

Bagley and Duffey also carried out an energy balance on the fluid as it emerged from the capillary and arrived at the expression:

$$\sigma^2 = \left(\frac{D_j}{D}\right)^4 + 2\left(\frac{D_j}{D}\right)^{-2} - 3 \qquad (20)$$

Comparing these expressions with experimental results found differences of up to 50 percent between calculated values of σ^2 and experimental values (3).

Graessley, Glasscock and Crawley (29) assumed the die swell to be caused by the release of elastic energy stored in the fluid inside the capillary. Graessley obtained the equation:

$$\left(\frac{D_j}{D}\right)^4 - 2\left(\frac{D_j}{D}\right)^{-2} - 3 = \frac{J_o \tau_w^2}{2G_s} \quad \frac{\int_0^1 \xi^5 \, d\xi/(\eta/\eta_o)}{\int_0^1 \xi^3 \, d\xi/(\eta/\eta_o)} \qquad (21)$$

where $\xi = r/R$, is the dimensionless radial position, τ_o is the experimental shear compliance and G_s is the modulus of elasticity estimated from the theory of rubber elasticity in terms of the average molecular weight between entanglements and τ_w is the shear stress at the capillary wall. The factor

$$\frac{1}{2} \quad \frac{\int_0^1 \xi^5 \, d\xi/(\eta/\eta_o)}{\int_0^1 \xi^3 \, d\xi/(\eta/\eta_o)} \qquad (22)$$

accounts for the velocity and stress distribution across the capillary. These results can be simplified by assuming a parabolic velocity profile inside the capillary and thus becomes

$$\sigma_w^2 = 3\left[\left(\frac{D_j}{D}\right)^4 + 2\left(\frac{D_j}{D}\right)^{-2} - 3\right] \qquad (23)$$

where σ_w is the recoverable shear at the wall. This work has one

inherent difficulty, in that it is also based on uniaxial stretching instead of recovery from shear. This analysis does give σ_w values in the correct range, but the calculated values differ from experimental by as much as 200 percent at low shear stresses.

Lodge (41) has shown theoretically that a sheared piece of viscoelastic material exhibits elastic recovery and a lateral swelling upon being released from stress and that a slow secondary recovery takes place. Lodge used a constitutive equation equivalent to Equation 10 with a_2 equal to zero and $a_1(t)$ independent of the invariants. For simple shear, Lodge's analysis yields:

$$\frac{\ell_j}{\ell_o} = (1 + \tau_1^2 \dot{\gamma}^2)^{1/6} \tag{24}$$

Tanner (66) assumed (1) isothermal and incompressible flow, (2) very long die, (3) negligible inertial effects, (4) the small slow recovery far away from the die is ignored. Tanner assumes that the Kaye, Bernstein, Kearsley and Zapas form of constitutive equation is relevant, such that

$$\tau_{ij} = -p\delta_{ij} + \int_{-\infty}^{t} \left(\frac{\partial U}{\partial I_B} C_{ij}^{-1} - \frac{\partial U}{\partial I_C} C_{ij}\right) ds \tag{25}$$

where U is a function of $I_{c^{-1}}$, I_c and $t - s$. $I_{c^{-1}}$ and I_c are the traces of the strain tensors C_{ij}^{-1} and C_{ij}, respectively. By introducing the condition of simple shear and neglecting the second normal stress difference, Tanner obtained the relation for the radial

expansion:

$$\frac{D_j}{D} = \left\{ \frac{\int_0^{D/2} (N_1 + G - \tau^2/G)\, r\, dr}{\int_0^{D/2} Gr\, dr} \right\}^{1/6} \qquad (26)$$

where N_1 is the first normal stress difference, $(\tau_{11} - \tau_{22})$, G is an elastic modulus and τ is the local shear stress in the capillary. For materials with a single time constant,

$$\frac{N_1}{2\tau} = \frac{\tau}{G} \qquad (27)$$

and G is a constant. For such materials it is possible to simplify Tanner's equation to the form:

$$\frac{D_j}{D} = \left(1 + \frac{(N_1/2\tau)^2}{2}\right)^{1/6} \qquad (28)$$

Considering experimental data which indicates D_j/D approaches 1.1 for slow Newtonian flows and polymer melts, Tanner revises his equation to

$$\frac{D_e}{D} = \frac{D_j}{D} + 0.1 \qquad (29)$$

This seems to give reasonable agreement between predicted swelling ratios and experimental values for polystyrene, however, little has been done to compare this theory to other polymeric melts (73).

White (74) proposed a model to relate entrance flow patterns

to extrudate quality. The model consisted of five regions:

(1) Virgin melt

(2) A funnel shaped region through which melt moves from region one to the die

(3) Dead spaces

(4) Area within the capillary itself

(5) Emerging extrudate.

In region one the normal stresses are equal to the hydrostatic pressure and the shear stresses are zero. As the polymer proceeds to the die entry the stresses reach a maximum. As the melt emerges from the die, it remembers its previous deformation. Here, White uses a single integral constitutive equation to describe the flow through the slit.

CHAPTER III

RHEOLOGICAL PROPERTIES

A. MATERIALS

Six commercial polymers were chosen for this study. These were:

(1) A branched low density polyethylene (LDPE, MI = 5.0), Dow Chemical 610M, with a melt index of 5.0 and density of 0.92 gm/cc^3;

(2) A linear high density polyethylene (HDPE, MI = 0.1), Phillips Petroleum, Marlex EHM6001, with a melt index of 0.1 and a density of 0.96 gm/cc;

(3) A linear high density polyethylene (HDPE, MI = 5.0), Phillips Petroleum, Marlex EMB6050, with a melt index of 5.0 and a density of .96 gm/cc^3;

(4) A linear high density polyethylene (HDPE, MI = 0.02, Union Carbide DMDJ1155 with a melt index of 0.02 and a density of 0.96 gm/cc^3;

(5) Polystyrene (PS), Dow Chemical Styron polystyrene 678 with a density of 1.02 gm/cc^3; and

(6) Polypropylene (PP), Hercules, Inc., Profax 6523F with a density of 0.89 gm/cc^3.

B. MEASUREMENTS

Capillary Rheometer

The Instron Capillary Rheometer (72) was used to carry out

viscosity measurements. Pallets of polymer were fed into the Instron barrel heated to 180°C, the temperature at which measurements were carried out. The polymer reached thermal equilibrium after forty-five minutes. After the polymer had achieved thermal equilibrium it was forced through a capillary die by the downward motion of a constant speed plunger fitted to the barrel. Eight stainless steel capillaries of varying lengths and diameters were used. These are listed in Table I. The lengths were determined with Vernier calipers and the diameters were measured from photomicrographs of the capillaries at a known magnification by the Lietz orthoplan microscope.

The shear stress and viscosity characteristics of the polymer were determined from plunger speed and force data for a series of capillaries. In particular the shear stress $(\tau_{12})_w$, and the shear viscosity, η, were determined from the Instron capillary rheometer using the Equations (12), (40) and (51):

$$\mu = (\tau_{12})_w / \dot{\gamma}_w \tag{30}$$

$$P = P_{ENT} + 4(\tau_{12})_w \left(\frac{L}{D}\right) \tag{31}$$

$$\dot{\gamma}_w = \left[\frac{3n' + 1}{4n'}\right] \frac{8V}{D} \tag{32}$$

where $n' = d \log (\tau_{12})_w / d \log \frac{8V}{D}$ (33)

TABLE I

CAPILLARY DIMENSIONS

Capillary	Diameter (Inch)	Length (Inch)	$\frac{L}{D}$
2S	.022	.200 (8)	8.96
2M	.023	.601 (5)	25.61
2L	.023	.960 (0)	40.64
5S	.052	.512 (0)	9.85
5M	.052	1.512 (5)	29.08
5L	.054	2.578 (0)	47.50
8S	.079	.402 (0)	5.04
8M	.080	.797 (5)	9.96

Rheogoniometer

The shear viscosity and the first normal stress difference were determined from the Weissenberg rheogoniometer in the region of low shear. The polyolefins have been know to degrade easily at high temperatures. Before making rheological measurements on polyethylene melts, it was necessary to homogenize and stabilize the sample as suggested by Chen (14):

Prepare a five percent solution of the polymer in p-xylene at 120-130°C, and slowly add this to five to ten times its volume of well stirred methanol at room temperature. Filter out the precipitated polymer and wash on the filter with additional quantities of methanol. Dry the polymer for two hours in a vacuum oven with a maximum temperature of 105°C.

A dilute chloroform solution of the stabilizer (0,2 weight percent of the polymer) is then sprinkled over the dry polymer and thoroughly mixed. The polymer is then dried in a vacuum oven for two hours with a maximum temperature of 105°C.

The dry polymer was then molded into discs having a diameter of 2.5 centimeters using a laminating press.

The experiments were carried out at 180°C using a two degree cone angle and a 2.5 cm diameter cone and plate. A heating period of approximately two hours was necessary to reach thermal equilibrium.

The shear viscosity was determined from the Weissenberg rheogoniometer in the low shear rate region using these Equations, (12), (40) and (51):

$$\mu = \frac{\tau_{12}}{\dot{\gamma}} \tag{34}$$

$$\tau_{12} = \frac{3M}{2\pi R^3} \tag{35}$$

$$\dot{\gamma} = \frac{\Omega}{\phi} \tag{36}$$

where M is the torque, Ω is the angular velocity, ϕ the gap angle and R the radius of the cone.

The first normal stress difference, N_1, was determined in the region of low shear rates from the Weissenberg rheogoniometer using the Equations (27) and (51).

$$N_1 = \frac{2F}{\pi R^2} \tag{37}$$

where F is the force pushing the platens apart.

Results

The viscosity-shear rate properties are given by Figure 1. The low shear rate data was obtained from the Weissenberg rheogoniometer and the Instron capillary rheometer was used for shear rates above one sec^{-1}.

The first normal stress difference-shear rate properties are given by Figure 2. N_1 is seen to be in the range of 10^4 to 10^5 dynes/cm^2 in the range of shear rates covered. The first normal stress difference-shear stress relationships at low shear rates are plotted

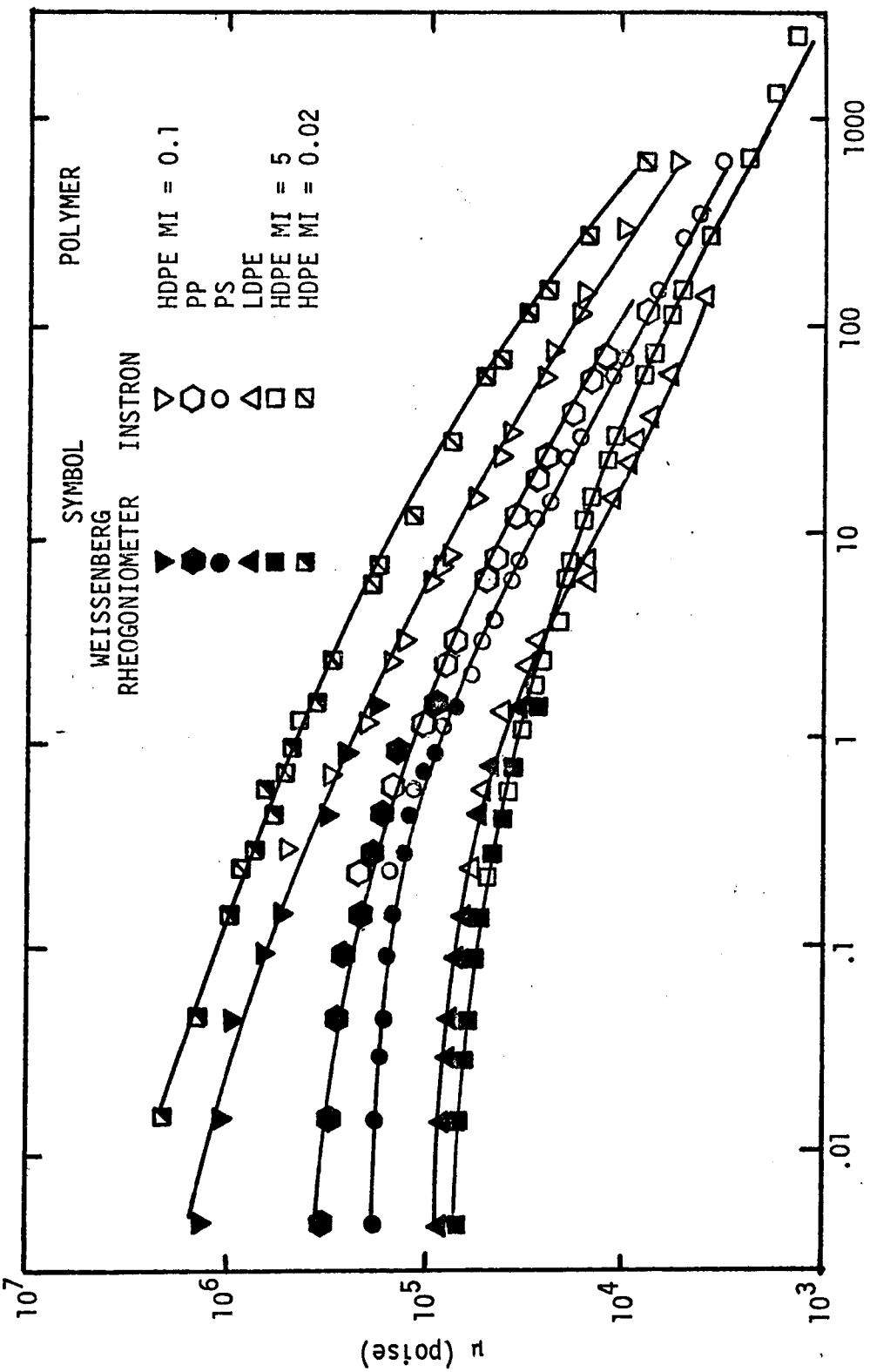

Figure 1. Non-Newtonian Shear Viscosity as a Function of Shear Rate

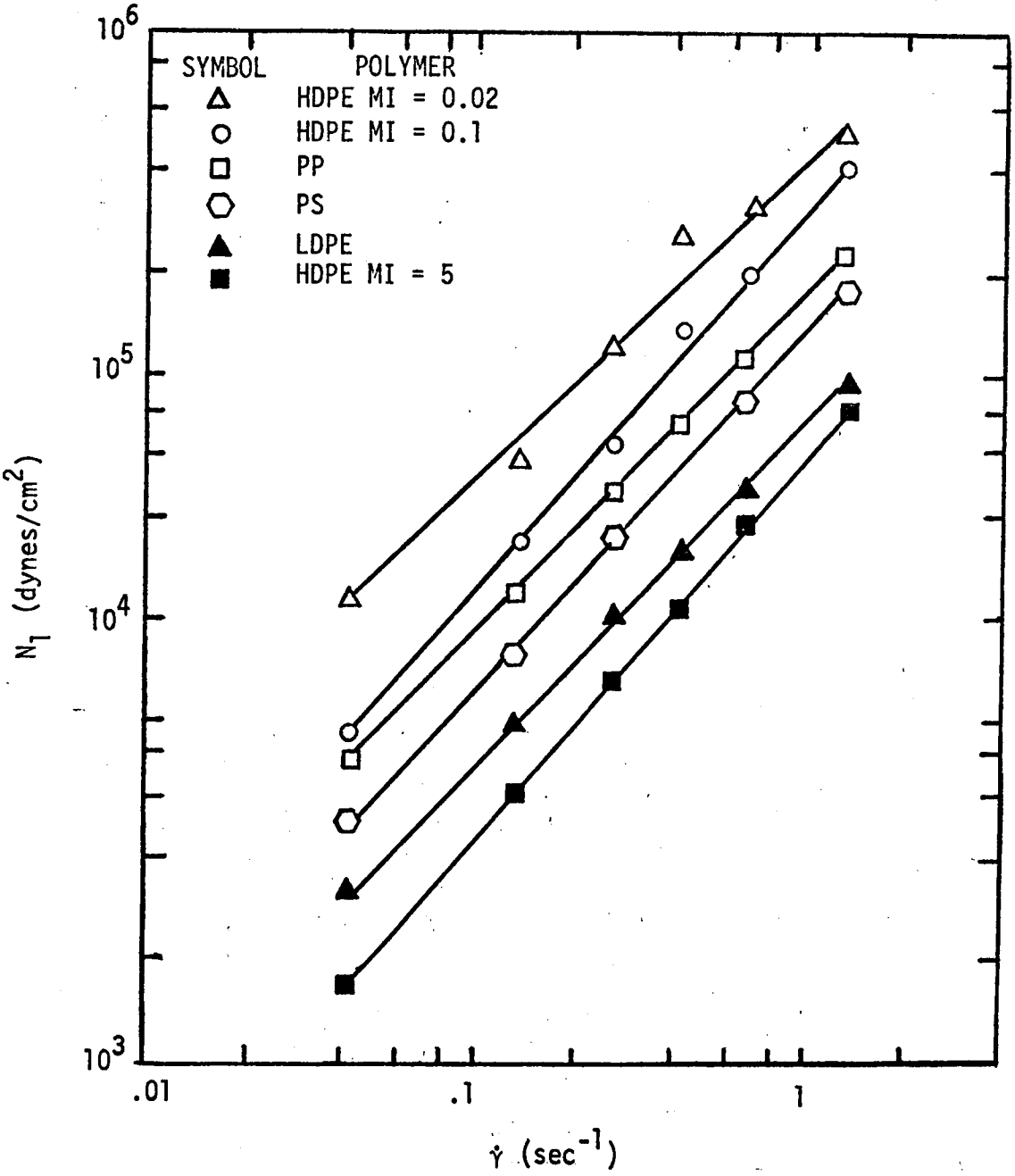

Figure 2. First Normal Stress Difference as a Function of Shear Rate

in Figure 3.

Interpretation

The viscosity measurements from the Weissenberg rheogoniometer and the Instron rheometer agree reasonably well in the range of overlap, as seen in Figure 1.

The three high density polyethylenes used show very different viscosities at 180°C. The high density polyethylene melt index 0.02 (HDPE MI = 0.02) has a viscosity in the range of 2.0 - 3.0 x 10^6 poise at very low shear rates. The high density polyethylene melt index 0.1 (HDPE MI = 0.1) is not quite as viscous, the viscosity ranging from 1 - 2 x 10^6 poise at low shear rates. The high density polyethylene melt index 5.0 (HDPE MI = 5) has a much lower viscosity than the other two melts, ranging from 6.5 - 7.5 x 10^4 poise at low shear rates. This is shown more clearly in Figure 4. Also shown is viscosity data from the literature.

Dharod (23) used the same HDPE MI = 0.1 and presented viscosity-shear rate data very similar to that in Figure 1. He also presents data for a high density polyethylene melt index six, which is slightly lower than that shown for our HDPE MI = 5 shown in Figure 1. Schroff and Shida (61) measured the viscosities of high density polyethylene melts at 190°C. The shear rate-viscosity curve for HDPE MI = 5 shows a similar shape to viscosity-shear rate curves for high density polyethylenes of 4.0 and 6.0 melt indices. The curve for the HDPE MI = 5 lies slightly below that of the melt index 4.0 polyethylene and well above that of the melt index 6.0 polyethylene. Han, Yu and

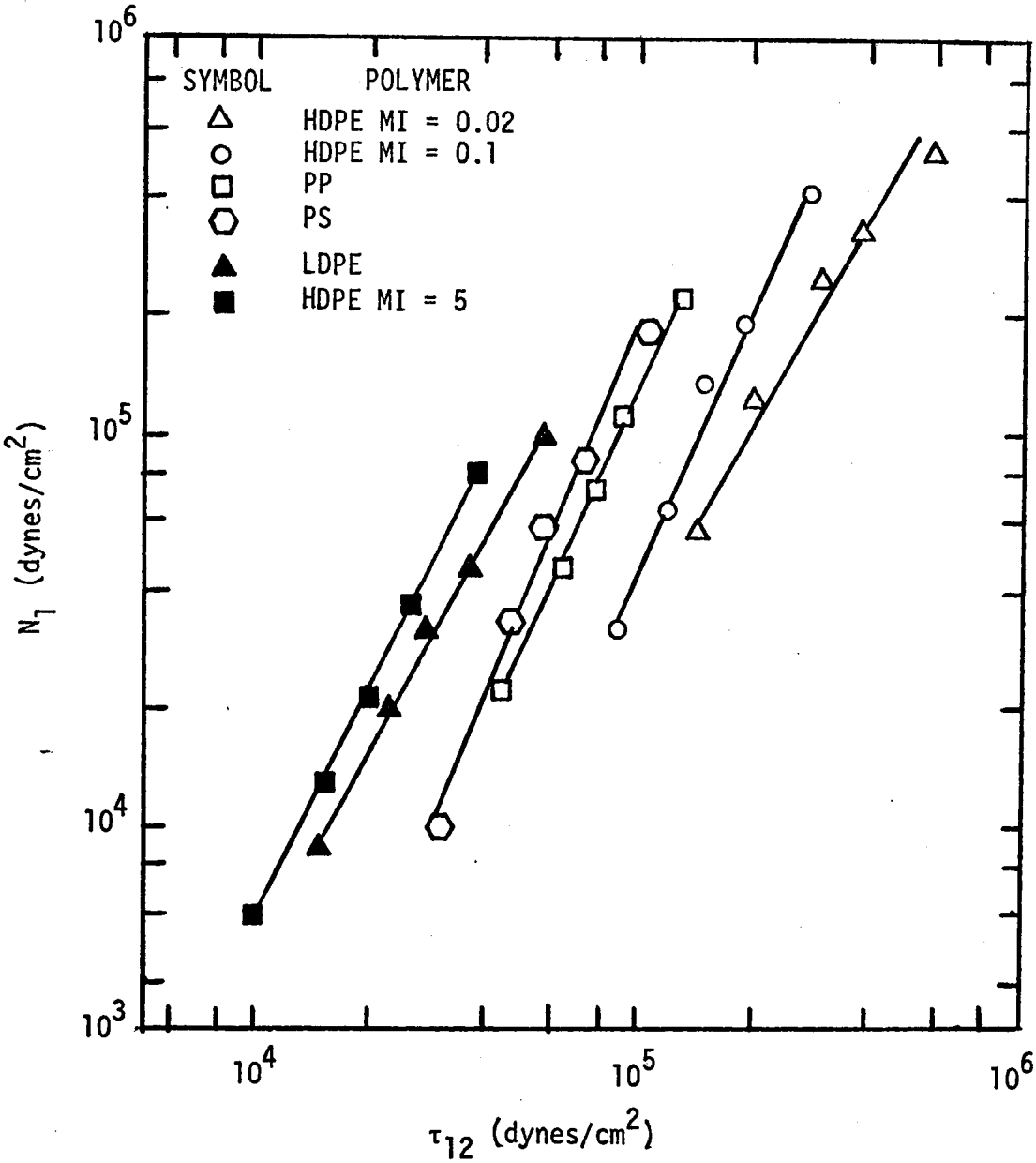

Figure 3. First Normal Stress Difference as a Function of Shear Stress

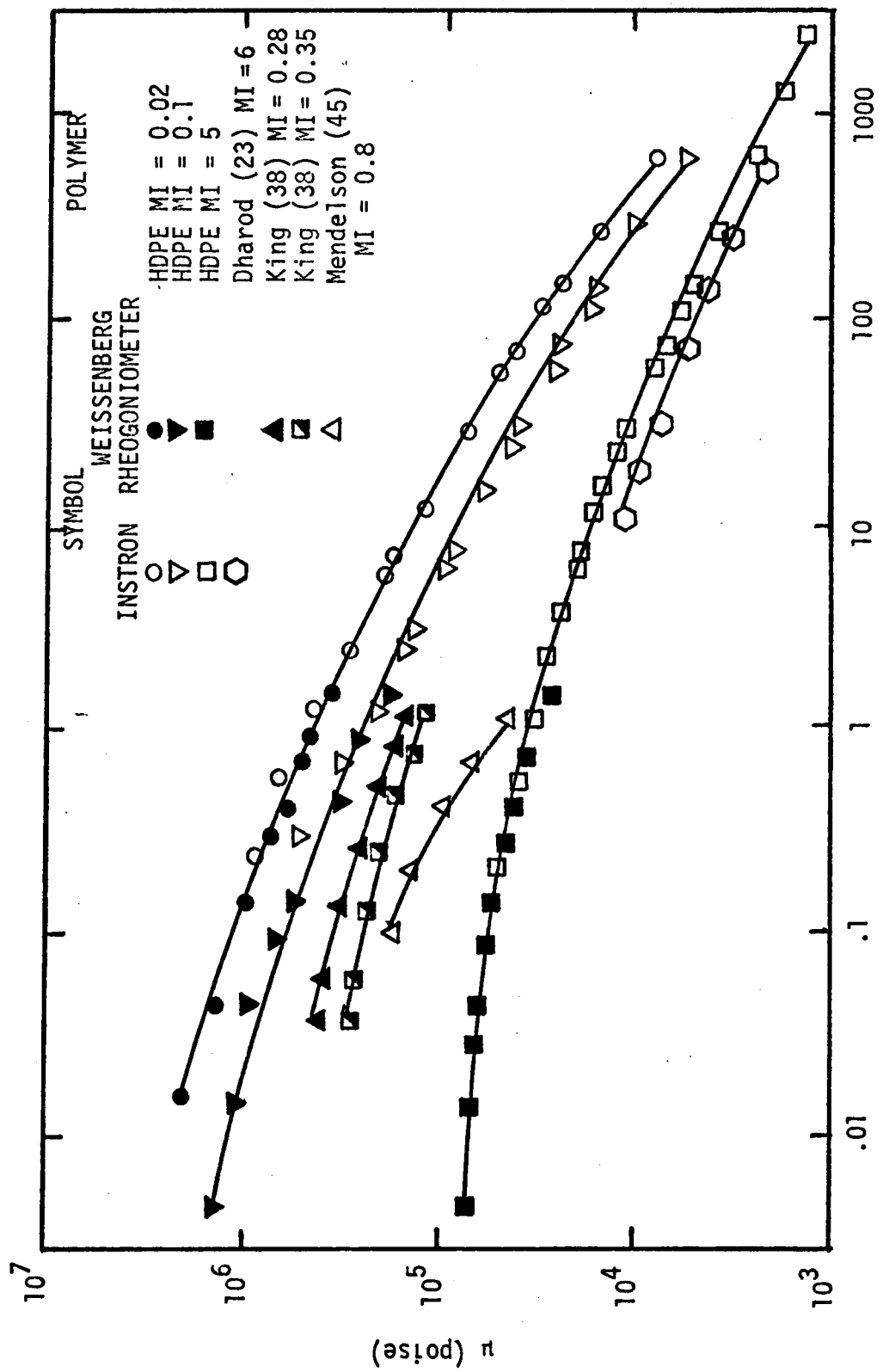

Figure 4. Shear Viscosity as a Function of Shear Rate for HDPE's and Literature Data

Kim (35) used high density polyethylenes of melt indices 0.2 and 0.8 and obtained viscosity measurements for these polymer melts at 200°C. The high density polyethylene data for these polymers lies between that of the HDPE MI = 0.1 and HDPE MI = 5. It is difficult to compare viscosities of different polymers at different temperatures. These comparisons at least give us a rough idea of the order of magnitude of the viscosity.

Dharod (23) obtained viscosity-shear rate data for the low density polyethylene (LDPE) used in this study. The data he presents is in agreement with that in Figure 1. Schroff and Shida (61) determined the viscosities of low density polyethylene. The LDPE used in this study was similar to a low density polyethylene of melt index 3.2 used by Schroff and Shida. The viscosities were roughly in the same range and the curves differed only at high shear rates, where the LDPE used in this work curves off to one side. Han and coworkers (35) also present viscosity data on a low density polyethylene, melt index 3.5. The viscosity of this low density polyethylene was slightly higher than viscosities obtained for the LDPE used in this study.

White and coworkers (82) present data on the polypropylene (PP) used in this work. Reasonable agreement exists between the two sets of viscosity data.

White and coworkers (81) determined the molecular weight of the polystyrene (PS) used here in previous work. The number average molecular weight being 78,000 and M_w/M_n = 3.1. Dalton (20) used a

polystyrene of M_n = 48,000 and M_w/M_n = 3.9. His viscosity at 180°C is roughly 30 percent lower than that obtained for the PS in Figure 1. Ballenger (4) measured the viscosity of polystyrene at 180°C with M_n = 311,000 and M_w/M_n = 2.82. That viscosity data appeared well above that of PS in Figure 1. Graessley (29) used a polystyrene of M_w = 220,000 and M_w/M_n = 3.1 at 180°C in his work. Compared to the PS in Figure 1, the viscosities were roughly 50 percent higher, although not as high as Ballenger's. Chen and Bogue (15) measured the viscosity of a polystyrene of M_n = 90,000 and M_w/M_n of 2.54 at 180°C. The viscosities obtained by Chen and Bogue were slightly higher when compared to Figure 1.

Mendelson (44) measured the first normal stress difference of four high density polyethylenes of melt indices 0.8 and 0.2 at 200°C. Comparison of this data with that of Figure 2 shows the first normal stress difference for high density polyethylenes to be in roughly the same range, 10^4 - 10^5 dynes/cm^2. Looking more closely, the high density polyethylenes of melt indices 0.8 and 0.2 show first normal stress differences lying between those of HDPE MI = 0.1 and HDPE MI = 5 in Figure 2. This comparison is limited because of the difference in temperature, however, the N_1 values are of the appropriate order of magnitude. King (38) measured the first normal stress difference at 190°C using high density polyethylenes of melt indices of approximately 0.3. N_1 ranged from 10^4 dynes/cm^2 at shear rates of .1 sec^{-1} to 10^5 dyne/cm^2 at shear rates of approximately 1 sec^{-1}. These values give reasonable agreement with those in

Figure 2. Cooper and Pollett (19) measured the first normal stress difference of high density polyethylene at 180°C. Measurements of N_1 fall into the range of 10^5 dynes/cm^2 at shear rates of approximately 1 sec^{-1}. These measurements appear to agree with Figure 2. Plots of N_1 versus τ_{12} show reasonable agreement with Figure 3. Sakamoto and Porter (60) measured the first normal stress difference of high density polyethylene and found N_1 values in the range of 10^4 to 10^5 dynes/cm^2 for shear rates ranging from .1 to 1 sec^{-1}. These values are similar to those in Figure 2. Lee (39) obtained first normal stress data for high density polyethylene with a viscosity comparable to that of the HDPE MI = 0.02 in Figure 1. The N_1 values obtained are similar to those of the HDPE MI = 0.02 in Figure 2. Han (32) presents values of the first normal stress difference in the range of 10^4 to 10^5 dynes/cm^2 for high density polyethylene, in agreement with Figure 2. Normal stress data from the literature for different high density polyethylene melts is compared in Figure 5.

Lee (39), Han (32) and Chen and Bogue (15) present first normal stress data for polystyrene. The values of N_1 lie in the range of 10^4 to 10^5 dynes/cm^2 in the shear rate range of .1 to 1 sec^{-1}. This is in rough agreement with Figure 2.

Chen and Bogue (15), Han (32) and Lee (39) also present first normal stress differences for low density polyethylene in the range of 10^4 to 10^5 dynes/cm^2 at shear rates between 0.1 and 1 sec^{-1}. These values are in rough agreement with those in Figure 2.

One may define a characteristic relaxation time from the

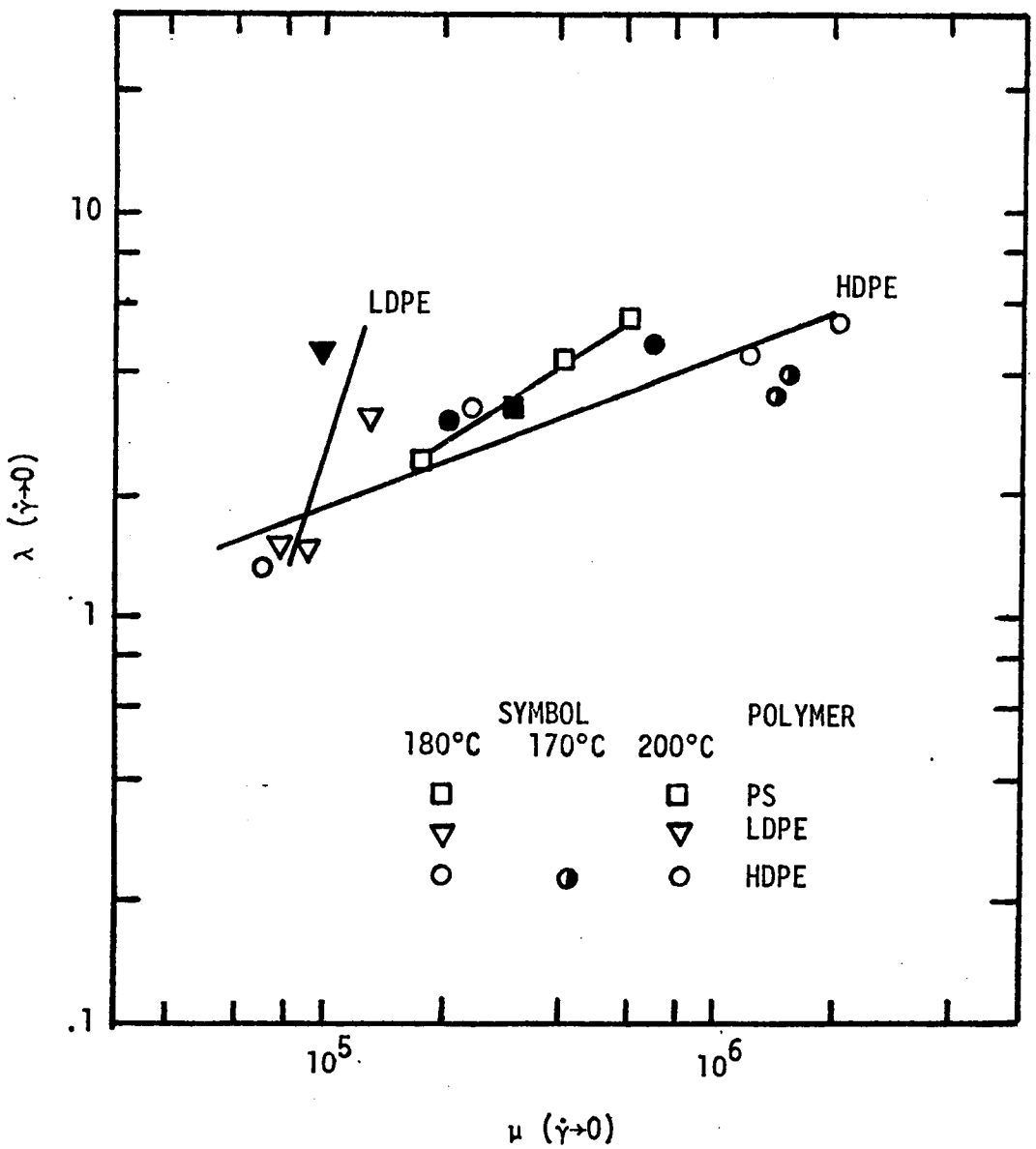

Figure 5. Relaxation Time ($\dot{\gamma}\to 0$) as a Function of Viscosity ($\dot{\gamma}\to 0$) for the PS, LDPE and HDPE's and Literature Data

theory of second order fluids, which is equivalent to a normalized first moment of the relaxation modulus of linear viscoelasticity G(t)

$$\lambda = \frac{\int_0^\infty SG(s)\,ds}{\int_0^\infty G(s)\,ds} \tag{38}$$

As the shear approaches zero,

$$N_1 = 2\left[\int_0^\infty SG(s)\,ds\right]\dot{\gamma}^2 = 2\lambda\eta\dot{\gamma} \tag{39}$$

As

$$\tau_{12} = \eta\dot{\gamma} \tag{40}$$

$$N_1 = 2\lambda\dot{\gamma}\tau_{12} \tag{41}$$

$$\lambda = \frac{1}{2}\,\frac{N_1}{\tau_{12}\dot{\gamma}} \tag{42}$$

The relaxation time as a function of shear rate is shown in Figure 6. Included is high density polyethylene melt index 0.8 used by Mendelson (44). The relaxation time calculated from the data of Mendelson seems to agree quite well with that of the other high density polyethylenes. These values are similar to those computed from data compiled by Lee (39), Dee (21), King (38) and Chen (15). Figure 6 shows the relationship between viscosity as shear rate approaches zero and relaxation time as shear rate approaches zero

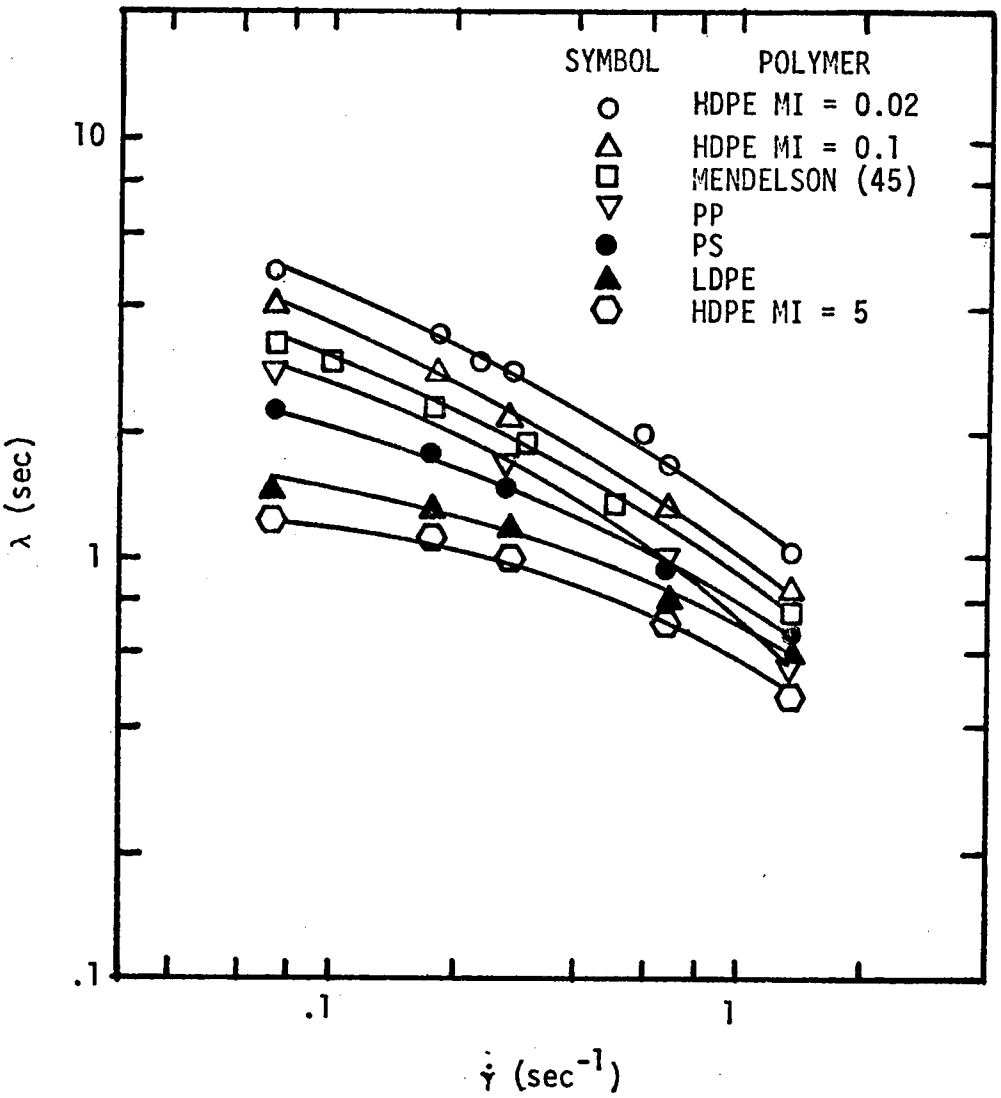

Figure 6. Relaxation Time as a Function of Shear Rate

for the polymer melts used in this study and literature data. This gives a comparison between the different commercial polymers.

The relaxation time of the high density polyethylenes was observed to decrease with increasing melt index, or equivalently, to decrease with decreasing viscosity. This was also true for the other melts shown in Figure 5.

In later chapters, we will use an elastic modulus G, as a means of characterizing the melts. Since according to the second order fluid theory

$$N_1 = 2\,Je\,\eta\dot{\gamma}^2 = 2Je\,\tau_{12}^2 \tag{43}$$

$$\frac{N_1}{\tau_{12}} = 2Je\,\tau_{12} \tag{44}$$

$$2Je = \frac{1}{G} \tag{45}$$

where G is a constant and Je is a shear compliance. Using the first normal stress difference and the shear stress, it is possible to calculate G and Je for each melt. These values are shown in Table 2.

TABLE II

MODULUS OF RECOVERY AND SHEAR COMPLIANCE OF POLYMERS USED

Polymer	G (dynes/cm^2)	Je (cm^2/dyne)
PS	1.68×10^{-5}	2.98×10^{4}
PS	1.60×10^{-5}	3.12×10^{4}
LDPE	4.82×10^{-5}	1.04×10^{4}
HDPE MI = 5	5.14×10^{-5}	0.97×10^{4}
HDPE MI = 0.1	5.31×10^{-6}	0.94×10^{5}
HDPE MI = 0.02	2.28×10^{-6}	2.19×10^{5}

CHAPTER IV

DIE SWELL--QUALITATIVE STUDIES

A. PROCEDURE

The die swell was measured using the Instron capillary rheometer. Pallets of polymer were fed into the Instron barrel, heated to 180°C and then forced through a capillary by the downward motion of a constant speed plunger fitted to the barrel. The capillaries used were listed in Table I. Approximately 80 different experimental runs were made using the Instron rheometer. During each run, the plunger speed was varied from .002 inch/minute to five inch/minute. At each speed the force pushing on the plunger was allowed to reach steady state and samples of the extrudate were taken. Five to ten samples were taken at each new plunger speed, depending on the run.

The die swell of the frozen extrudates was measured approximately 0.2 inches from the initially extruded end using micrometers.

The cooled extrudates were annealed in silicone oil at a temperature above the melting point of the polymer in order to allow the extrudates to relax to a stress free state. For most of the polymers this was taken to be 160°C. A temperature of 180°C was used for polypropylene, since it is still in the solid state at 160°C. The samples were annealed for approximately fifteen minutes. This was a long enough period of time to allow the extrudates to reach a constant diameter. After annealing, the extrudates were removed and

again measured using micrometers.

For selected runs a 35 mm camera with fine grain film was used to take photographs of the extrudate as it emerged from the capillary. The photographs had an enlargement of 1/1 to 2/1 depending upon the experimental run. The negatives were "blown up" on a grid screen using a slide projector and the diameter of the extrudates was measured. Enlargement on the grid screen was 50/1 to 100/1 depending upon the run.

The polymers were also extruded into a bath of silicone oil at 180°C and photographs were taken of the extrudate in an effort to approximate the isothermal state. The photographs were taken between five and ten minutes after the extrudate emerged from the capillary. At slower speeds, the extrudate took longer to reach the plane of the camera. The photographs were processed according to the previous description and the die swell was measured from them. A sketch of the oil bath is shown in Figure 7.

B. APPEARANCE

Polypropylene

The polypropylene (PP) extrudates appeared smooth and translucent over the shear rate range of .07 sec^{-1} to 72 sec^{-1}, equivalent to a shear stress at the wall of 1.1×10^6 $dyne/cm^2$, the extrudate appeared to take on a helical shape. Above shear rates of 333 sec^{-1} the extrudate became more grossly distorted. The extrudate appeared bent and twisted on a larger scale, while still retaining the helical

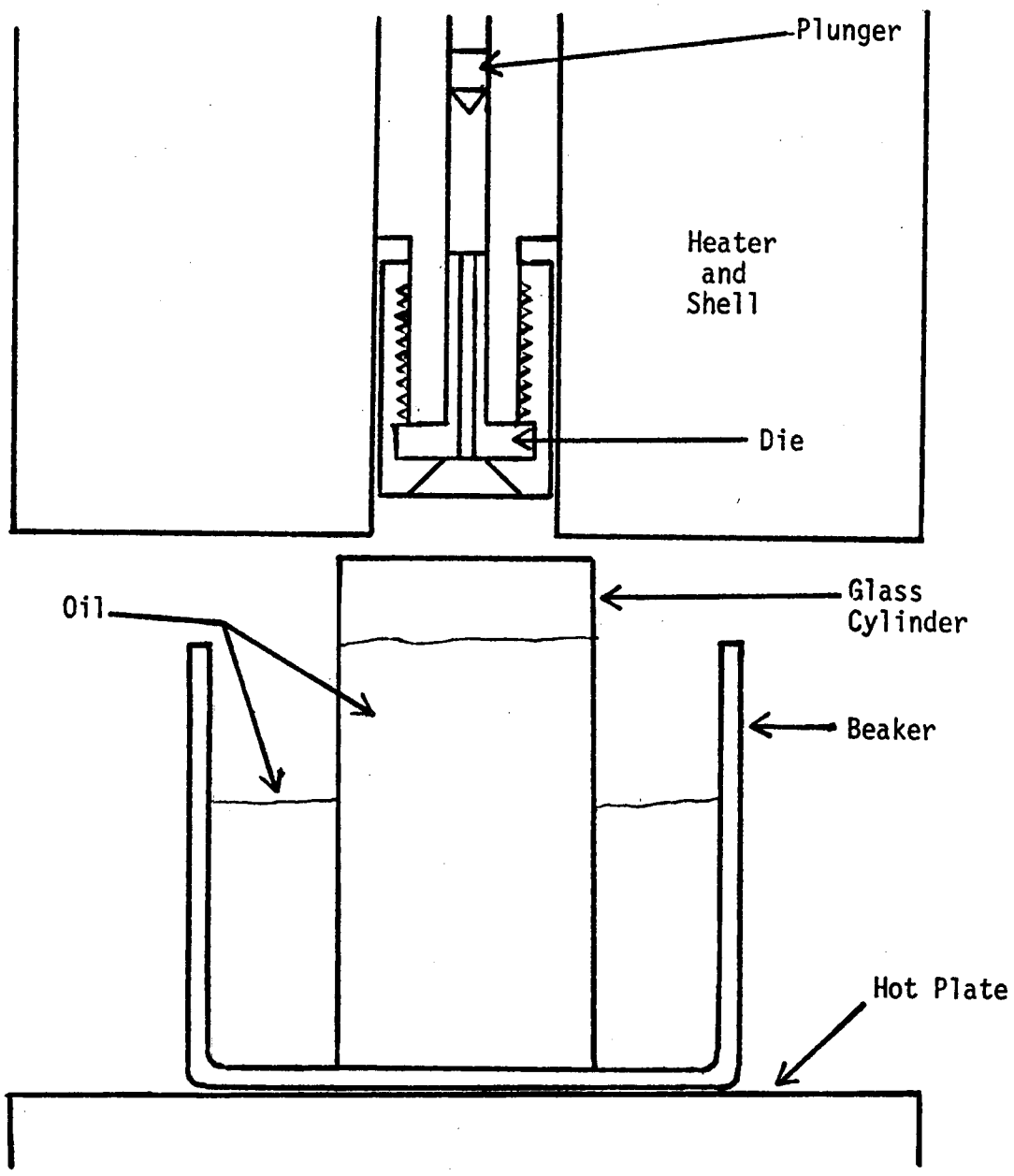

Figure 7. Diagram of Isothermal Extrusion Apparatus

appearance. Increasing the L/D ratio of the die appeared to damp out the distortion.

Polystyrene

The polystyrene (PS) extrudates appeared smooth and clear over a shear rate range of .07 sec^{-1} to 580 sec^{-1}. At a wall shear rate of about 666 sec^{-1}, equivalent to a shear stress at the wall of 2.4×10^6 $dynes/cm^2$, the emerging extrudate took on a helical appearance. Small fluctuations in the pressure were observed. At shear rates above 3330 sec^{-1} the extrudate became grossly distorted, taking on the appearance of small jagged pieces joined together haphazardly. Larger fluctuations in the pressure were observed. Increasing the L/D ratio tended to damp out disturbances in the melt and lead to a smoother extrudate.

Low-Density Polyethylene

The low density polyethylene (LDPE) extrudates appeared smooth and translucent over the shear rate range of .07 sec^{-1} to 133 sec^{-1}. At a wall shear rate of 133 sec^{-1}, equivalent to a shear stress of 1.0×10^6 $dyne/cm^2$, the emerging extrudate appeared very slightly rippled, as though forming a helix. At a shear rate of 166 sec^{-1} the extrudate is clearly seen to assume the form of a helix. At the next change in flow rate, the extrudate assumed the shape of a linked-sausage as sections of the extrudate were alternately smooth and grossly distorted. At higher shear rates, in the range of 3330 sec^{-1}, the extrudate became grossly distorted, with the appearance of jagged

segments joined haphazardly. There were no alternating smooth sections observed. In the unstable flow regime, increasing the L/D ratio tended to decrease the distortion of the extrudate.

High Density Polyethylene

Extrudates of the high density polyethylene melt index 5.0 (HDPE MI = 5) appeared smooth and white over the shear rate range .07 sec^{-1} to 7260 sec^{-1}. At a shear rate of 7260^{-1}, equivalent to a shear stress of 4.0×10^6 $dyne/cm^2$, the emerging extrudate appeared to change from a smooth surface to a helical screw thread. This was accompanied by large fluctuations in pressure.

The high density polyethylene melt index 0.1 (HDPE MI = 0.1) exhibited similar characteristics to the polyethylene of melt index five, with distortion appearing at a shear rate of 666 sec^{-1}, equivalent to a shear stress of 4.0×10^6 $dyne/cm^2$. At a shear rate of 1450 sec^{-1} the extrudate became grossly distorted resembling jagged pieces joined together and only slightly resembling a screw thread. Increasing the L/D ratio of the capillaries appeared to have no effect on the distortion.

The high density polyethylene melt index 0.02 (HDPE MI = 0.02) appeared jagged and rough over the entire shear rate range. This was not the helical screw thread type of distortion as observed in the other two high density polyethylenes. At a shear rate of 666 sec^{-1}, equivalent to a shear stress of 4.5×10^6 $dyne/cm^2$ the extrudate did exhibit a transition from the rough extrudate to a rough helical screw thread appearance. This was accompanied by large fluctuations

in the pressure. At shear rates of 1450 sec^{-1} the extrudates became more grossly distorted, similar to the HDPE MI = 0.1.

Appendix B lists the critical parameters at which extrudate distortion was observed for both the helical or screw thread instability and the gross distortion.

C. SOLIDIFIED EXTRUDATE SWELL

Polypropylene

The die swell of the frozen extrudate was observed to increase with increasing shear rate until the extrudate became distorted. The die swell was observed to be a function of the shear rate, independent of the capillary diameter. This is shown in Figure 8. Increasing the L/D ratio of the capillaries caused the amount of swell to decrease, at a constant shear rate. This is shown in Figure 9. For dies with L/D ratios greater than 40, the die swell seemed almost independent of L/D ratio. The die swell approached a lower limit of 1.1 at low shear rates.

Polystyrene

The die swell was observed to increase with increasing shear rate until the extrudate became distorted. The die swell was observed to be a function of the shear rate, independent of the capillary diameter. Increasing the L/D ratio of the capillaries caused the amount of swell to decrease, at a constant shear rate. For dies with an L/D ratio greater than 25, the die swell seemed almost independent of the L/D ratio. The die swell approached a lower limit

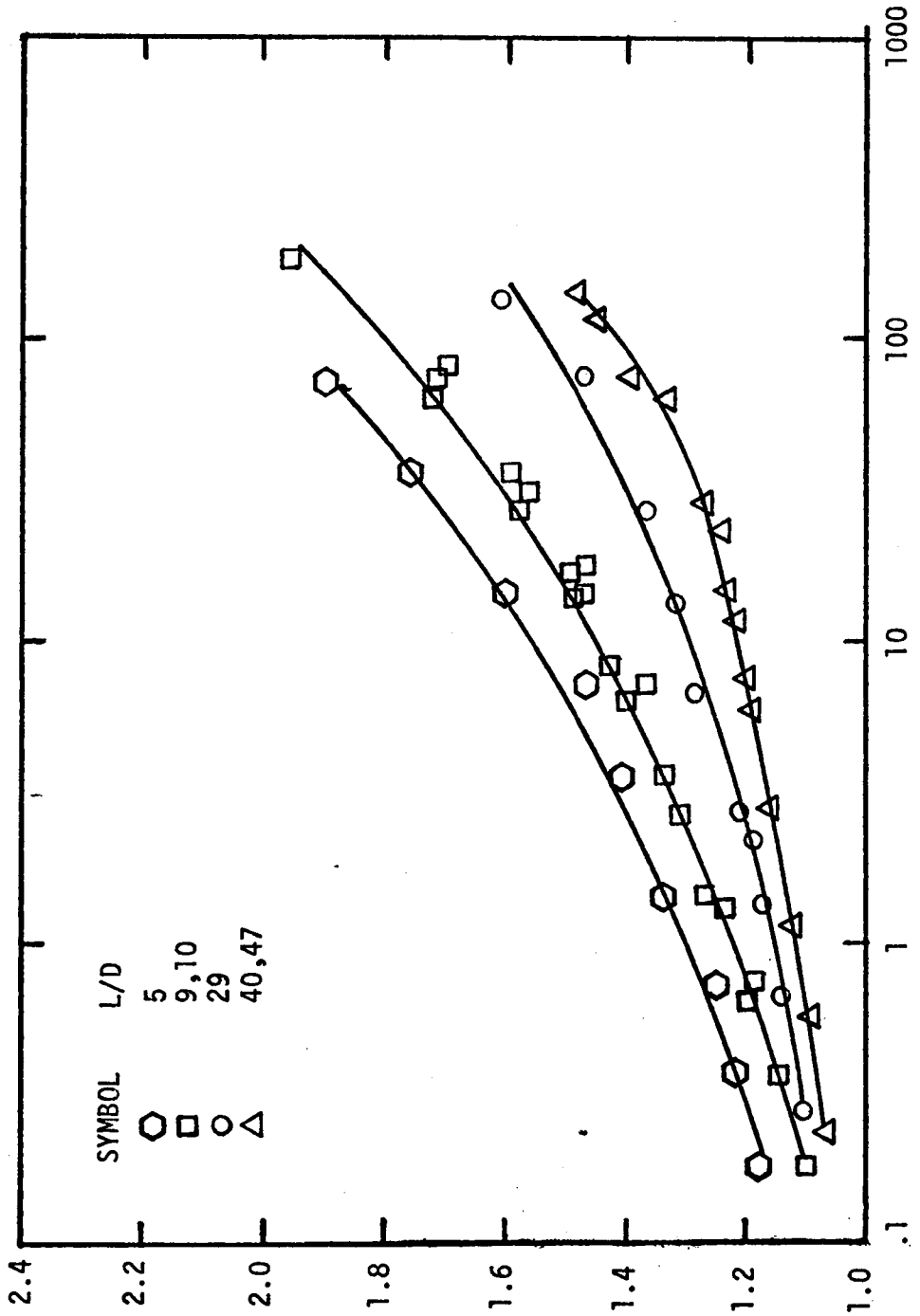

Figure 8. Die Swell of PP as a Function of Shear Rate

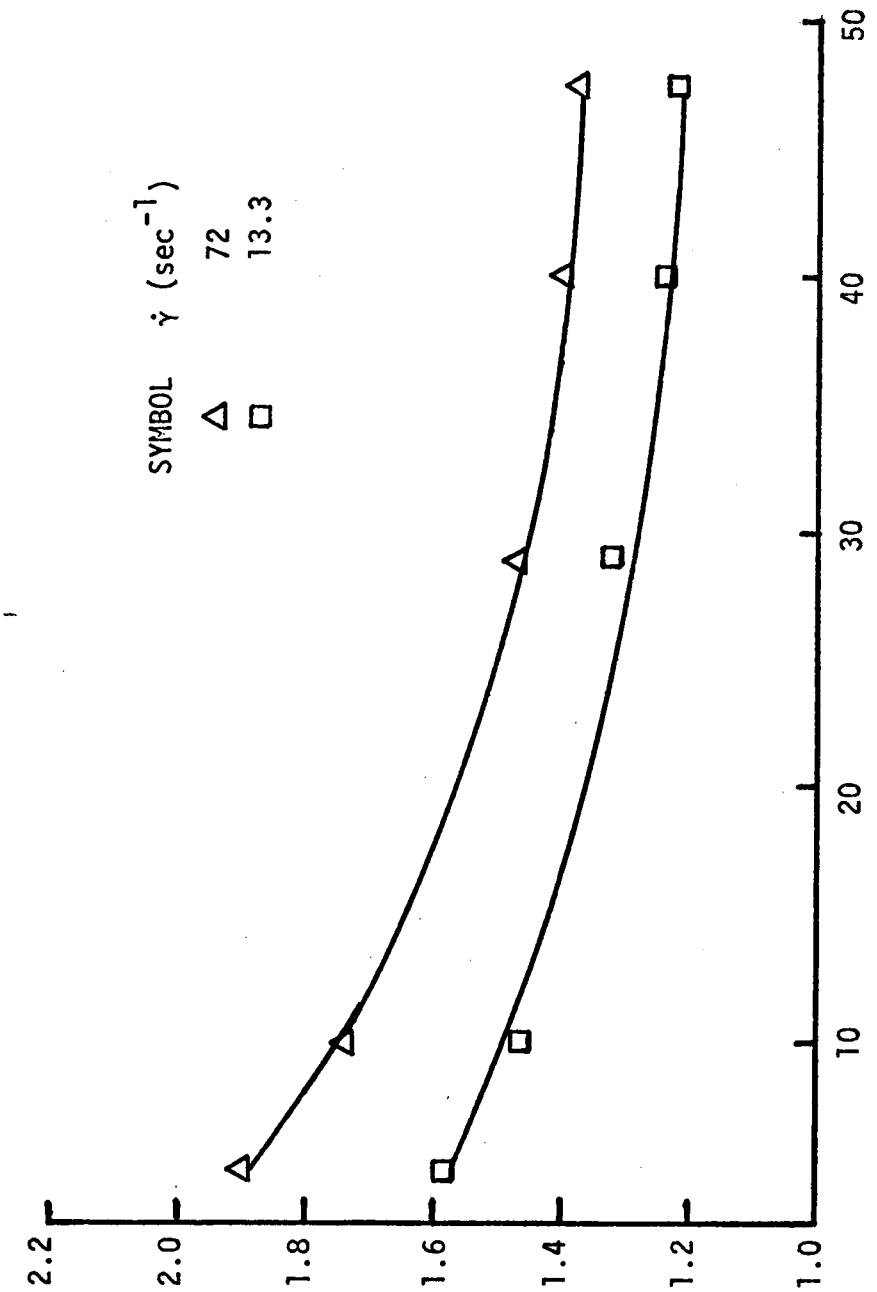

Figure 9. Die Swell of PP as a Function of L/D Ratio

of 1.1 at low shear rates. These effects are shown in Figures 10 and 11.

High Density Polyethylene

The die swell of the polyethylene extrudates was observed to increase with increasing shear rate until the extrudate became distorted. The die swell was observed to be a function of shear rate, independent of the capillary diameter. The low melt index polyethylenes, HDPE's MI = 0.1 and MI = 0.02, appeared to have an almost constant die swell over a range of shear rates from .07 to 10 sec^{-1}. Increasing the L/D ratio of the capillaries caused the amount of swell to decrease, at constant shear rate.

The HDPE MI = 5 had die swell almost independent of L/D ratio for L/D's greater than 25. The other polyethylenes did not display this tendency. All three polyethylene melts had die swell approaching a lower limit of 1.1 at low shear rates. The HDPE MI = 0.1 and HDPE MI = 0.02 never quite reached 1.1 even at the lowest shear rates. The behavior of these melts with respect to shear rate and changing L/D is shown in Figures 12 and 13 for MI = 0.1, Figures 14 and 15 for MI = 5 and Figures 16 and 17 for MI = 0.02.

Low Density Polyethylene

The die swell of the LDPE extrudates was observed to increase with increasing shear rate until the extrudate became distorted. The shape of the curve displayed a different character than the curves of die swell versus shear rate for the other polymers. From a lower

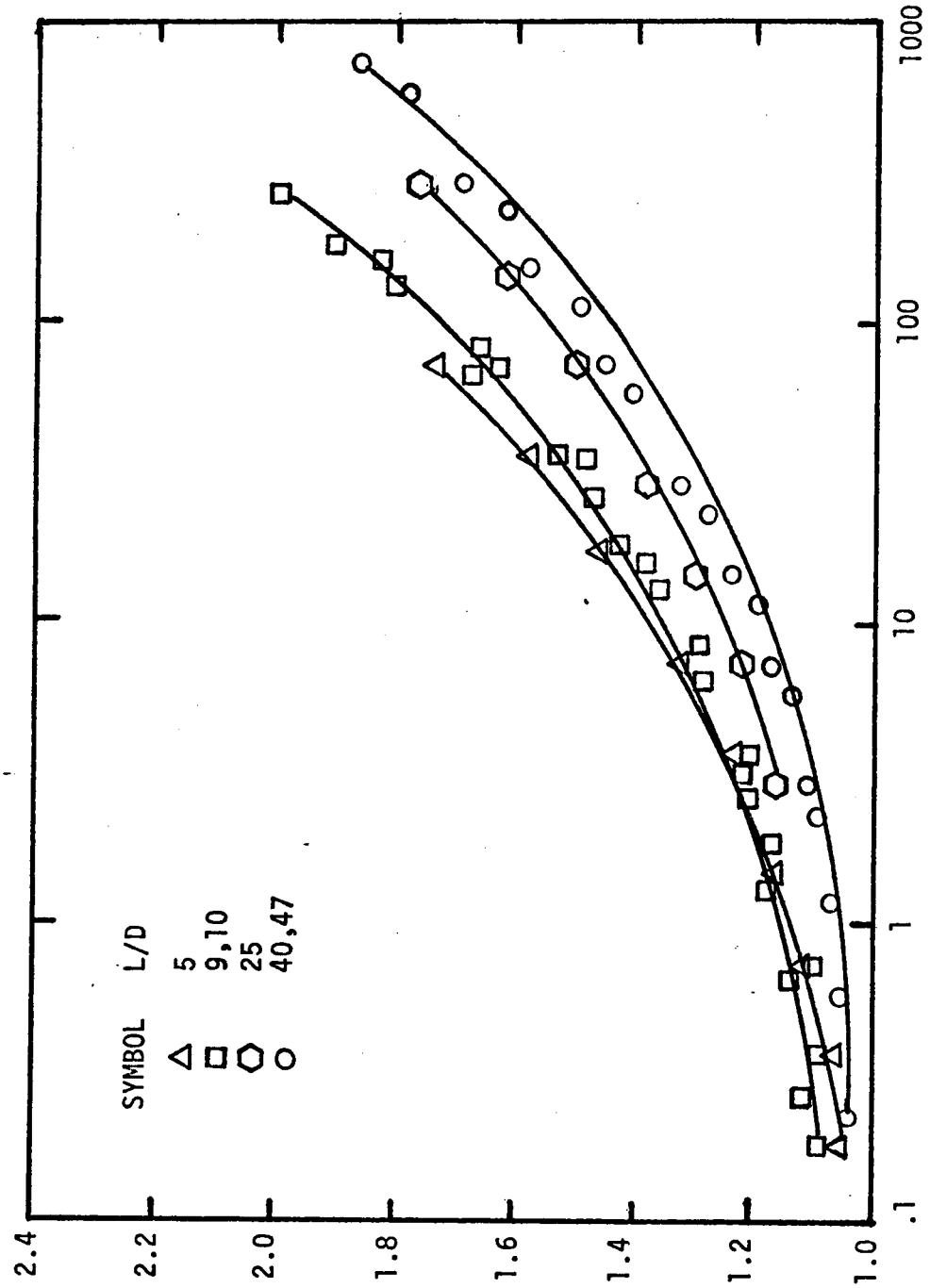

Figure 10. Die Swell of PS as a Function of Shear Rate

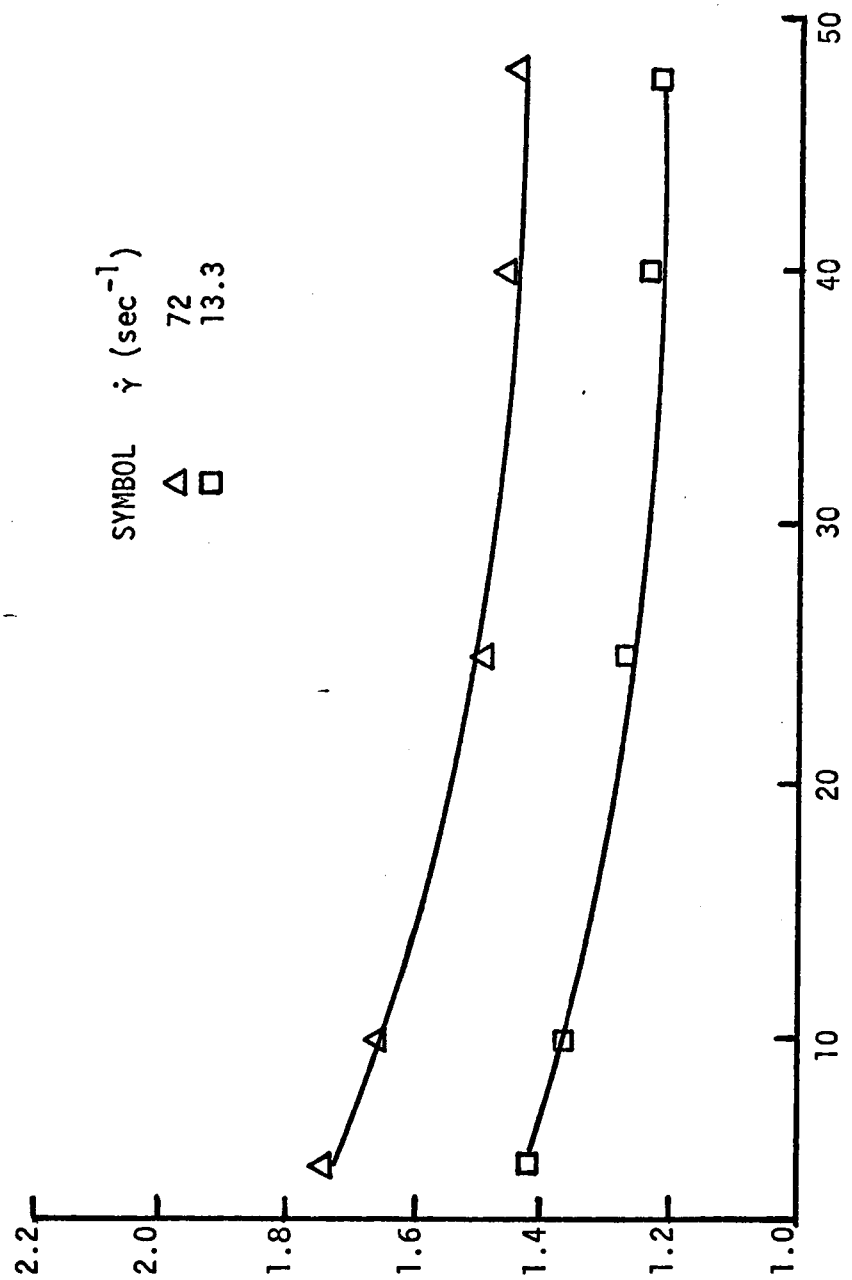

Figure 11. Die Swell of PS as a Function of L/D Ratio

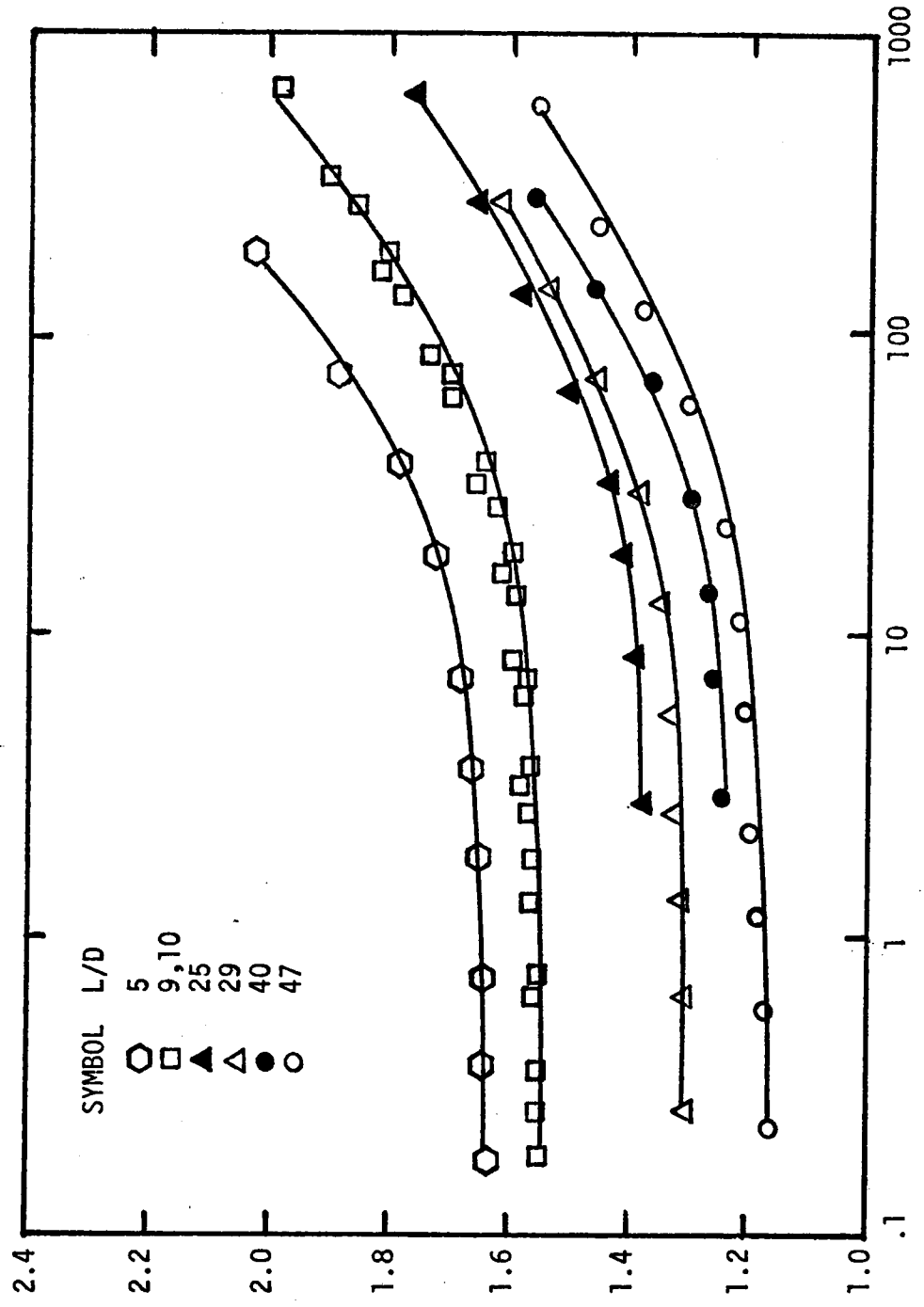

Figure 12. Die Swell of HDPE MI = 0.1 as a Function of Shear Rate

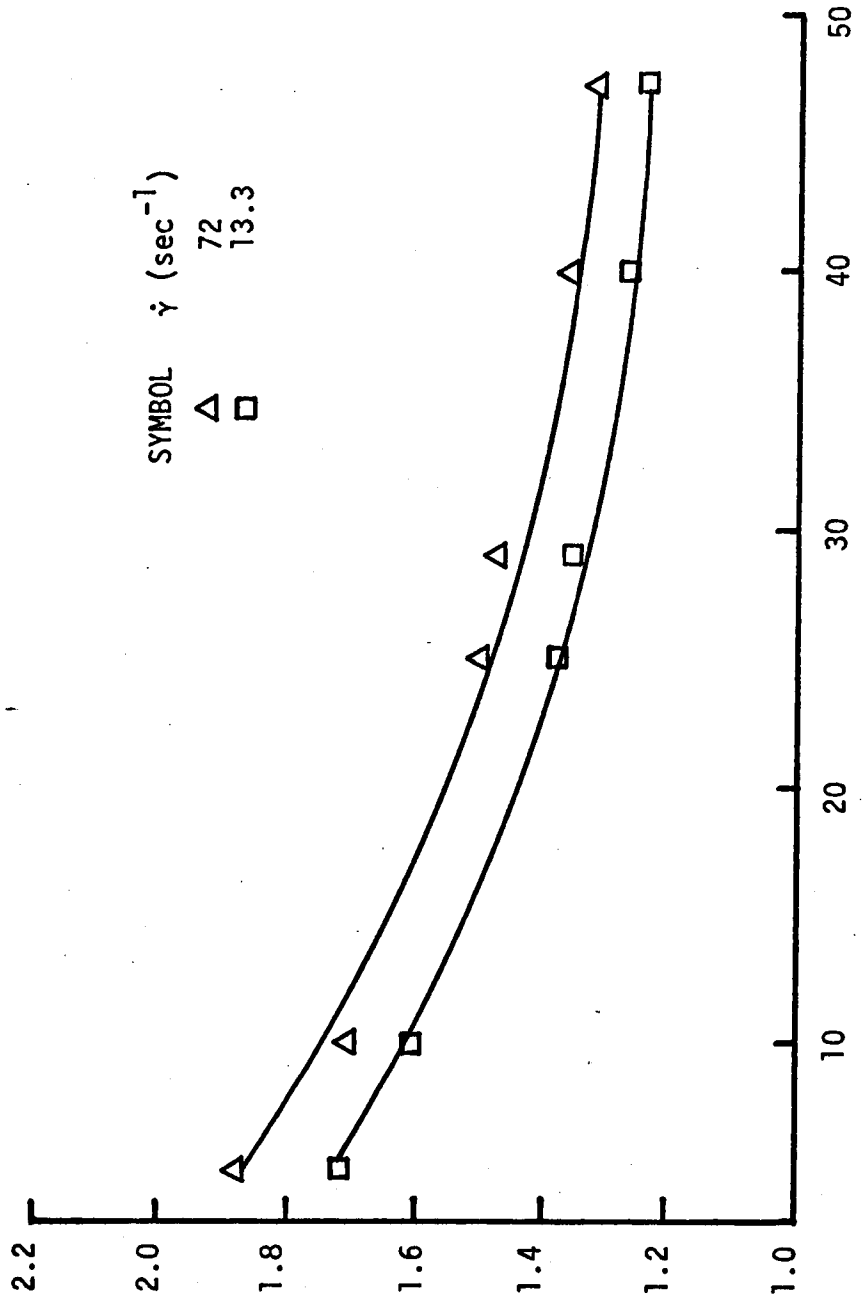

Figure 13. Die Swell of HDPE MI = 0.1 as a Function of L/D Ratio

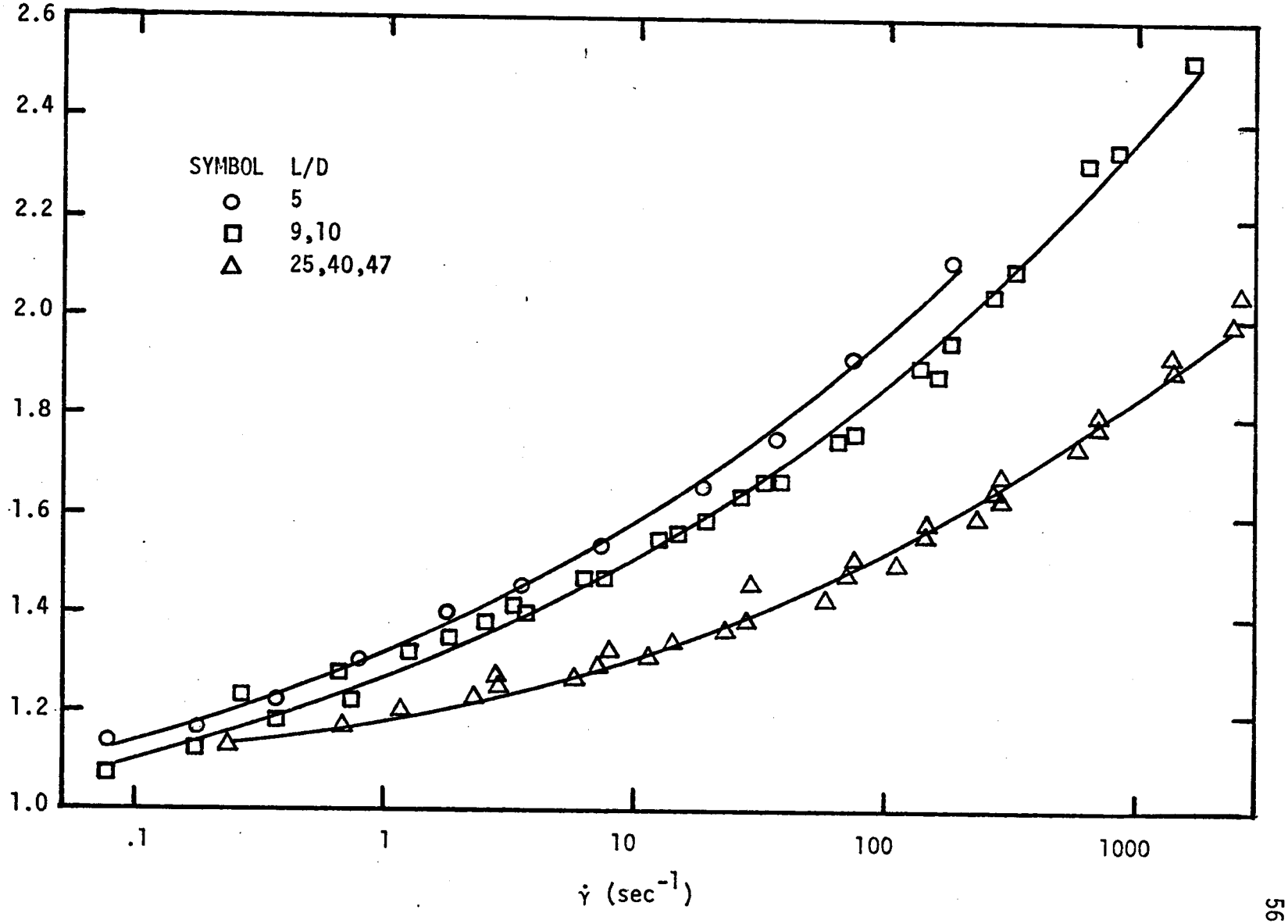

Figure 14. Die Swell of HDPE MI = 5 as a Function of Shear Rate

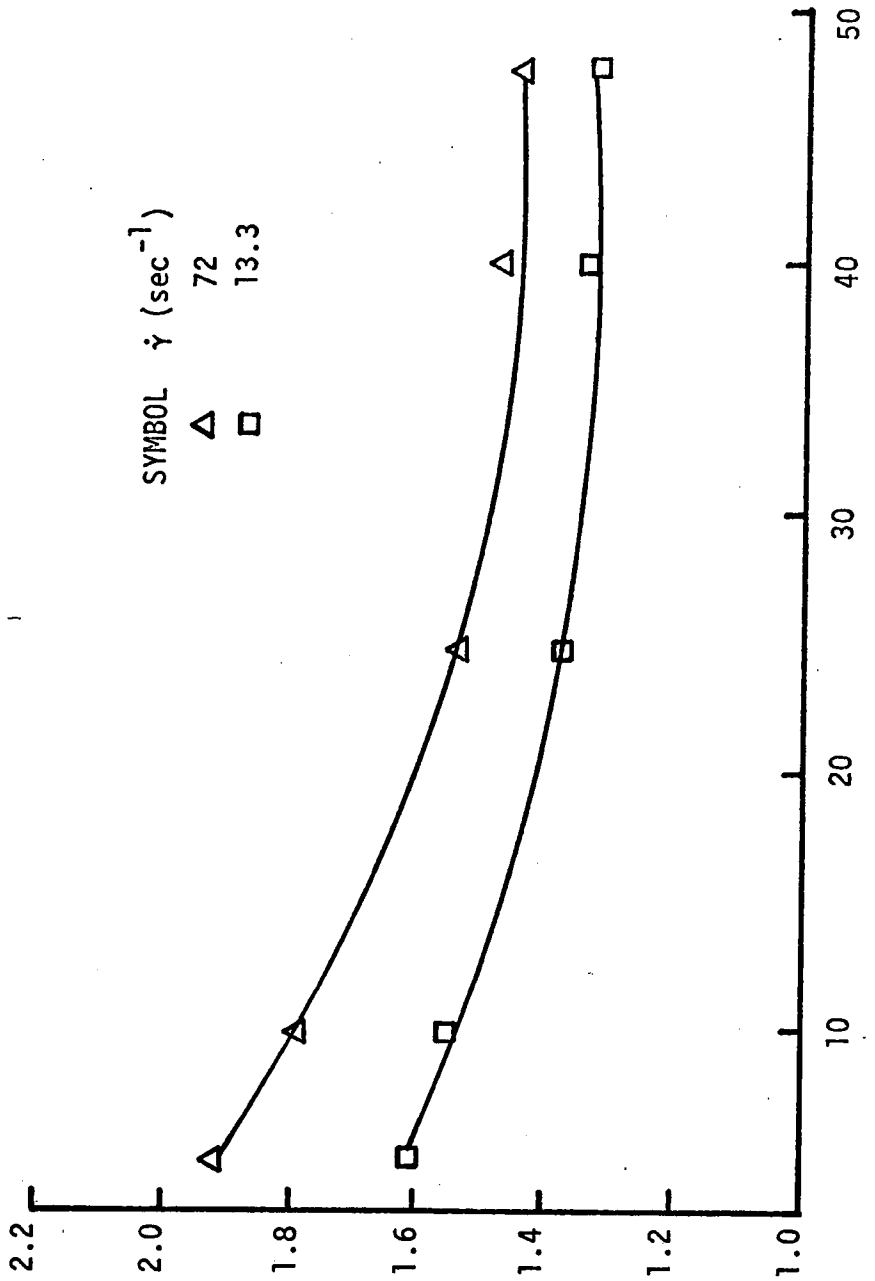

Figure 15. Die Swell of HDPE MI = 5 as a Function of L/D Ratio

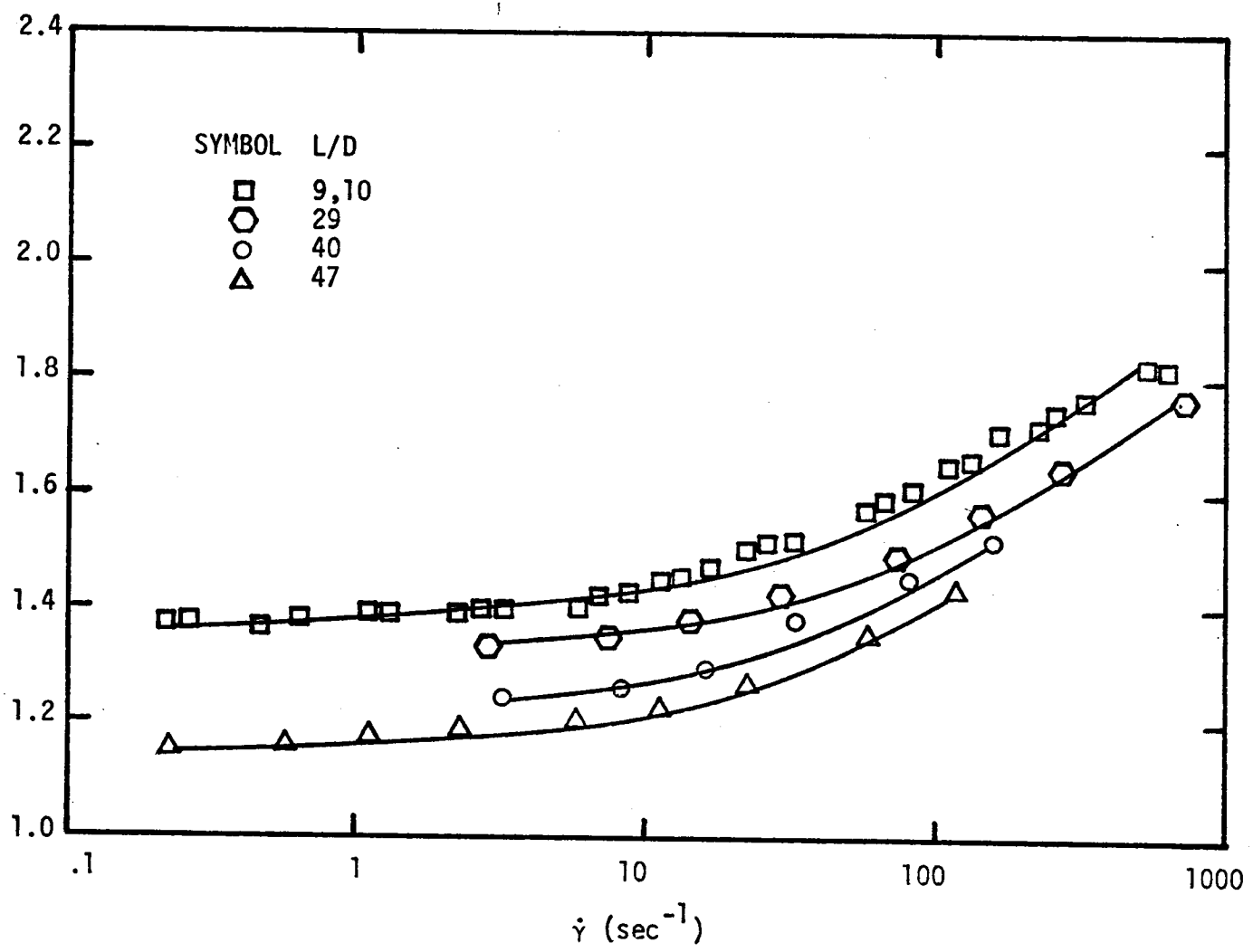

Figure 16. Die Swell of HDPE MI = 0.02 as a Function of Shear Rate

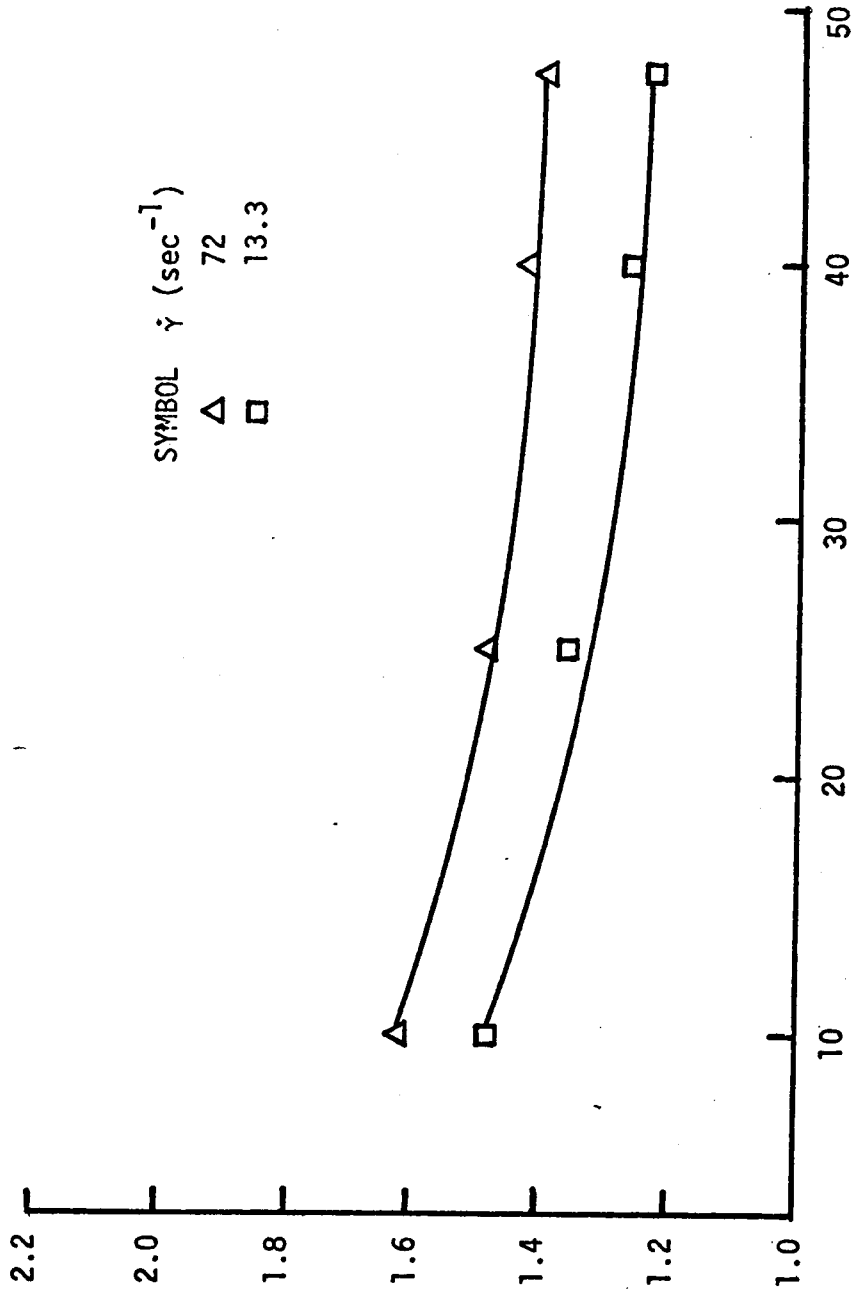

Figure 17. Die Swell of HDPE MI = 0.02 as a Function of L/D Ratio

limit approaching 1.1 at low shear rates, the die swell increased by increasing increments over the range of shear rates from 0.07 to 2 sec^{-1}, at shear rates greater than 2 sec^{-1} the die swell increased by smaller amounts than the previous increase for a change in shear rate. This die swell behavior was observed to be a function of shear rate, independent of the capillary diameter. The effect of increasing the L/D ratio was to decrease the die swell, at constant shear rate. The amount of swell was quite dependent on the L/D ratio. These characteristics are shown in Figures 18 and 19.

Comparison of All Polymers

Comparing the die swell of all polymers for one of the capillaries shows they all approach a lower limit at low shear rates. All the curves of die swell versus shear rate have the same form, except for the low density polyethylene. From shear rates of 1 sec^{-1} to approximately 100 sec^{-1} the LDPE had a consistently higher die swell ratio than the other polymers. This comparison can be made from Figure 20.

Comparing the die swell of the polymers at a constant shear rate, the LDPE shows the largest amount of die swell. The die swell is seen to diminish as the L/D ratio of the capillary increases. The HDPE MI = 5 shows a higher amount of die swell at this shear rate than the other two high density polyethylenes. Generally, the curves for all polymers excluding LDPE cluster together. These observations are seen in Figure 21.

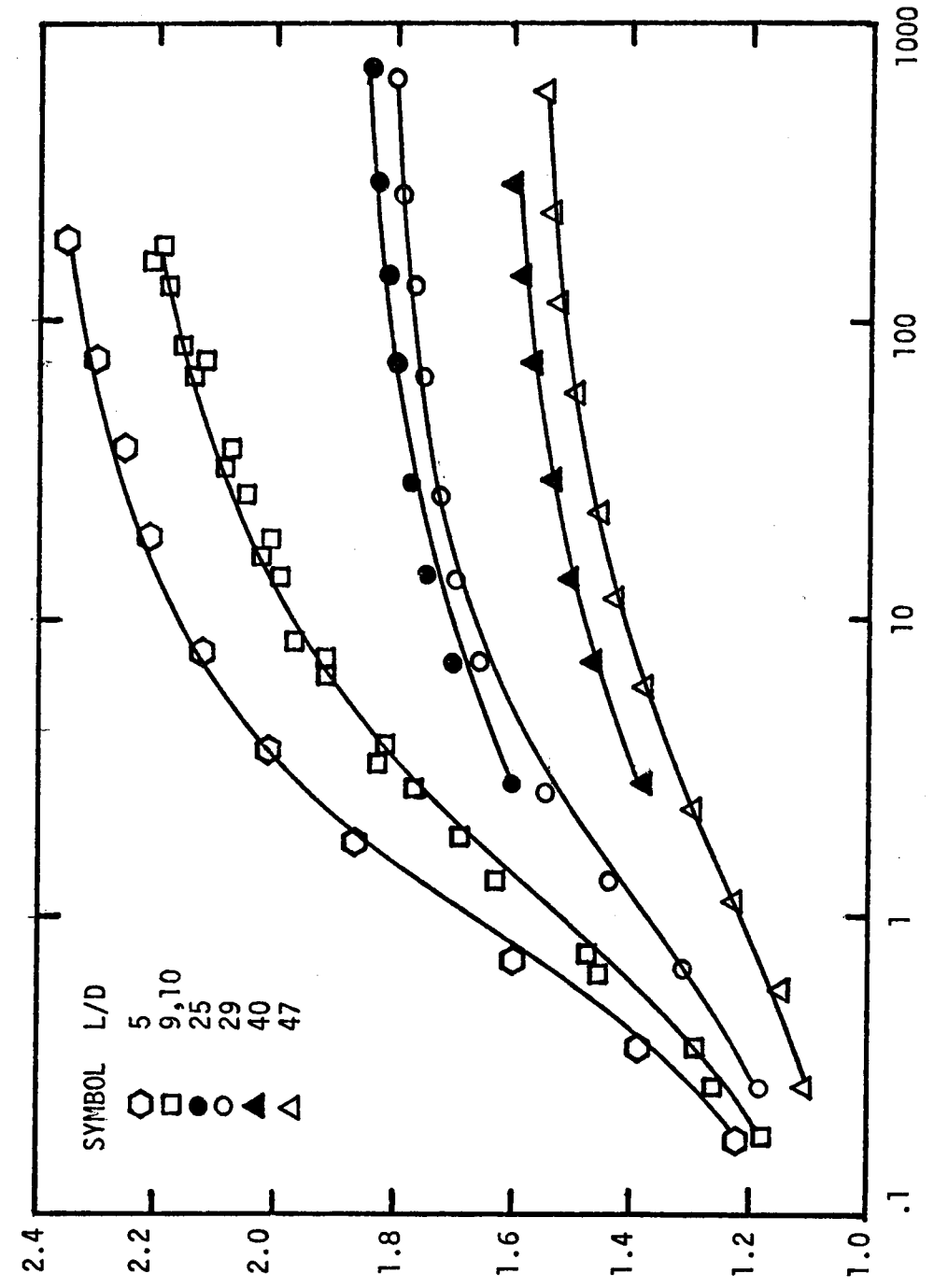

Figure 18. Die Swell of LDPE as a Function of Shear Rate

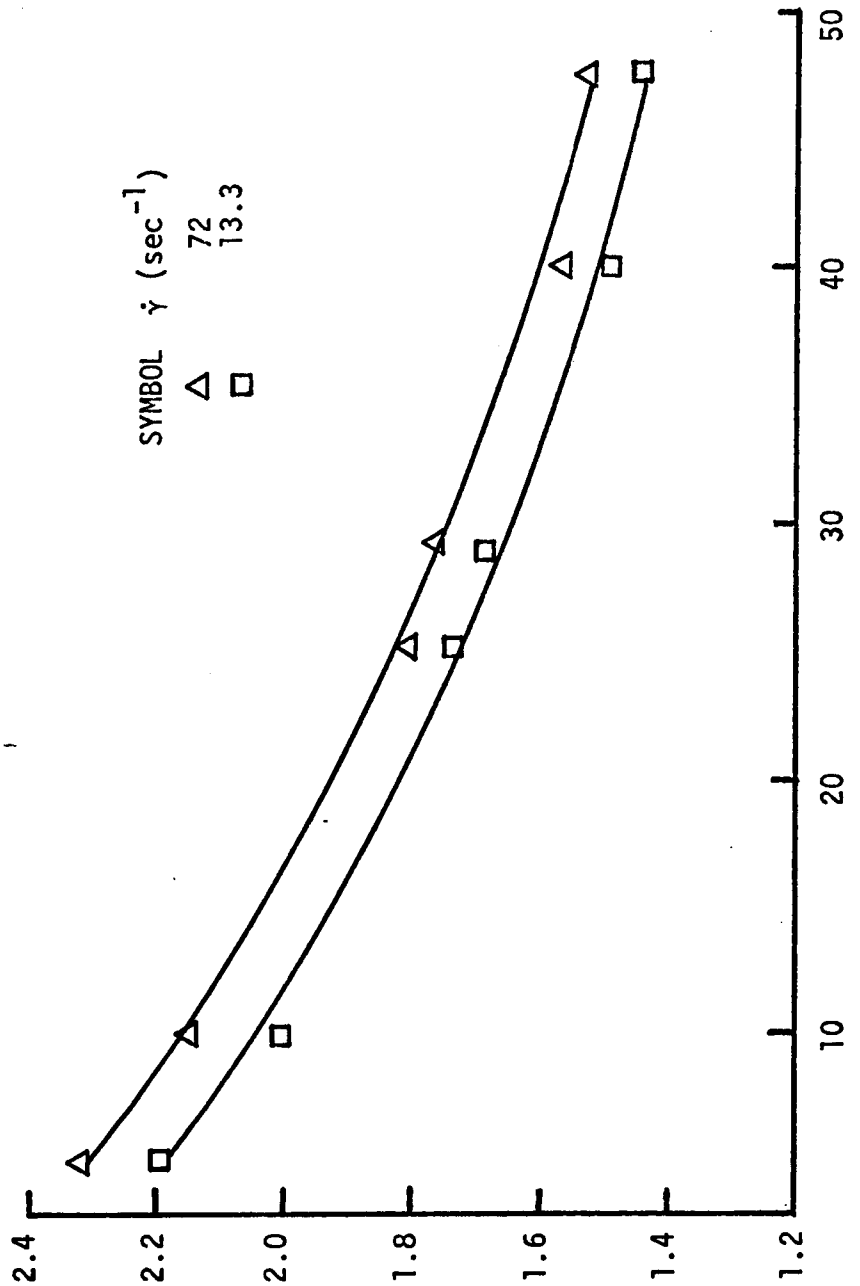

Figure 19. Die Swell of LDPE as a Function of L/D Ratio

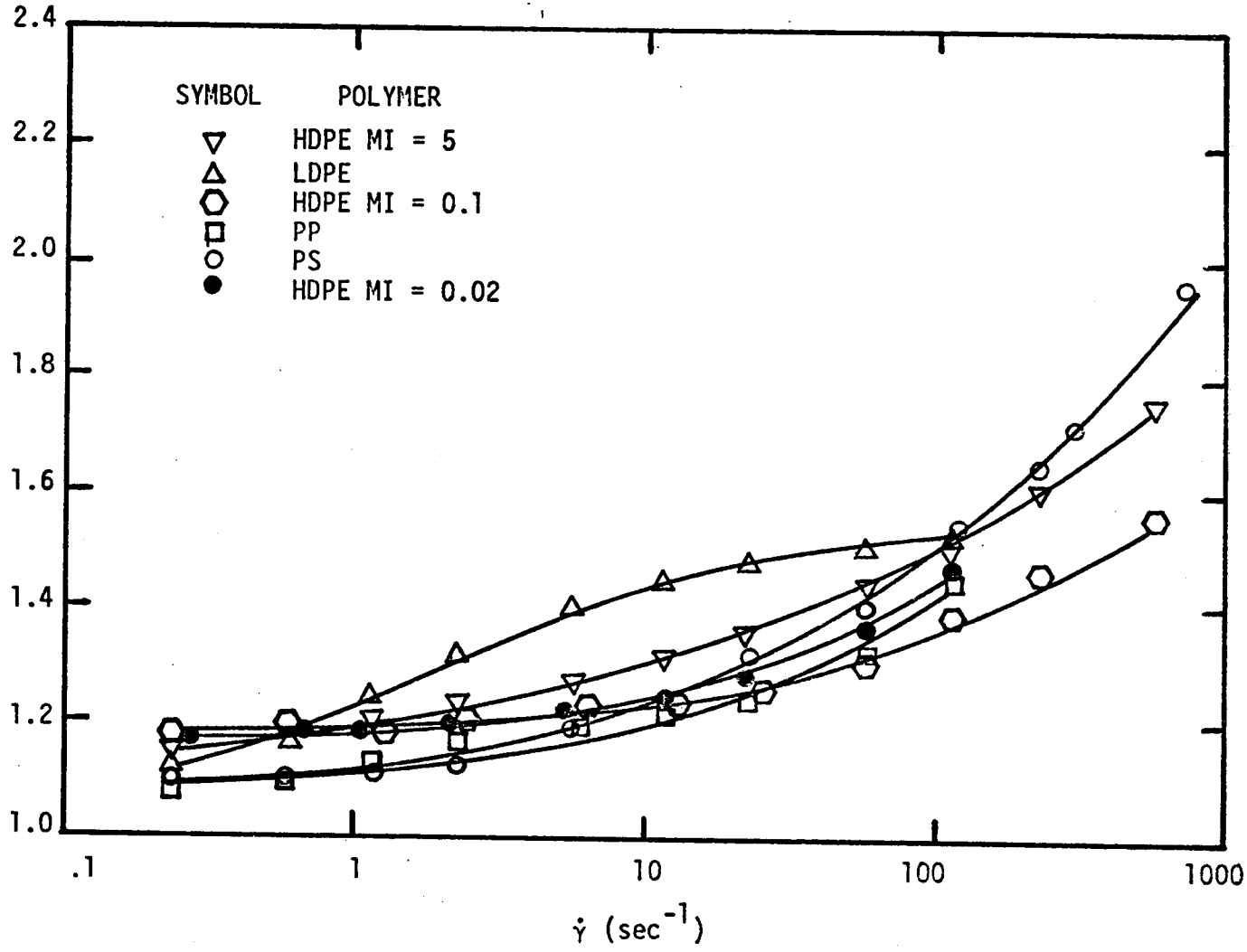

Figure 20. Comparison of Die Swell of Polymer Melts as a Function of Shear Rate, L/D = 48

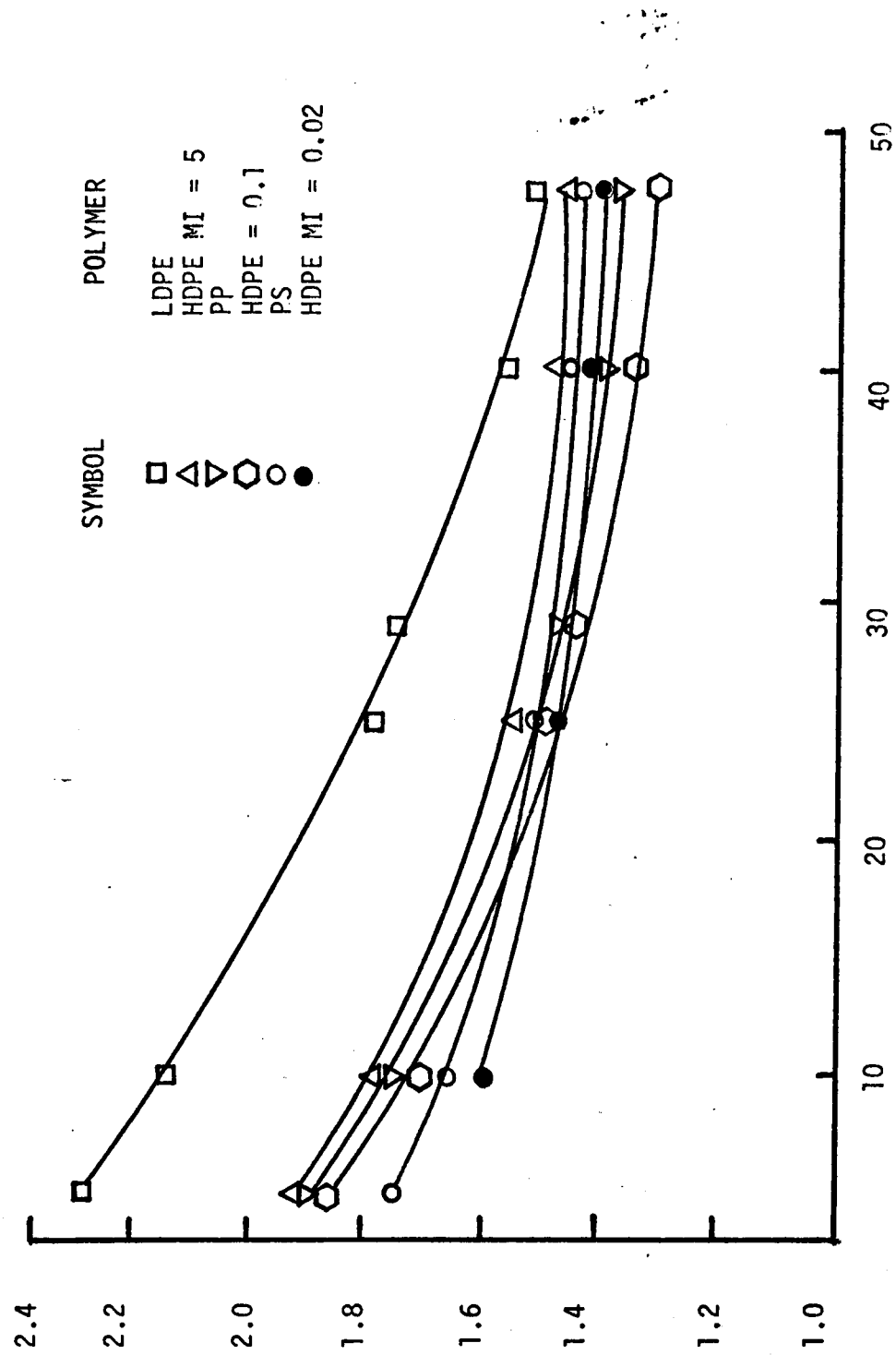

Figure 21. Comparison of Die Swell as a Function of L/D Ratio for Six Polymer Melts

D. ANNEALED EXTRUDATES

Polypropylene

The annealed PP displayed a consistently higher die swell ratio than the unannealed samples. The annealed samples were approximately seven to eight percent larger than unannealed samples at the low shear rates. As the shear rate at which the samples were taken increased, the difference became larger. At 116 sec^{-1}, the shear rate at which the last sample was taken, the annealed samples were almost 15 percent larger than unannealed samples. This is shown in Figure 22.

Polystyrene

The annealed PS samples exhibited behavior similar to that of polypropylene. At low shear rates the annealed samples were two to four percent larger than unannealed samples. At higher shear rates, this difference became more pronounced. At shear rates above 100 sec^{-1} the difference was greater than 25 percent. This is shown in Figure 23.

Low Density Polyethylene

The annealed samples were again larger than unannealed samples. At low shear rates the difference was approximately 16 percent. At higher shear rates, the difference remained in the range of 16 percent. This shows an almost constant amount of swell over the range of shear rates used. This is shown in Figure 24.

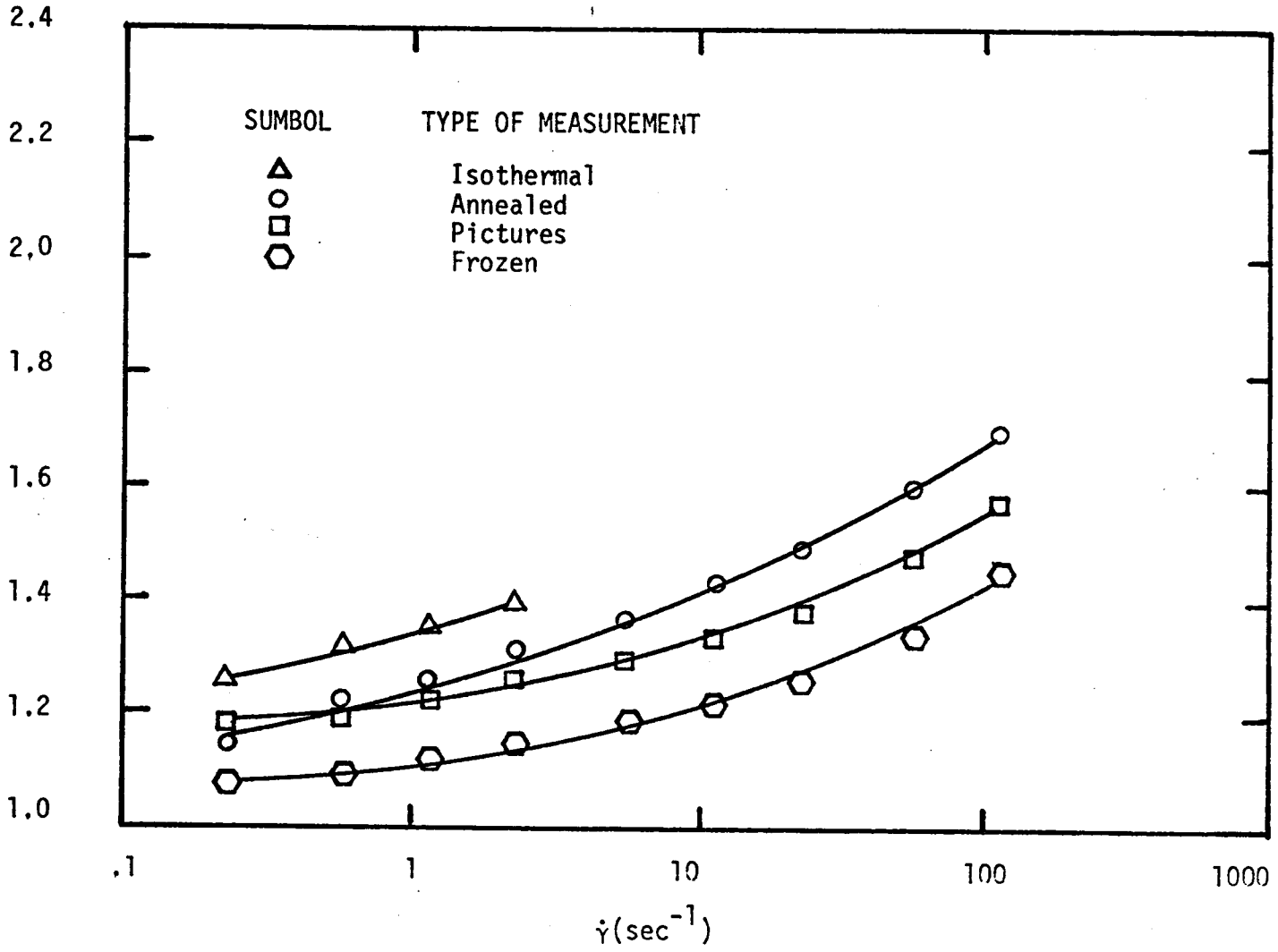

Figure 22. Comparison of Die Swell from Frozen, Annealed, Photography and Isothermal Measurements as a Function of Shear Rate for PP

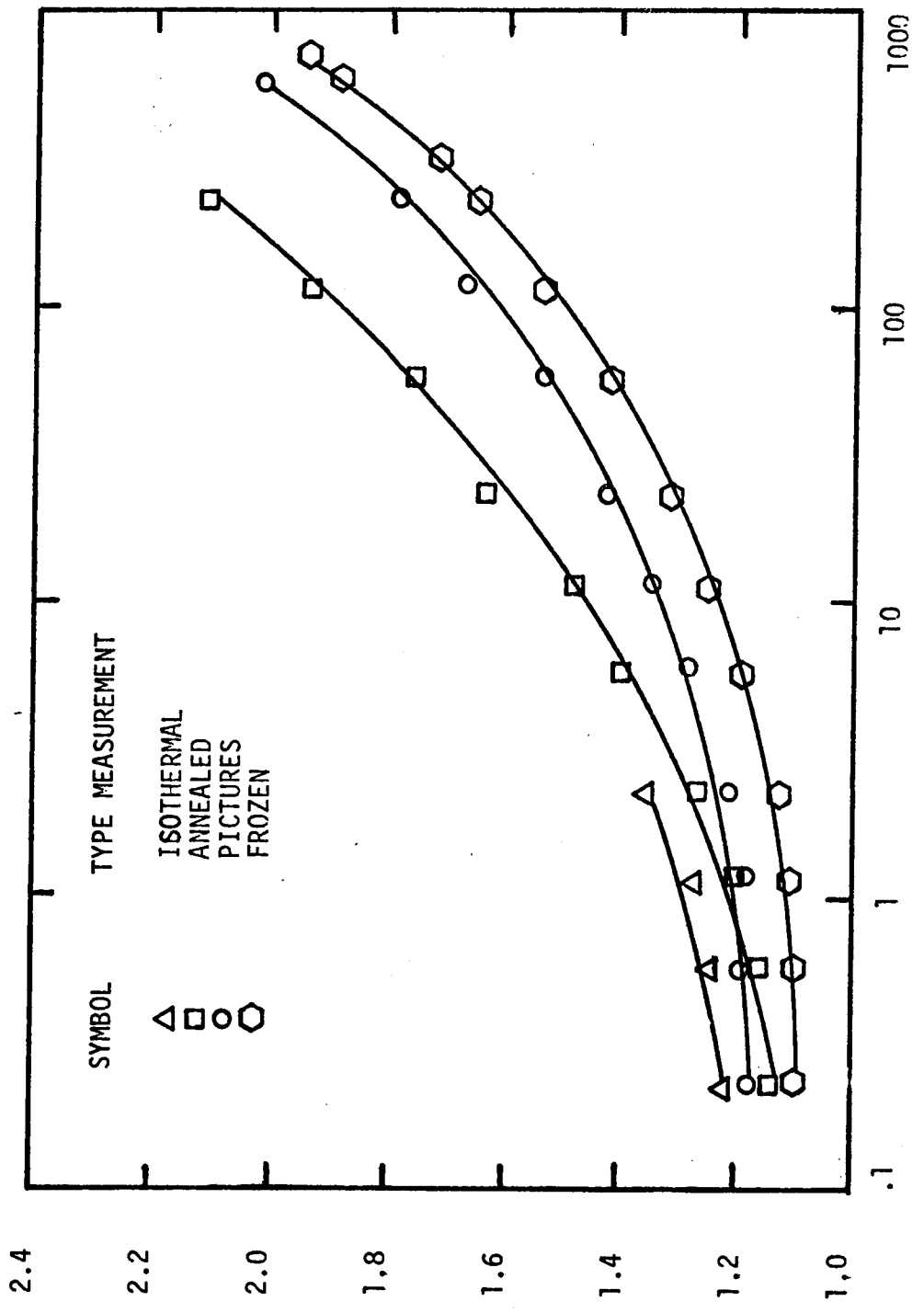

Figure 23. Comparison of Die Swell from Frozen, Annealed, Photographic, and Isothermal Measurements as a Function of Shear Rate for PS, L/D = 48.

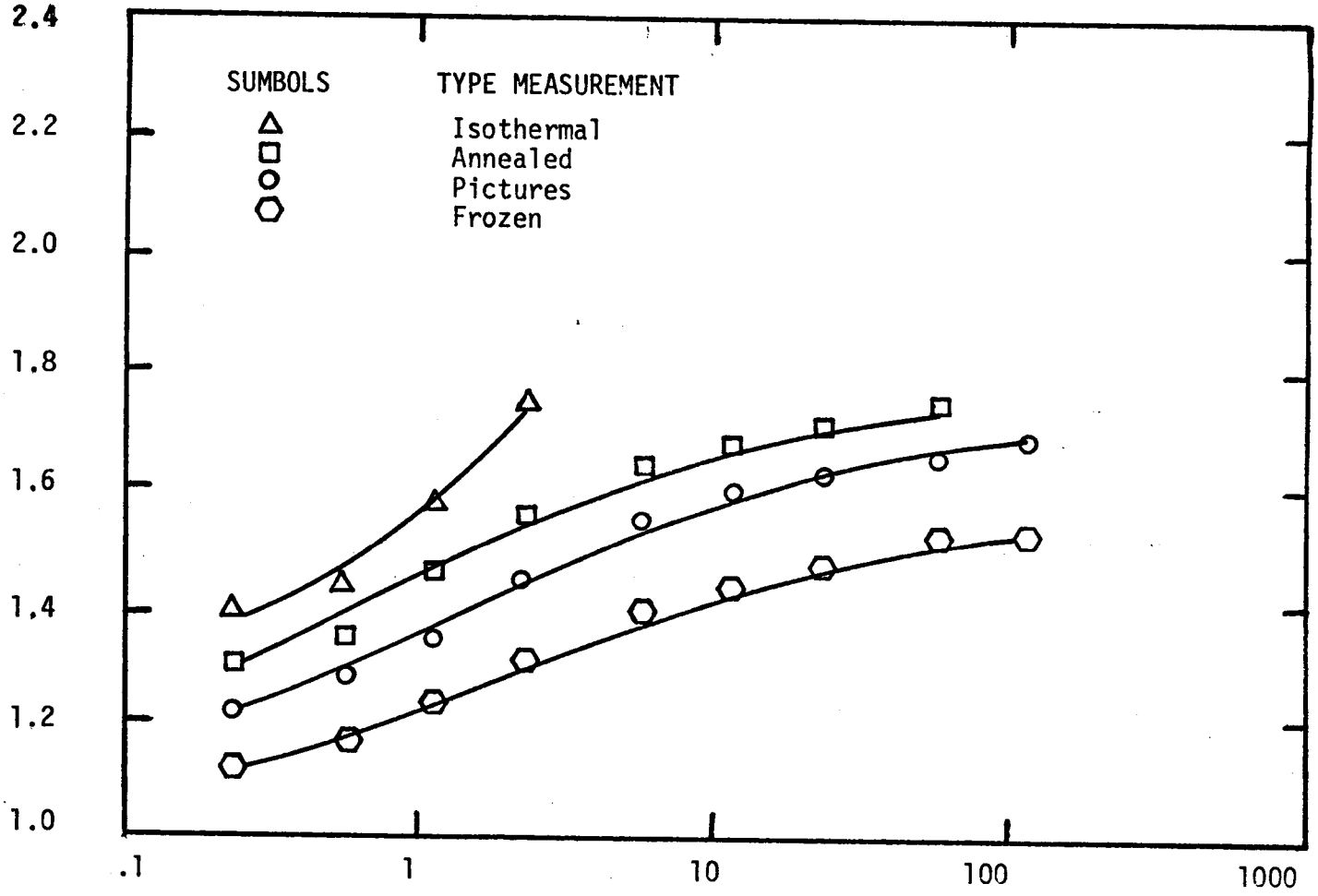

Figure 24. Comparison of Die Swell from Frozen, Annealed, Photographic and Isothermal Measurements as a Function of Shear Rate for LDPE, L/D = 48

High Density Polyethylene

All HDPE samples which were annealed were larger than unannealed samples at their respective shear rates. The HDPE MI = 5, upon annealing, showed an increase in die swell ratio of about 20 percent at low shear rates. At higher shear rates, this difference became slightly greater, increasing to about 25 percent. This change was only slight as compared to the large change in polystyrene at high shear rates. This is shown in Figure 25.

The HDPE MI = 0.1 and HDPE MI = 0.02 displayed a more pronounced change in die swell ratio. At low shear rates the annealed extrudates were greater by almost 21 percent for HDPE MI = 0.02 and 27 percent for HDPE MI = 0.1. As the shear rates were increased the differences between the unannealed samples and the annealed extrudates became greater. At high shear rates, the difference between annealed and unannealed became as large as 37 percent for HDPE MI = 0.02 and 38 percent for HDPE MI = 0.1. The HDPE MI = 0.02 polyethylene showed the greatest change in the annealed samples, going from 21 percent greater at low shear rates to 37 percent greater at high shear rates, These observations can be seen in Figures 26 and 27.

Comparison of All Polymers

Comparison of the die swell ratio of all the annealed extrudates over the range of shear rates used can be seen in Figure 28. Comparing just the annealed values, the HDPE MI = 0.1 and HDPE MI = 0.02 display the largest die swell. The HDPE MI = 0.1 is largest at lower shear rates and HDPE MI = 0.02 is slightly lower, but increases in such a

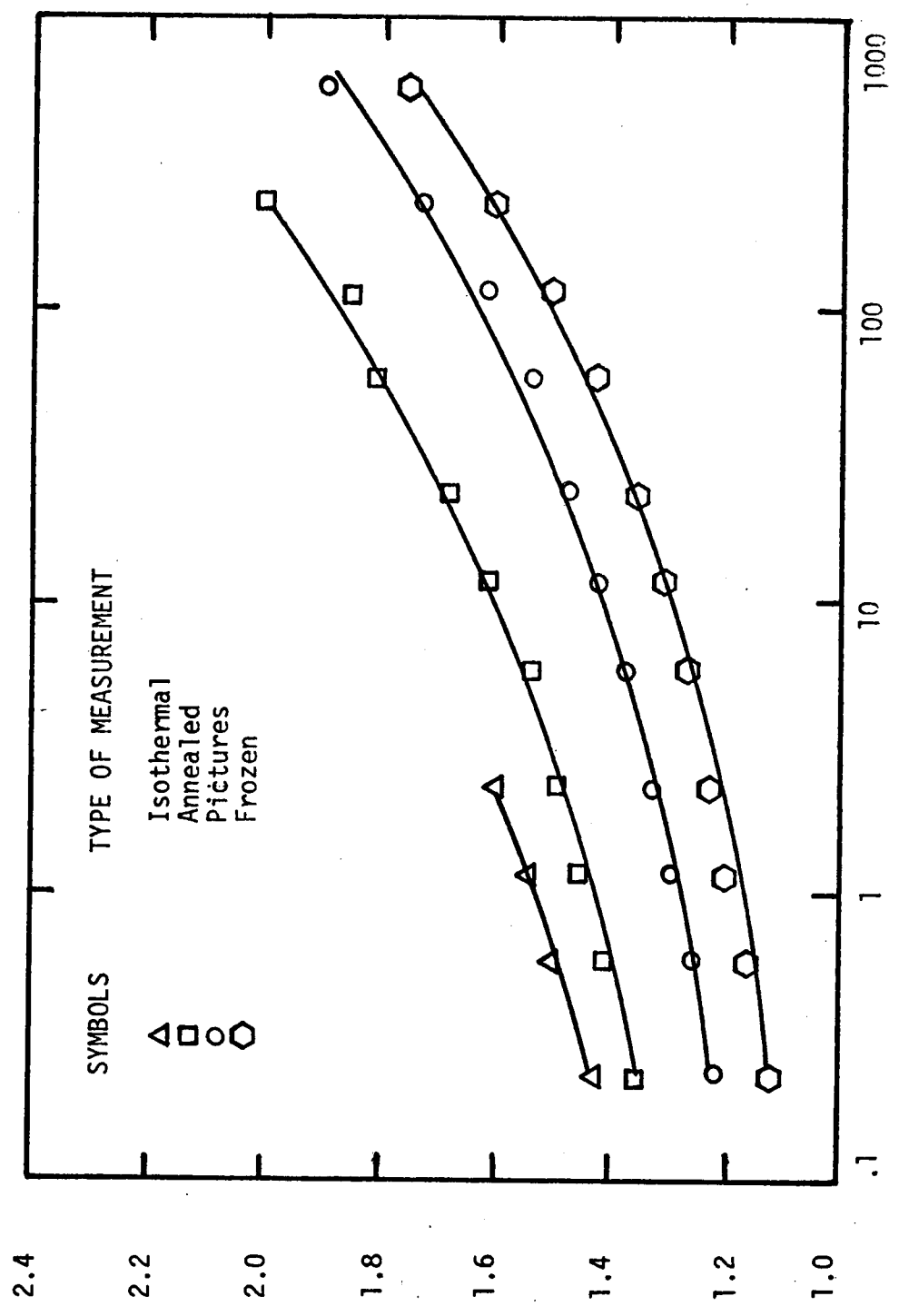

Figure 25. Comparison of Die Swell from Frozen, Annealed, Photographic and Isothermal Measurements as a Function of Shear Rate for HDPE MI = 5, L/D = 48.

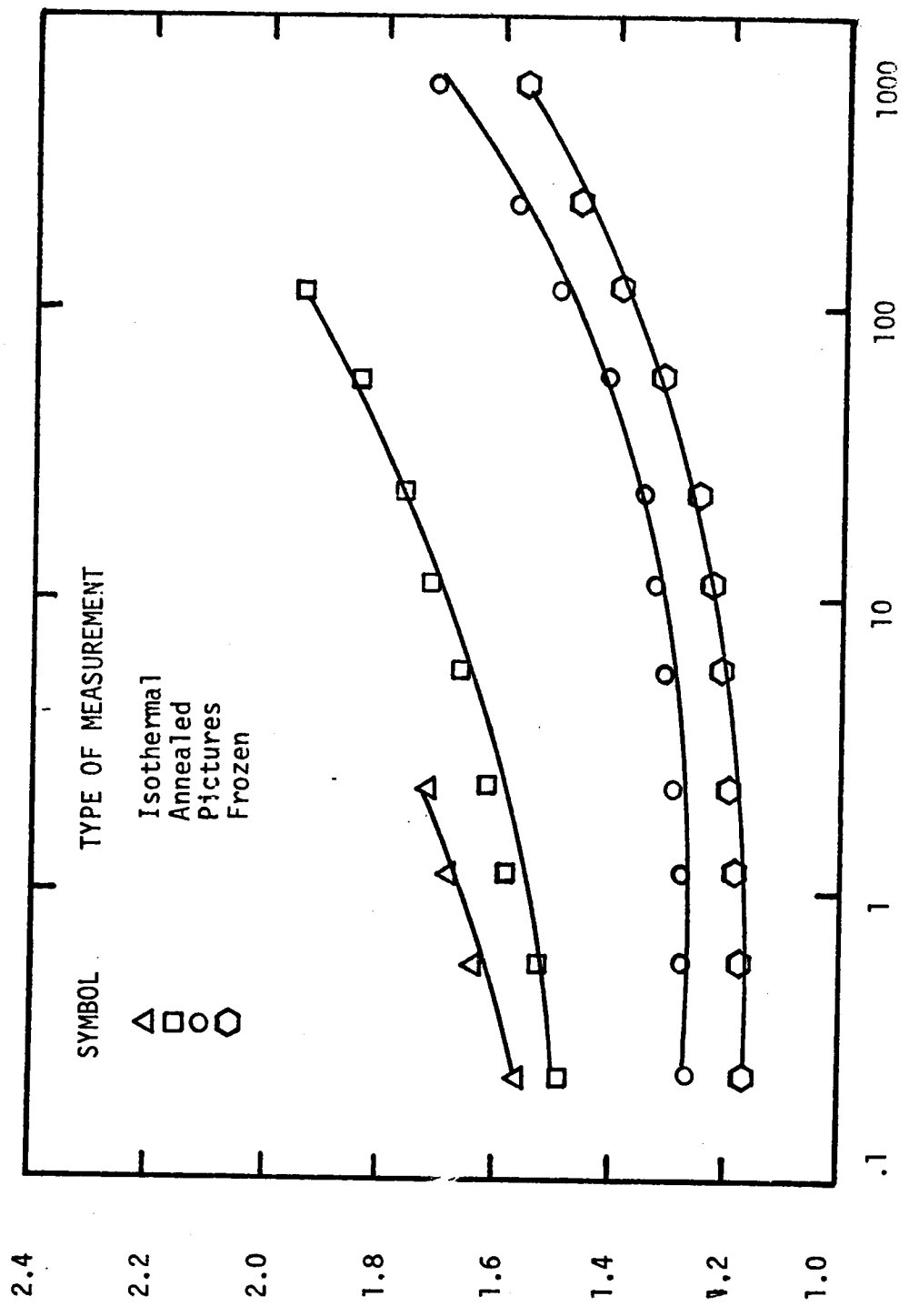

Figure 26. Comparison of Die Swell from Frozen, Annealed, Photographs and Isothermal Measurements as a Function of Shear Rate for HDPE MI = 0.1, L/D = 48.

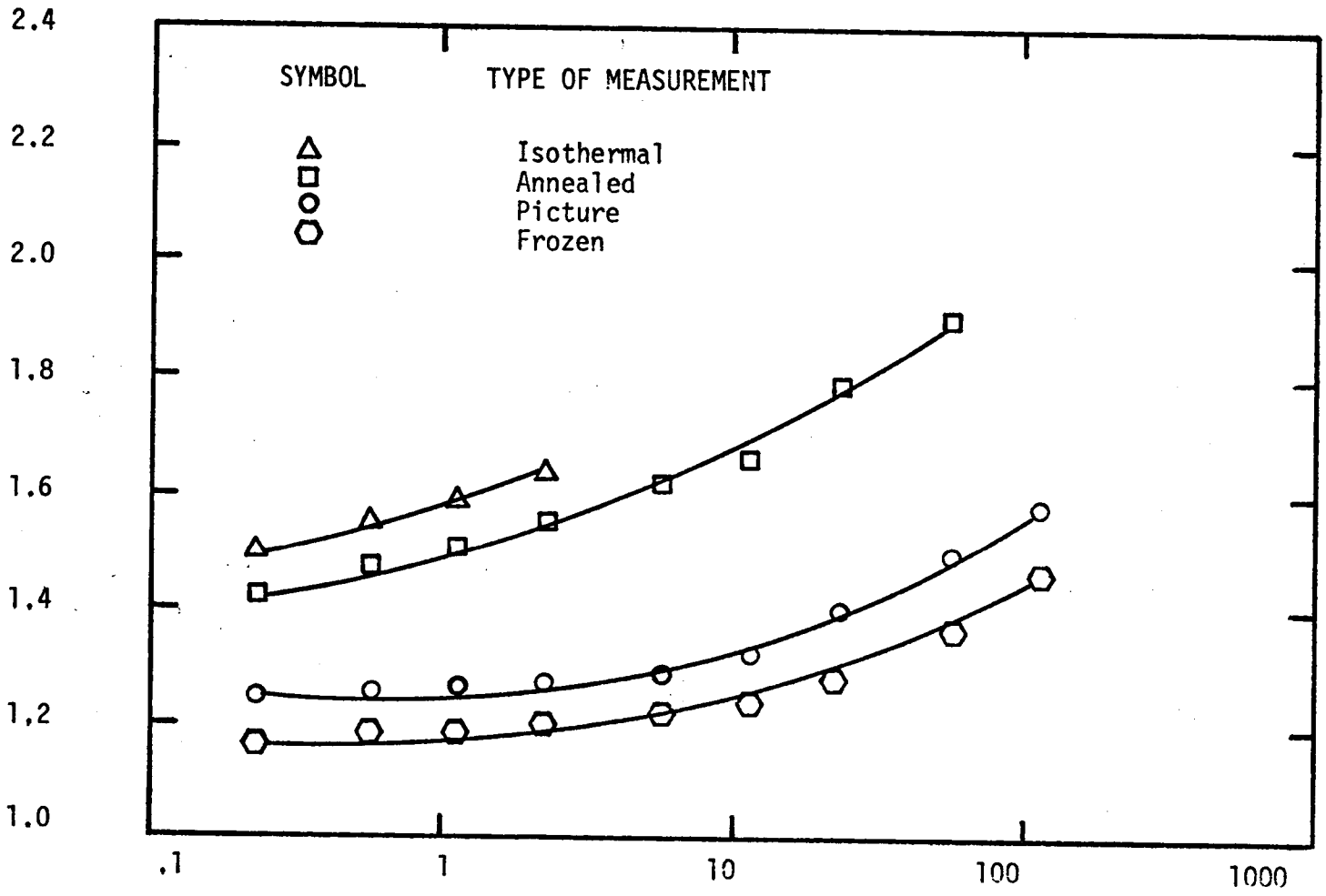

Figure 27. Comparison of Die Swell from Frozen, Annealed, Photographic and Isothermal Measurements as a Function of Shear Rate for HDPE MI = 0.02, L/D = 48

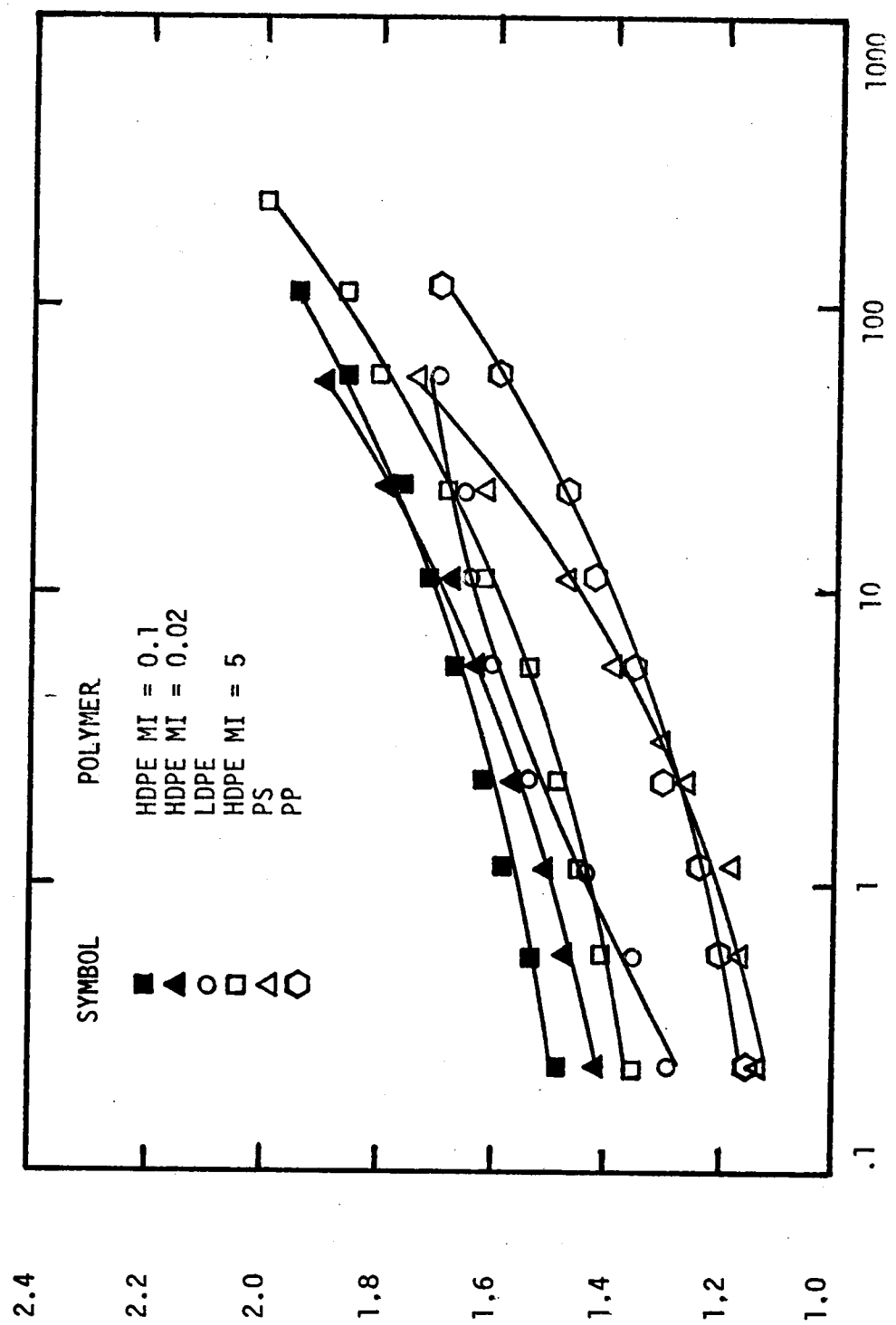

Figure 28. Comparison of Die Swell of the Annealed Extrudates for all Polymer Melts as a Function of Shear Rate, L/D = 48

manner that the swell becomes largest of all polymers above shear rates of 10-20 sec^{-1}. The PP and PS show the lowest swell over most of the range. The LDPE and HDPE MI = 5 show an intermediate amount of swell over most of the range of shear rates when compared with the other polymers.

E. PHOTOGRAPHS

Polypropylene

Photographs of extruded PP as it emerged from the capillary showed an almost constant difference in die swell when compared to the extrudates at that shear rate. The die swell measured from the photographs was consistently seven to nine percent higher than the die swell of the cooled extrudates. This observation was consistent over the entire range of shear rates used. This comparison is seen in Figure 22.

Polystyrene

Again, photographs of extruded PS showed an almost constant difference between the measured die swell and the die swell of the cooled extrudate, similar to polypropylene. The die swell measured from the photographs was five to six percent higher than the die swell measured from the cooled extrudates. This is shown in Figure 23.

Low Density Polyethylene

Die swell measured from the photographs was consistently eight

to nine percent above the die swell measured for the cooled extrudates. This is shown in Figure 24.

High Density Polyethylene

The die swell measured from the photographs was consistently eight to eleven percent above the die swell measured for cooled extrudates for all three of the high density polyethylenes used. This is shown in Figures 25, 26 and 27. The measurements for all three high density polyethylenes were very similar, little difference being noted for the difference in polymers.

Compairson of All Polymers

A comparison of the die swell for all of the polymers used measured from the photographs is shown in Figure 29. All curves except low density polyethylene have similar shapes. The low density polyethylene displays the largest die swell over most of the range of shear rates. This plot resembles very closely the plot of the die swell of the cooled extrudate versus shear rate. The major difference between the two plots is an upward displacement in the die swell measured from photographs as compared to the swell measured from cooled extrudate. This displacement is almost constant for each respective polymer over the range of shear rates used. It would appear that the photographs measure the thermal expansion of the polymers when they are raised from ambient temperature to 180°C.

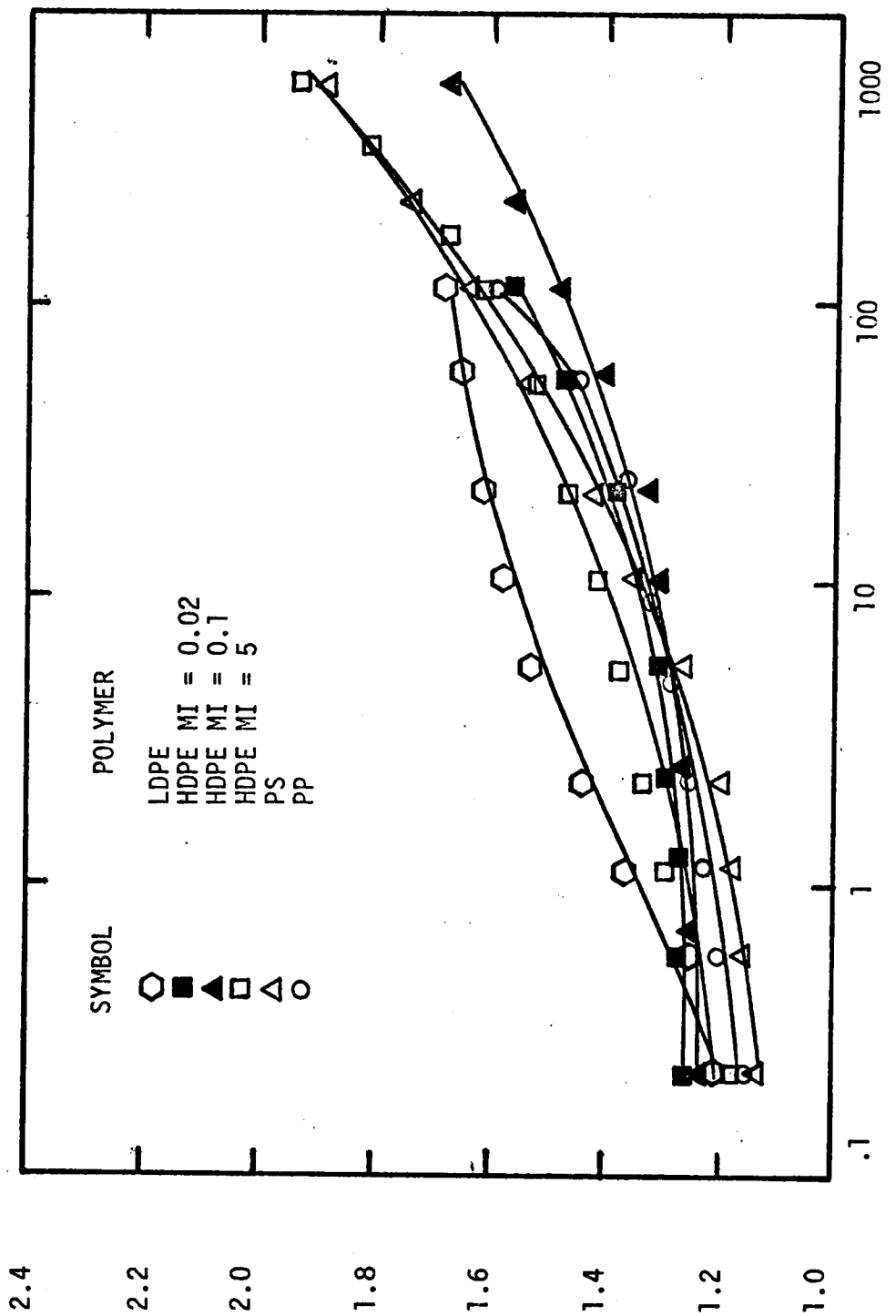

Figure 29. Comparison of Die Swell Measured from Photograph for Six Polymer Melts as a Function of Shear Rate, L/D = 48

F. ISOTHERMAL EXTRUSION

Polypropylene

The results of isothermally extruding PP and measuring the die swell from photographs are shown in Figure 22. At the low shear rates used, the isothermal swell was slightly greater than the annealed die swell, the difference being in the range of eight percent. This difference was almost constant over the range of shear rates used. The shear rate range was limited to very low shear rates because of the method used.

Polystyrene

The isothermal die swell for PS is shown in Figure 23. At the low shear rates, the isothermal die swell was slightly greater than the annealed die swell, the difference being in the range of five to six percent.

Low Density Polyethylene

The isothermal die swell was somewhat larger than the die swell of the annealed extrudates. This difference appeared to be in the range of seven to eleven percent. This is shown in Figure 24.

High Density Polyethylene

For all three high density polyethylenes, the isothermal die swell was larger than the annealed die swell. The isothermal die swell was in the range of five to seven percent larger than the annealed die swell. All three polyethylenes showed isothermal die swell

larger than annealed swell by approximately the same amount. These results are shown in Figures 25, 26 and 27.

Comparison of All Polymers

The die swell measured isothermally was higher than the die swell measured by any of the other methods. The method used limited the die swell measurements to low shear rates. The HDPE MI = 0.1 exhibited the highest value of isothermal die swell over most of the range of shear rates. The PS had the lowest isothermal die swell in this range. These observations are seen in Figure 30.

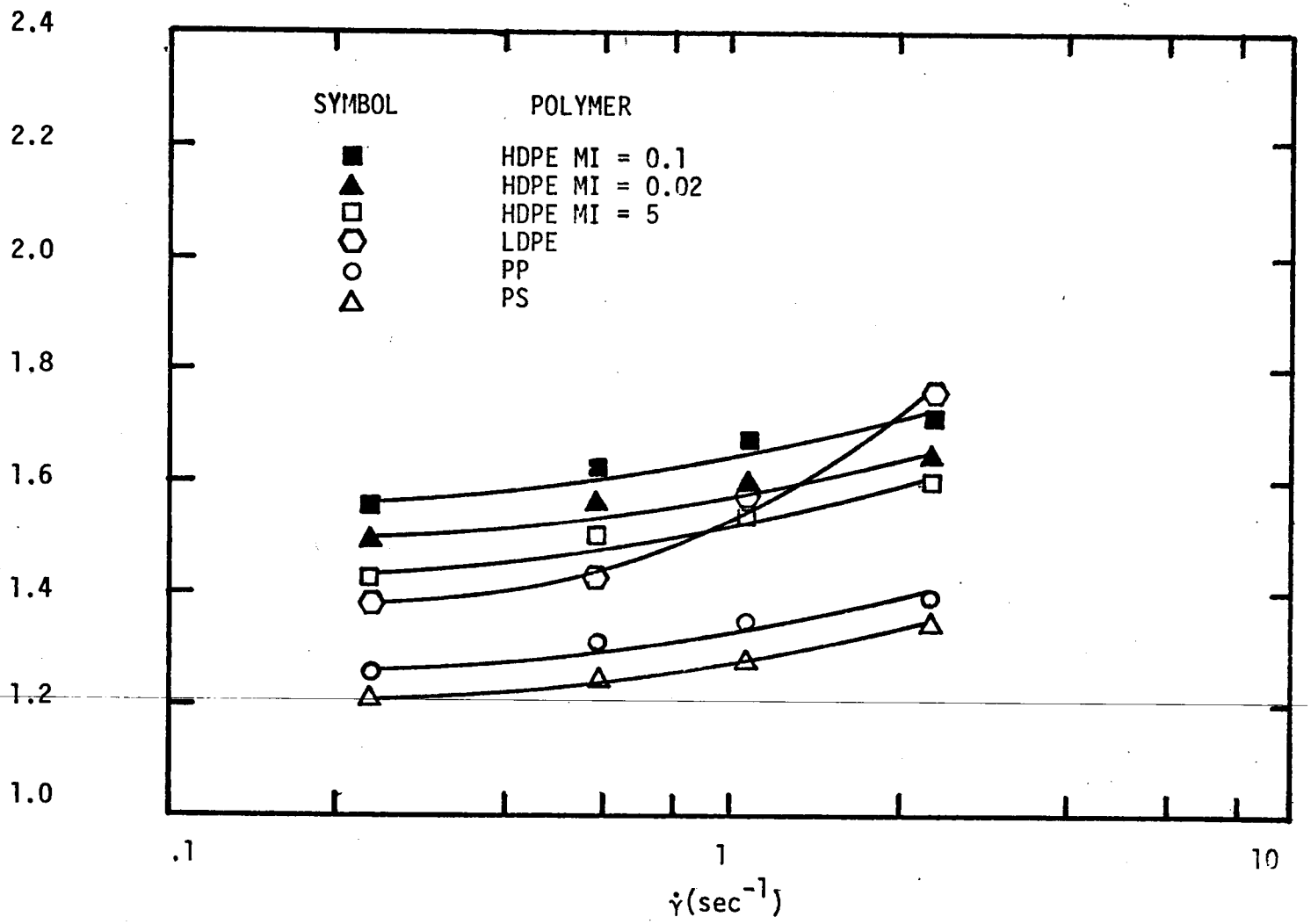

Figure 30. Comparison of Die Swell Measured Isothermally for Six Polymer Melts as a Function of Shear Rate, L/D = 48

CHAPTER V

INTERPRETATION

A. INTERPRETATION OF DIE SWELL

If polymer melts are viscoelastic fluids, then the method of fluid dynamics may be used to interpret the experimental data. The arguments of this section were developed with Professor J. L. White (78). If we assume a constitutive equation for the polymer melts, combine with the equation of motion and place in dimensionless form, then the die swell may be shown to be expressible in the form:

$$\frac{D_j}{D} = f(\lambda_{CH}\frac{V}{D}, \frac{DV}{\eta}, \frac{\gamma}{\eta V}, \frac{L}{D}, \text{"shape of functional"})$$

The Reynolds number effect for polymer melts is small. High viscosities should make $\gamma/\eta V$ small.

All of the theories of die swell are primitive, but their level of crudeness varies. The least primitive is that of Tanner (66). It argues that

$$\frac{D_j}{D} = g(\lambda_{CH}\frac{V}{D}, \frac{L}{D} \to \infty, \text{only}) = [1 + \frac{1}{2}\lambda_1^2 \dot{\gamma}_w^2]^{1/6} \qquad (31)$$

where

$$\lambda_{CH}\frac{V}{D} = C\frac{(N_1)_w}{(\tau_{12})_w} = C\,2\,J_e(\tau_{12})_w$$

$$\lambda_{CH} = 2\ C\ J_e \frac{(\tau_{12})_w}{(V/D)} = \frac{C}{8}\ J_e\ n(\dot{\gamma})$$

The unique dependence of D_j/D means that a specific shape was assumed for the functional. This may be seen to be the case. Tanner takes

$$F(\text{deformation}) = \int_{s=-\infty}^{s=t} \frac{G}{\lambda}\ e^{-s/\lambda}\ \underset{\sim}{C}^{-1}\ ds \qquad (32)$$

Consider the alternative theory (78)

$$F(\text{deformation}) = \int_{s=-\infty}^{s=t} \frac{G}{\lambda}\ e^{-z/\lambda}\ \underset{\sim}{C}\ dz \qquad (33)$$

This will result in a different D_j/D function.

We can use the constitutive equation

$$\tau = -p\delta_{ij} + \int_{-\infty}^{t} a_1(t-s)\ \underset{\sim}{C}^{-1}_{ij} - a_2(t-s)\ \underset{\sim}{C}_{ij}]\ ds \qquad (34)$$

where

$$a_1(t) = G_1/\lambda\ e^{-t/\lambda}$$

$$a_2(t) = G_2/\lambda\ e^{-t/\lambda}$$

For simple shear we have

$$\underset{\sim}{C}^{-1} = \begin{vmatrix} 1 + \dot{\gamma}^2 z^2 & \dot{\gamma}z & 0 \\ \dot{\gamma}z & 1 & 0 \\ 0 & 0 & 1 \end{vmatrix}$$

and

$$\underset{\sim}{C} = \begin{vmatrix} 1 & -\dot{\gamma}z & 0 \\ -\dot{\gamma}z & 1 + \dot{\gamma}^2 z^2 & 0 \\ 0 & 0 & 1 \end{vmatrix} \tag{35}$$

Looking at the limit of $t \to \infty$ we have

$$G^*(\underset{\sim}{C}^{-1})^* - H^*(\underset{\sim}{C})^* = \begin{vmatrix} \mu_{10} + \mu_{12}\dot{\gamma}^2 & \mu_{11}\dot{\gamma} & 0 \\ \mu_{11}\dot{\gamma} & \mu_{11} & 0 \\ 0 & 0 & \mu_{10} \end{vmatrix}$$

$$- \begin{vmatrix} \mu_{20} & \mu_{21}\dot{\gamma} & \\ -\mu_{21} & \mu_{22}+\mu_{22}\dot{\gamma}^2 & 0 \\ 0 & 0 & \mu_{20} \end{vmatrix} \tag{36}$$

where

$$\mu_{10} = \int_0^\infty a_1(z)\, dz \qquad \mu_{20} = \int_0^\infty a_2(z)\, dz$$

$$\mu_{11} = \int_0^\infty z a_1(z)\, dz \qquad \mu_{21} = \int_0^\infty z a_2(z)\, dz$$

$$\mu_{12} = \int_0^\infty z^2 a_1(z)\, dz \qquad \mu_{22} = \int_0^\infty z^2 a_2(z)\, dz$$

We can proceed by setting $G_1 = 0$ and $\det(C_{ij}) = 1$. This gives

$$H^{*3} = (\mu_{20} + \mu_{22}\,\dot{\gamma}^2)\,\mu_{20}^2 - (\mu_{21}\,\dot{\gamma})^2\,\mu_{20} \tag{37}$$

$$H^{*} = [\mu_{20}^3 + \mu_{20}^2\,\mu_{22}\,\dot{\gamma}^2 - \mu_{21}^2\,\dot{\gamma}^2\,\mu_{20}]^{1/3} \tag{38}$$

$$H^{*} = \mu_{20}\left[1 + \frac{\mu_{22}}{\mu_{20}}\,\dot{\gamma}^2 - \frac{\mu_{21}^2}{\mu_{20}^2}\,\dot{\gamma}^2\right]^{1/3} \tag{39}$$

Thus

$$\underset{\sim}{(C)}^{*} = \frac{1}{\mu_{22}\left[1 + \left(\frac{\mu_{22}}{\mu_{20}} - \frac{\mu_{21}^2}{\mu_{20}^2}\right)\dot{\gamma}^2\right]^{1/3}} \begin{vmatrix} \mu_{20} & -\mu_{21}\dot{\gamma} & 0 \\ -\mu_{21}\dot{\gamma} & \mu_{20}+\mu_{22}\dot{\gamma}^2 & 0 \\ 0 & 0 & \mu_{20} \end{vmatrix} \tag{40}$$

For a Cauchy fluid, the form of

$$\underset{\sim}{(C)}^{*}_{ab} = \frac{\partial \bar{x}^1\,(t)}{\partial \bar{x}^a\,(t+\delta t)} \quad \frac{\partial \bar{x}^1\,(t)}{\partial \bar{x}^b\,(t+\delta t)} \tag{41}$$

$$x_1(t_1 + \delta t_1) = \frac{1}{\alpha}\,x_1(t_1) + f(x_2(t_1))$$

$$x_2(t_1 + \delta t_1) = \alpha^2\,x_2(t_1)$$

$$x_3(t_1 + \delta t_1) = \frac{1}{\alpha}\,x_3(t_1)$$

Then

$$\underset{\sim}{C}^* = \begin{vmatrix} \frac{1}{\alpha^2} & \frac{1}{\alpha} f' & 0 \\ \frac{1}{\alpha} f' & f'^2 + \alpha^4 & 0 \\ 0 & 0 & \frac{1}{\alpha^2} \end{vmatrix} \partial \bar{x} \tag{42}$$

Equating components yields,

$$\frac{1}{\alpha^2} = \frac{1}{[1 + (\frac{\mu_{22}}{\mu_{20}} - \frac{\mu_{21}^2}{\mu_{22}^2}) \dot{\gamma}^2]^{1/3}} \tag{43}$$

$$f'^2 + \alpha^4 = \frac{1 + \frac{\mu_{22}}{\mu_{20}} \dot{\gamma}^2}{[1 + (\frac{\mu_{22}}{\mu_{20}} - \frac{\mu_{21}^2}{\mu_{20}^2}) \dot{\gamma}^2]^{1/3}} \tag{44}$$

$$\frac{1}{\alpha} f' = \frac{-\mu_{21}\dot{\gamma}}{\mu_{20} [1 + (\frac{\mu_{22}}{\mu_{20}} - \frac{\mu_{21}^2}{\mu_{20}^2}) \dot{\gamma}^2]^{1/3}} \tag{45}$$

Thus it would appear

$$\alpha^2 = \frac{\ell_2 (t_1 + \delta t_1)}{\ell_2(t_1)} = [1 + (\frac{\mu_{22}}{\mu_{20}} - \frac{\mu_{21}^2}{\mu_{20}^2}) \dot{\gamma}^2]^{1/3} \tag{46}$$

Since $\mu_{20} = G_2$, $\mu_{21} = G_2\lambda$, $\mu_{22} = 2G_2\lambda$, we obtain

$$\frac{\ell_2(t_1 + \delta t_1)}{\ell_2(t_1)} = [1 + \lambda_2^2 \dot{\gamma}^2]^{1/3} \tag{47}$$

The above result is for unconstrained recovery from a simple shear flow. The problem of die swell from a slit die or a capillary tube is more complex because of the distribution of shear rates. In a capillary tube the velocity field has the form

$$U = 2V [1 - (\frac{r}{R})^2] \tag{48}$$

with a shear rate varying radially according to

$$\dot{\gamma} = (- \frac{dU}{dr}) = \frac{4V}{R} (\frac{r}{R}) \tag{49}$$

To obtain the die swell, we must somehow average the recovery perpendicular to the direction of flow across the tube. If we presume that the recovery in the direction of flow may vary with position in such a way that all of the stresses are relieved at each point we have

Lodge fluid ($G_2 = 0$)

$$\frac{D_j}{D} = \int_0^1 [1 + \lambda_1^2 \dot{\gamma}^2]^{1/6} d(\frac{r}{R}) \tag{50}$$

Cauchy tensor fluid ($G_1 = 0$)

$$\frac{D_j}{D} = \int_0^1 [1 + \lambda_2^2 \dot{\gamma}^2]^{1/3} d(\frac{r}{R}) \tag{51}$$

In Tanner's approach, he presumes that the recovery in the direction of flow must be the same for each element but that the integral of the tensile stress across the radius must be zero. This leads to Lodge fluid ($G_2 = 0$) - Tanner approximation

$$\frac{D_j}{D} = \left[1 + \frac{1}{2}\ \lambda_1^2\ \dot{\gamma}_w^{\ 2}\ \right]^{1/6} \tag{52}$$

Cauchy fluid ($G_1 = 0$)

$$\frac{D_j}{D} = \left[1 + \frac{1}{2}\ \lambda_2\ \dot{\gamma}_w^2\right]^{1/3} \tag{53}$$

Equations 50 and 51 can be integrated using a digital computer and the result shown in Figure 31 is a function of $N_1 w/(\tau_{12})_w$. Also shown are the results of Tanner. The response of an actual fluid will differ somewhat and be more complicated, since the character of the functional will be different for each melt, so may the $\frac{D_j}{D} - \lambda\frac{V}{D}$ function. Of course, with a polymer family such as polystyrenes or polyethylenes, the behavior may be similar.

B. CORRELATION OF DIE SWELL AND FLOW RATE

If the preceding argument is proper, $\frac{D_j}{D}$ should depend not on the flow rate, Q, or the velocity, V_1, but on a shear rate such as Q/D^3 or V/D. Figure 32 shows the die swell of "frozen" extrudates of a high density polyethylene melt as a function of flow rate for dies of approximately the same L/D ratios. There is a significant

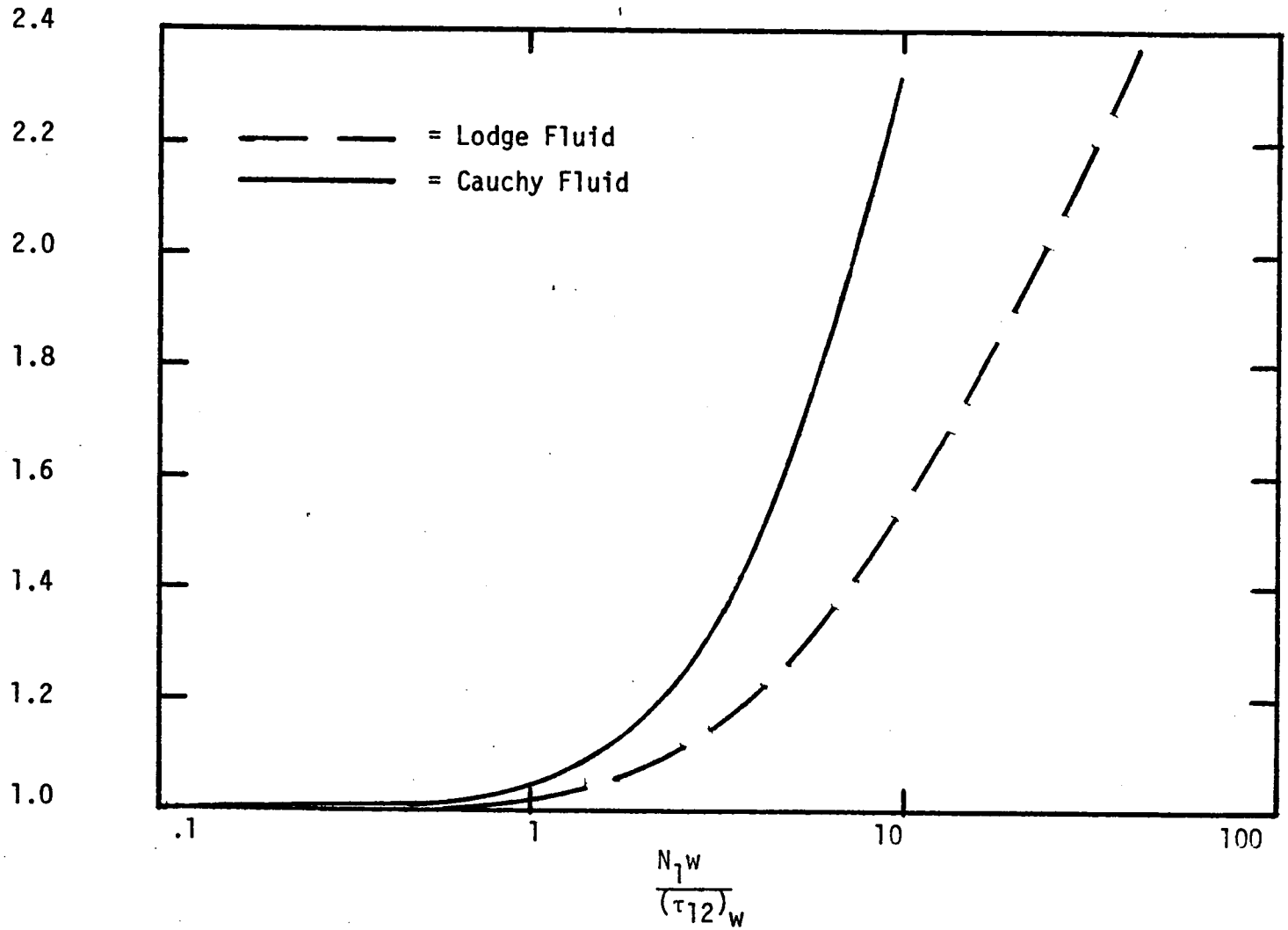

Figure 31. Die Swell as Predicted for a Lodge Fluid and a Cauchy Fluid as a Function of $\frac{N_1 W}{(\tau_{12})_W}$

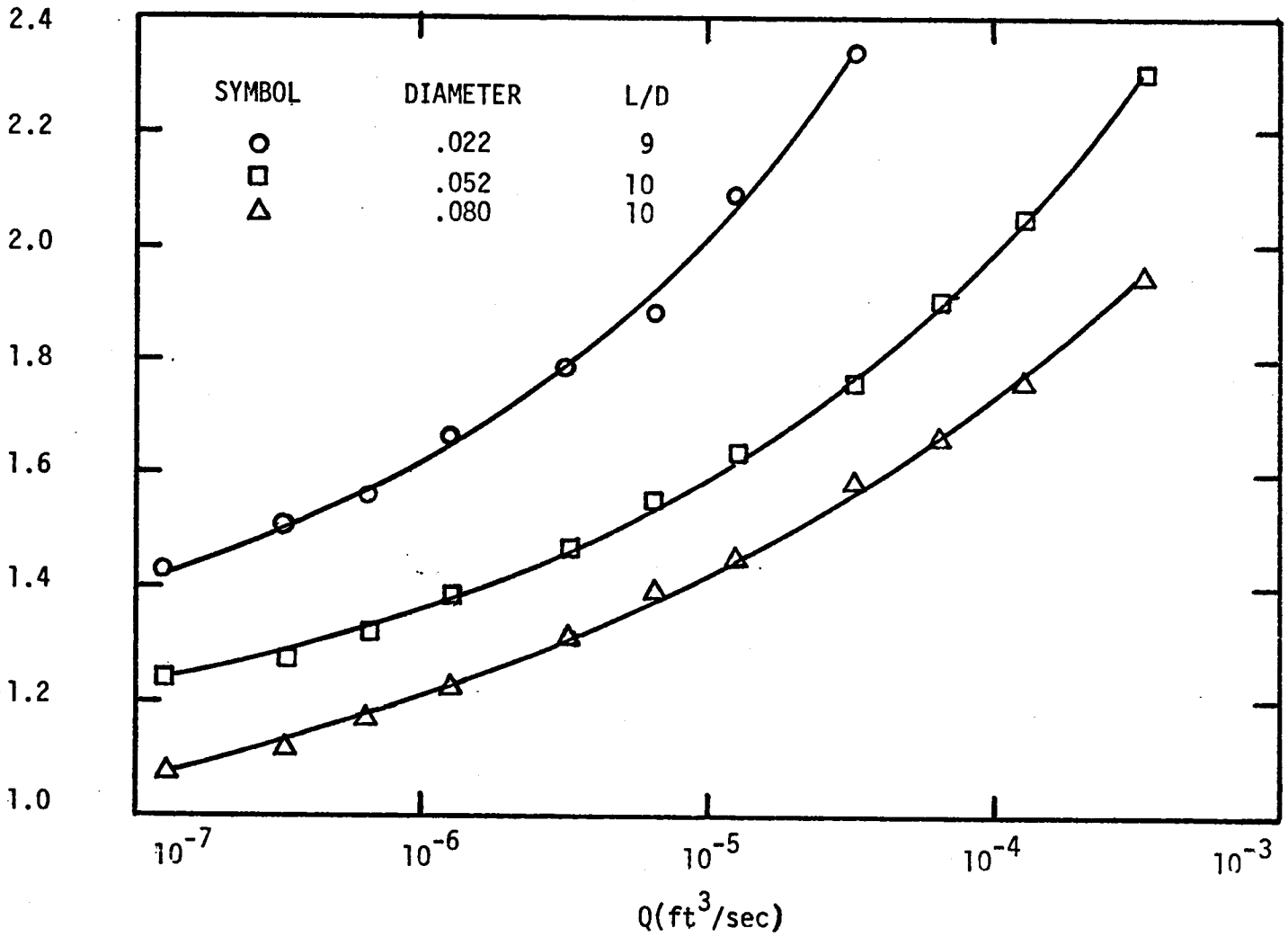

Figure 32. Die Swell as a Function of Flow Rate, for HDPE MI = 5

difference between the die swell recorded at the same flow rate for each die. Figure 33 shows the die swell as a function of shear rate. The die swell is observed to be approximately the same for each die at comparable shear rates. This is obviously a much better correlating parameter than just flow rate.

Figure 20 shows the comparison of the frozen die swell of the six polymer melts as a function of shear rate for a capillary of L/D = 47.5. All polymer melts except LDPE show die swell monotonically increasing with shear rate. The LDPE shows die swell increases monotonically with shear rate to approximately five sec^{-1} and then the die swell increases by an amount equal to or less than the previous increase for a change in shear rate..

Figure 28 shows a comparison of the die swell of the annealed extrudates as a function of shear rate for L/D = 47.5. The curves have separated compared to the plot of frozen die swell versus shear rate. The polyethylene melts locate in one area of the plot and the PP and PS melts locate in another. Again all curves except LDPE show monotonically increasing die swell with increasing shear rate. The LDPE curve shows the same character as previously described.

Figure 29 shows a comparison of the die swell measured from photographs as a function of shear rate for L/D = 47.5. All curves except LDPE show die swell increasing monotonically with increasing shear rate. The LDPE continues to have the shape previously described. This plot resembles the plot of frozen die swell versus shear rate. The curves are slightly higher in Figure 29, as if displaced upwards

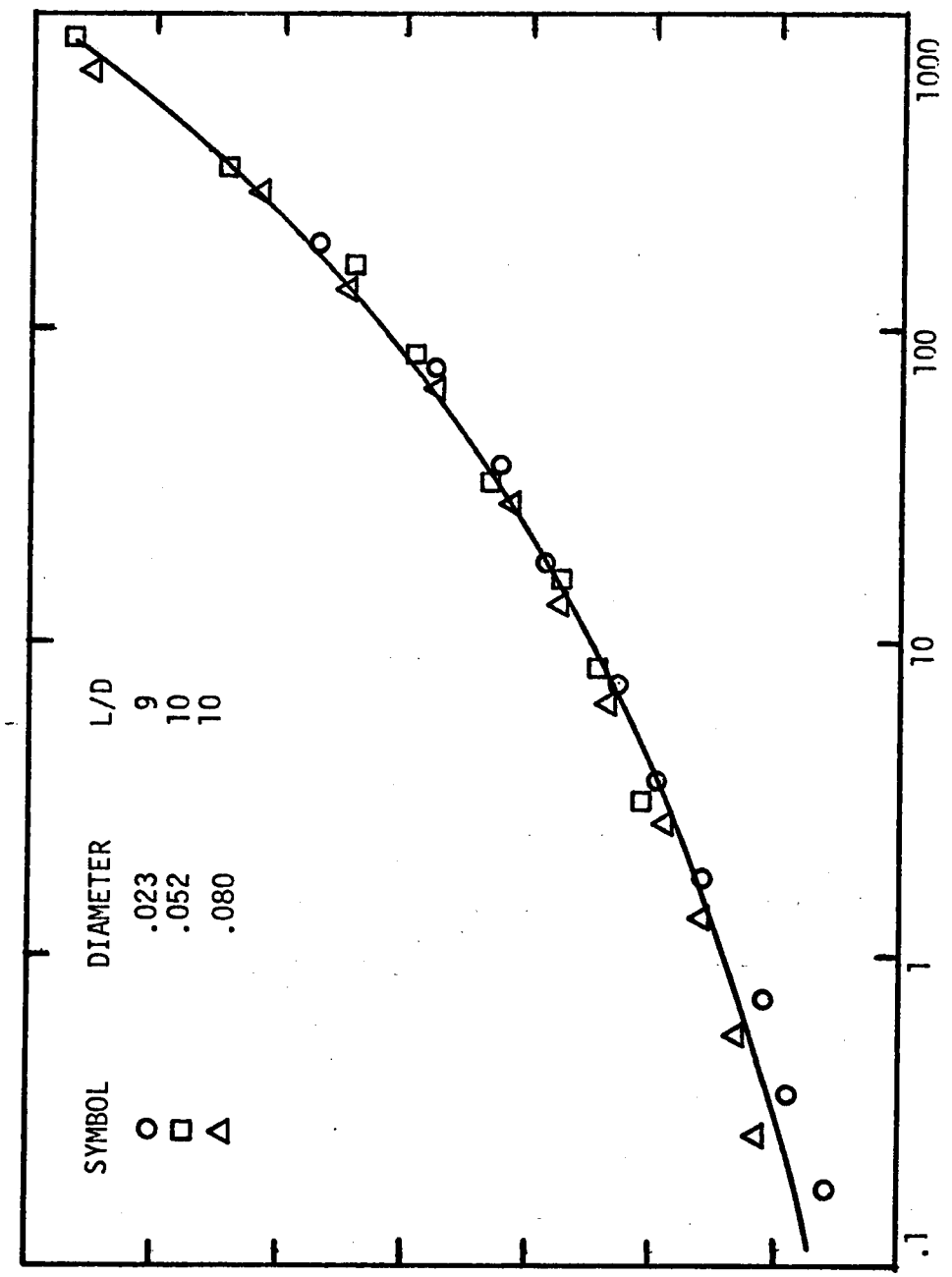

Figure 33. Die Swell as a Function of Shear Rate for HDPE MI = 5

by a constant amount. This would appear to be a result of thermal expansion.

Figure 30 compares the die swell of the six polymer melts measured isothermally as a function of shear rate for L/D = 47.5. All curves seem to increase monotonically with increasing shear rate. The polymer melts appear to separate into two groups. The polyethylenes locate in one area of the plot, while the PS and PP locate in another.

C. COMPARISON OF EXPERIMENTAL DATA WITH RHEOLOGICAL PROPERTIES

Die Swell as a Function of Shear Stress

Frozen Extrudates. As we have already compared die swell versus shear rate it would seem useful to compare die swell and shear stress (or the product of viscosity and shear rate). Figure 34 shows the die swell as a function of the shear stress at the wall for all six polymer melts. The shear stress at the wall is observed to vary between 10^3 and 10^7 dynes/cm^2 depending upon the shear rate. The capillary used has the largest L/D ratio available, L/D = 47.5. The die swell was observed to increase monotonically for all of the polymer melts, except the LDPE, as the shear stress increased. The LDPE showed die swell increasing monotonically with shear stress from 9×10^3 to 1.5×10^5 dynes/cm^2. At higher shear stresses the die swell for each incremental increase in shear stress was observed to increase by an amount less than or equal to the preceding increase. The LDPE and the HDPE MI = 5 showed the highest die swell over the range of shear

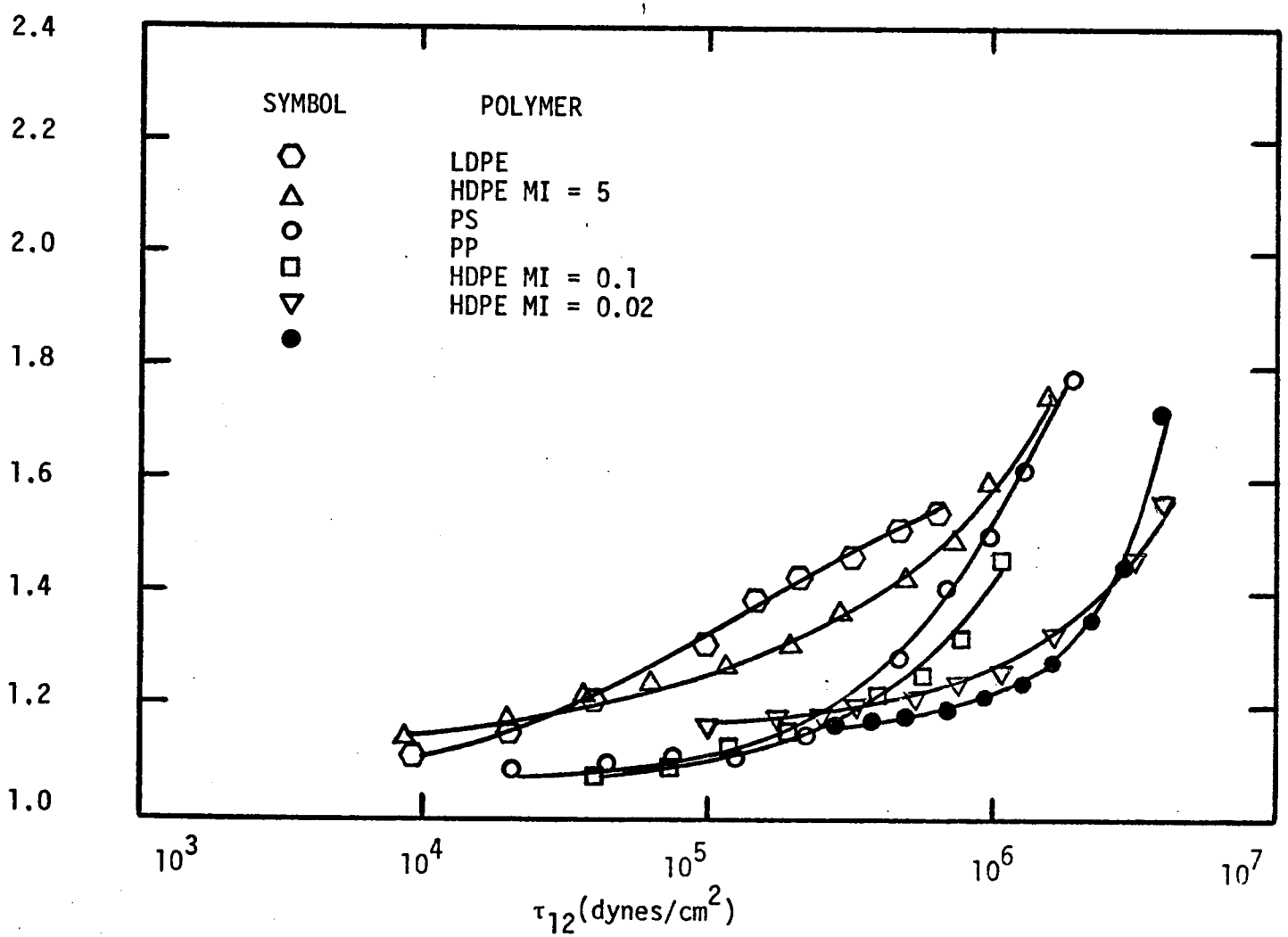

Figure 34. Die Swell as a Function of Shear Stress for Frozen Extrudates of Six Polymer Melts, L/D = 48

stresses. The PS and PP showed the least die swell at shear stresses from 2×10^4 to 2.5×10^5 dynes/cm^2. The HDPE MI = 0.02 showed the least die swell from 2.5×10^5 to 3×10^6 dynes/cm^2. The curves were observed to approach a lower limit of 1.1 at low shear stresses.

Photographs. The die swell measured from photographs as a function of shear stress for the six polymer melts is shown in Figure 35. The curves are very similar to those in Figure 34 except for the fact that they are displaced upwards by a constant amount. This amount of upward displacement has previously been suggested to show a density difference between the extrudates at 180°C and the cooled extrudates.

Annealed Data. The die swell as a function of shear stress for annealed extrudates is shown in Figure 36. The LDPE and HDPE MI = 5 showed the largest amount of die swell in the range of shear stresses covered. The PP and the HDPE MI = 0.02 were observed to show the least die swell in this range. The die swell was observed to increase monotonically with increasing shear stress for all polymer melts except the LDPE. The LDPE again showed a different character in the die swell-shear stress plot. The die swell was observed to increase monotonically from 9×10^3 to 1×10^5 dynes/cm^2. At higher shear stresses, the die swell increased by an equal or smaller amount than the preceding increase for each incremental increase in shear stress. The die swell measured from the annealed extrudates is observed to be noticeably larger than the die swell

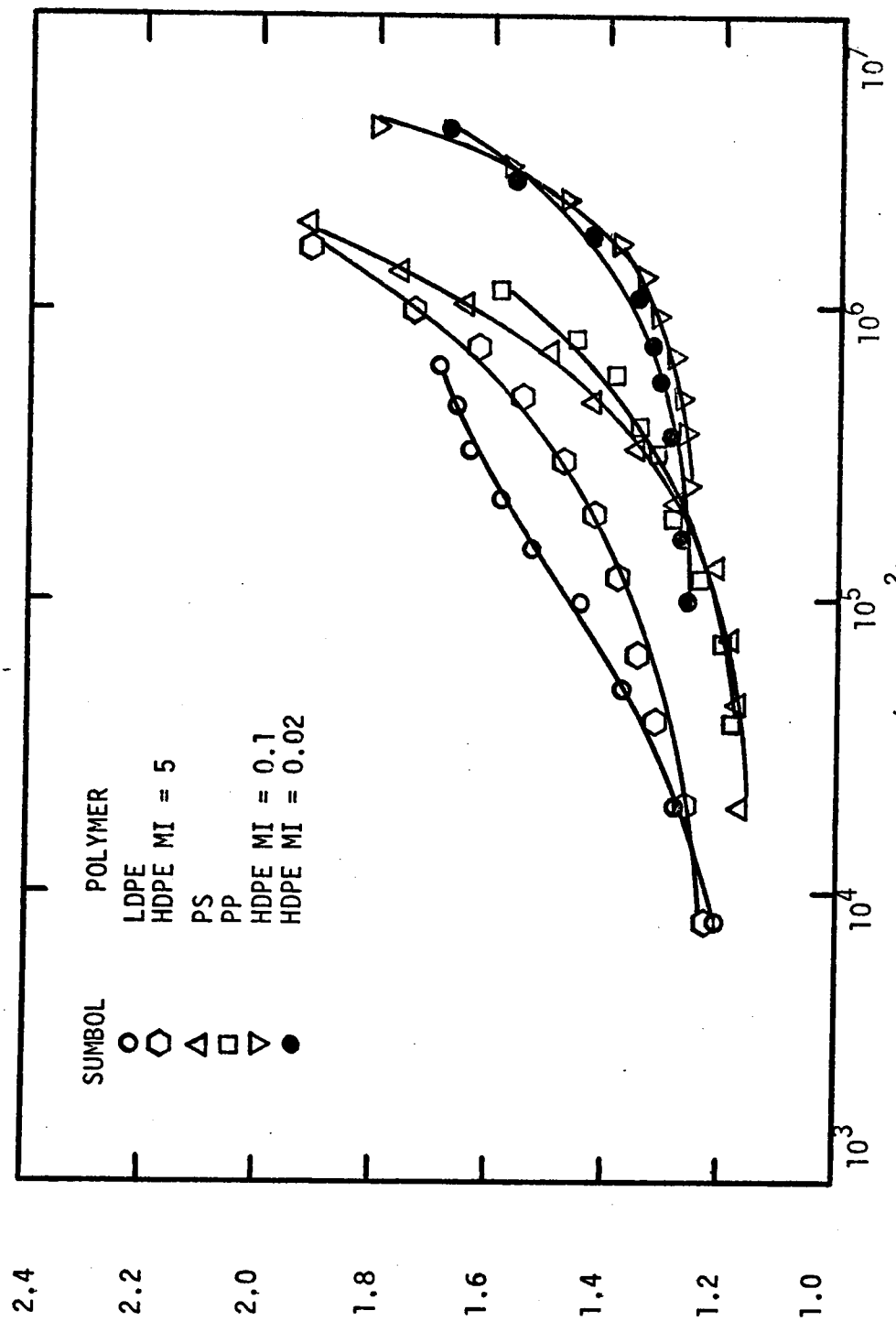

Figure 35. Die Swell Measured from Photographs as a Function of Shear Stress for Six Polymer Melts, L/D = 48

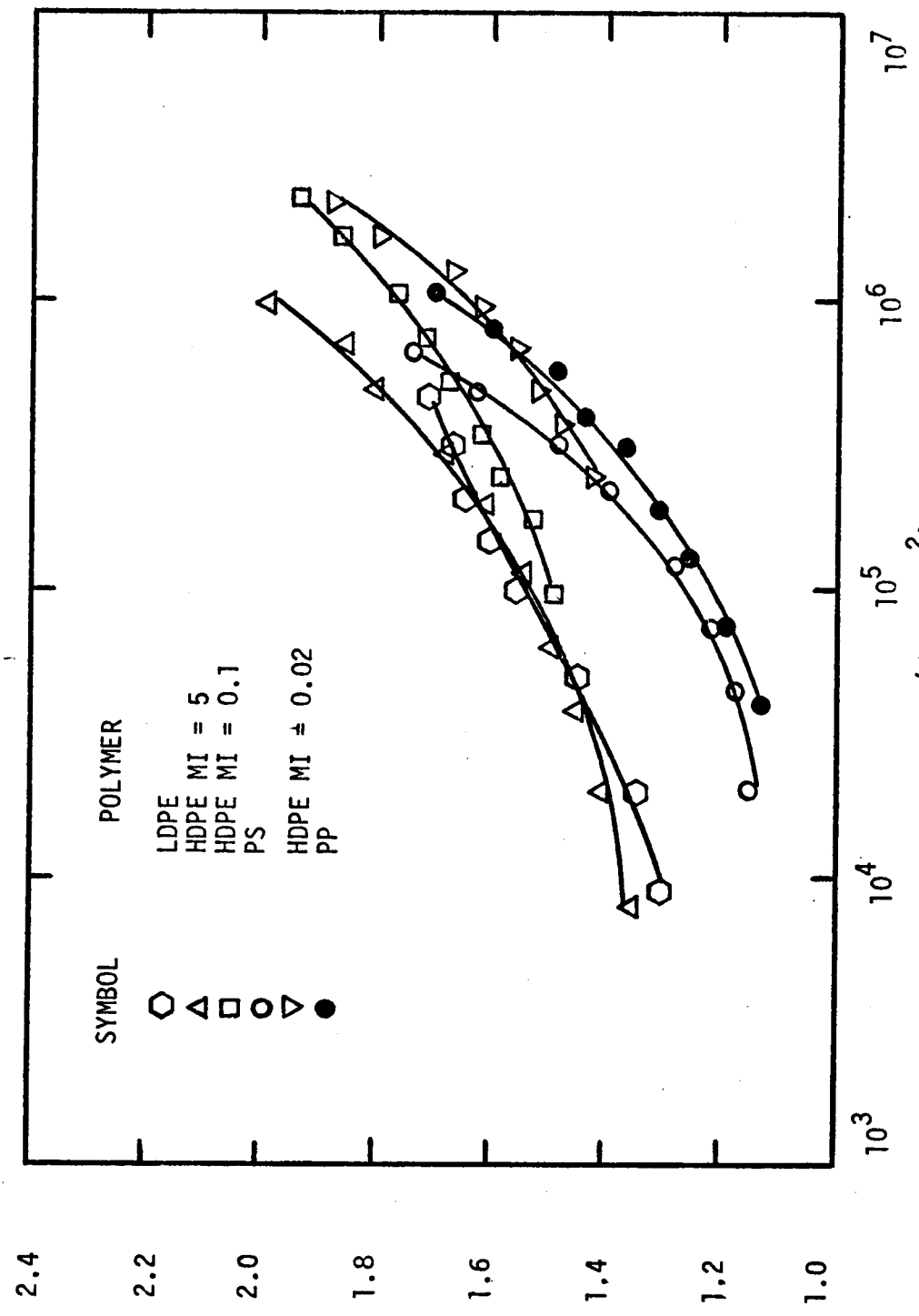

Figure 36. Die Swell of Annealed Extrudates as a Function of Shear Stress for Six Polymer Melts, L/D = 48

measured from the frozen extrudates.

Isothermal Swell. The die swell measured isothermally is shown in Figure 37 as a function of shear stress. The die swell measured in this manner is the highest of all the methods used. The die swell was observed to increase almost monotonically with increasing shear stress for all polymer melts. The LDPE data is below the point at which the curve changes its character, so the strange behavior of the LDPE noted previously is not observed here. The LDPE and the HDPE MI = 5 showed the largest amount of swell, while the PP and PS showed the least swell.

General Observations. The die swell was observed to increase with increasing shear stress, however, the character of the LDPE curve differed from the shape of the curves for the other melts. The isothermal data showed the largest swell for each melt. The polymer melts show quite a bit of separation from each other in the previous plots. The data for the six polymer melts is not as closely bunched together as in Figure 20 of die swell as a function of shear rate. This would seem to indicate that shear rate is a better correlating parameter than shear stress.

Die Swell as a Function of Normal Stress-Shear Stress Ratio

Shear Stress Ratio. The normal stress-shear stress ratio can be said to be a measure of the elastic forces of the melt to the viscous forces (see for example White, J. Appl. Poly. Sci. 8, 23339

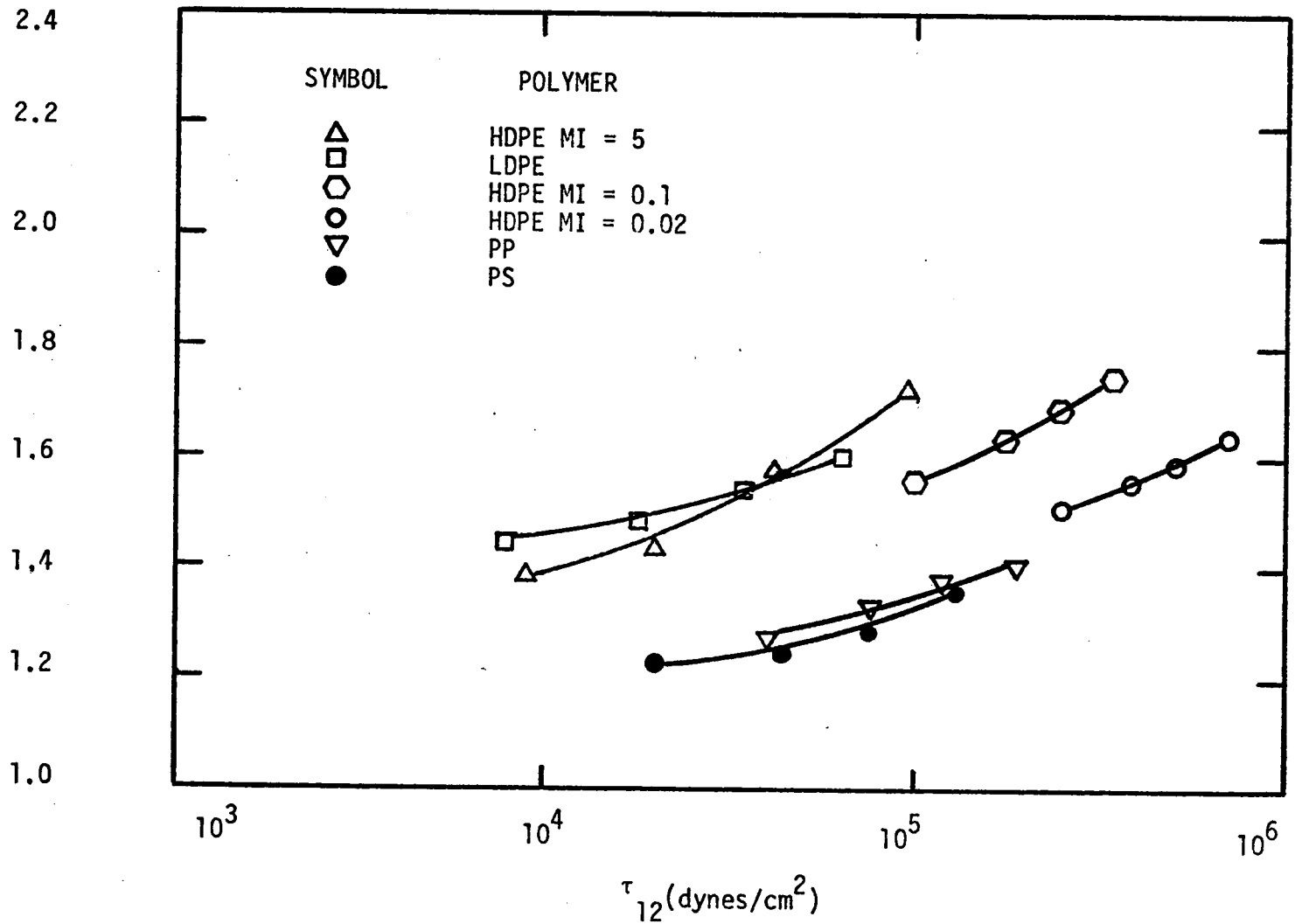

Figure 37. Isothermal Die Swell as a Function of Shear Stress for Six Polymer Melts

(1964)). Since the die swell is related to the elastic recovery, it would seem useful to compare die swell and the ratio of normal stresses to shear stresses. It is necessary to point out that normal stress data is limited to shear rates below 1.5 sec^{-1}. We can presume that J_e or G is a constant and use these constants to calculate normal stresses at higher shear rates.

Frozen Extrudates. The die swell as a function of normal stress-shear stress ratio $\frac{N_1 w}{(\tau_{12})_w}$, is shown in Figure 38 for the frozen extrudates. All of the curves fall in the same general area and approach a lower limit of 1.1 at low $\frac{N_1 w}{(\tau_{12})_w}$. At high $\frac{N_1 w}{(\tau_{12})_w}$ there is some spreading out of the curves. The HDPE MI = 0.02 appears to show the largest die swell over most of the range of $\frac{N_1 w}{(\tau_{12})_w}$. All of the die swell- $\frac{N_1 w}{(\tau_{12})_w}$ curves except for LDPE appear to increase monotonically. The LDPE increases monotonically from $\frac{N_1 w}{(\tau_{12})_w}$ of .4 to 7 and at greater values of $\frac{N_1 w}{(\tau_{12})_w}$ the increase in the die swell is less than or equal to the previous increase, for each change in $\frac{N_1 w}{(\tau_{12})_w}$. The PP seems to show the least die swell over the range of $\frac{N_1 w}{(\tau_{12})_w}$ values.

Photographs. The die swell measured from photographs is shown as a function of $\frac{N_1 w}{(\tau_{12})_w}$ in Figure 39. The die swell is greater by a constant smount, when compared to the frozen extrudates, as previously discussed. The curves follow the same pattern as those of the frozen extrudate.

Annealed Extrudates. The die swell of the annealed extrudates

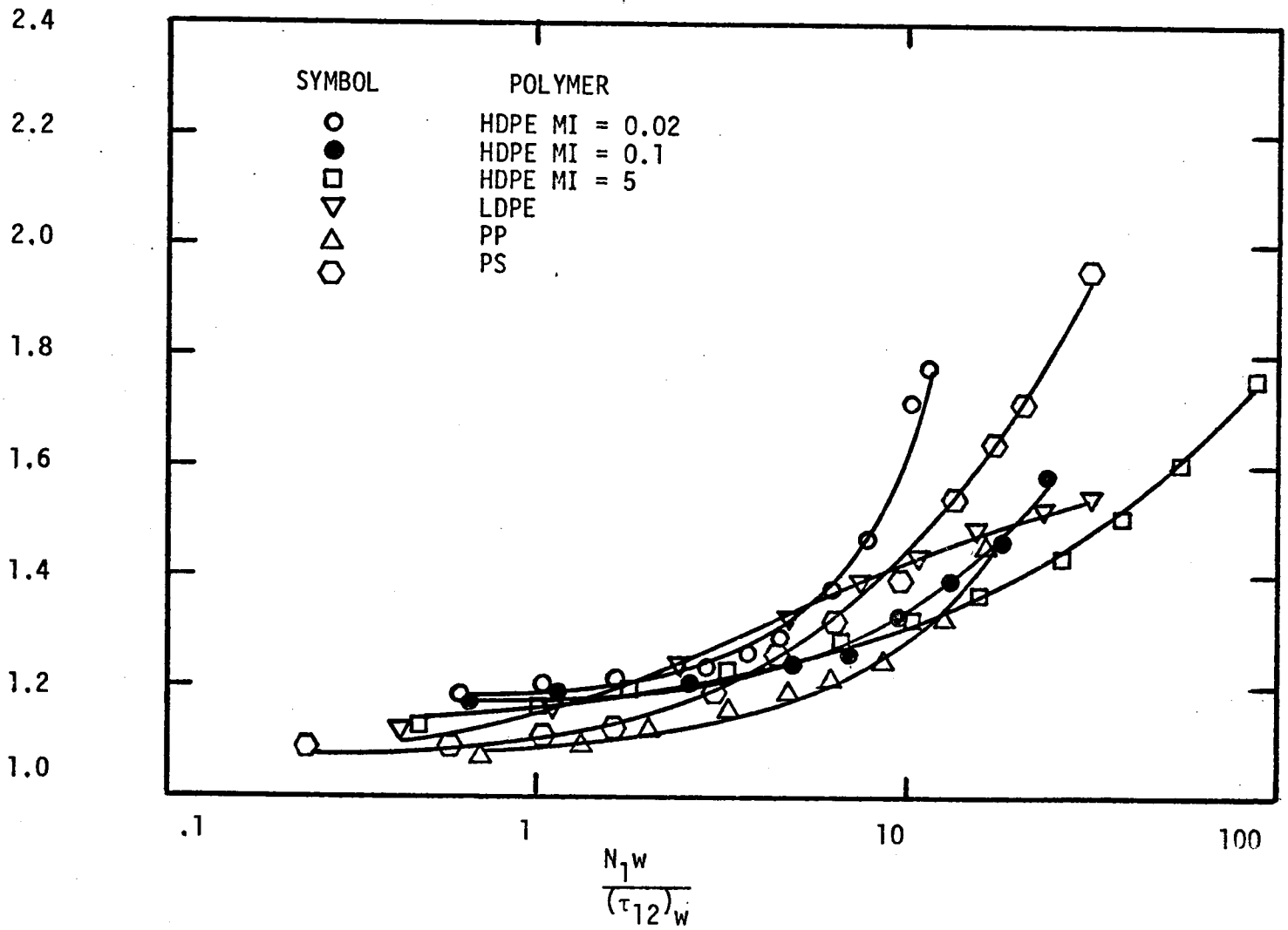

Figure 38. Die Swell of Frozen Extrudates as a Function of $\frac{N_1 w}{(\tau_{12})_w}$ for Six Polymer Melts, L/D = 48

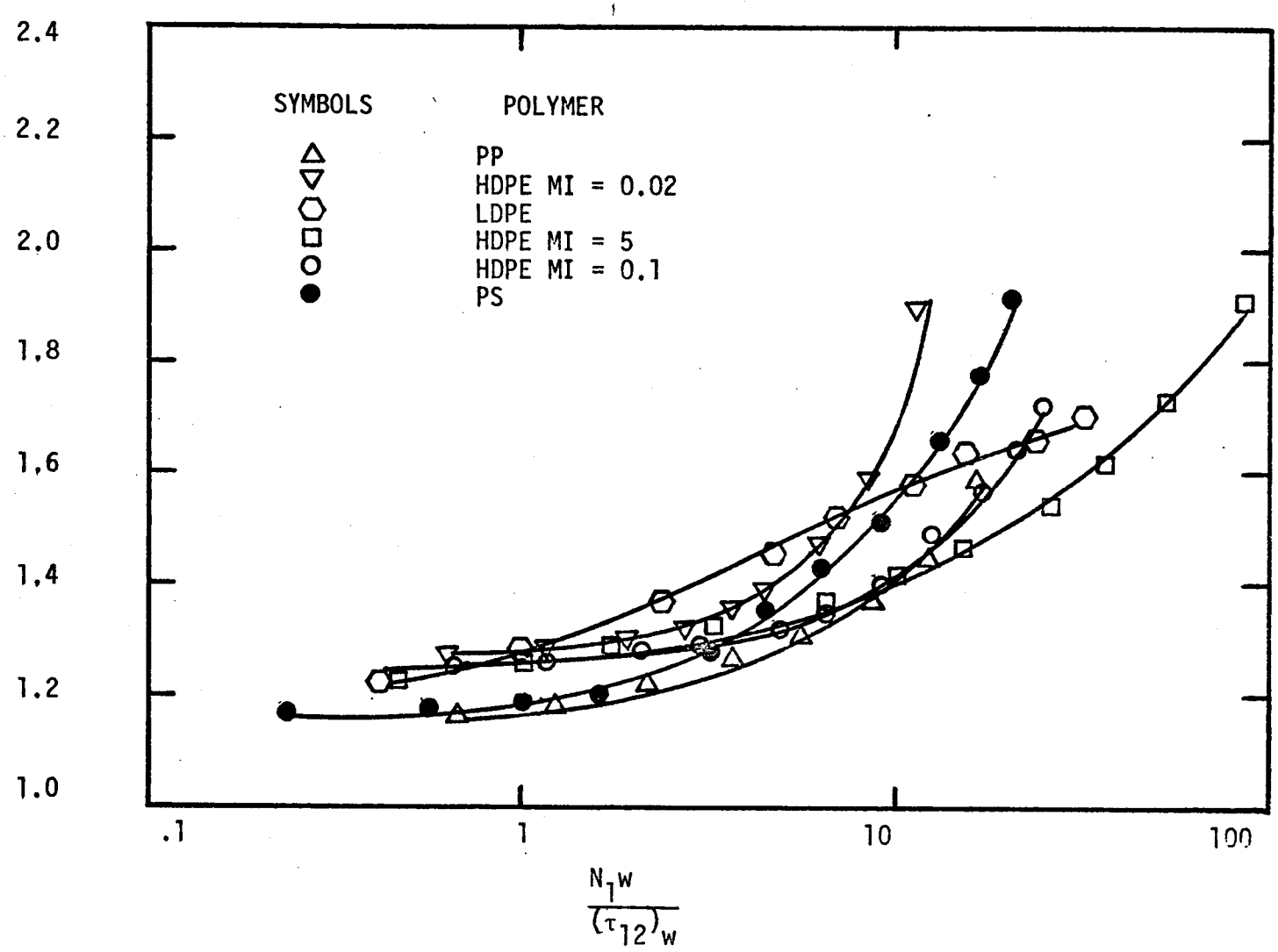

Figure 39. Die Swell Measured Photographically as a Function of $\frac{N_1 w}{(\tau_{12})_w}$ for Six Polymer Melts, L/D = 48

as a function of $\frac{N_1 w}{(\tau_{12})_w}$ is shown in Figure 40. The curves appear more spread out than in plots of frozen and photographic data. The die swell was observed to be monotonically increasing for all polymer melts except LDPE. The character of the LDPE curve again increased monotonically for a period and then at $\frac{N_1 w}{(\tau_{12})_w}$ greater than seven, for each subsequent increase in $\frac{N_1 w}{(\tau_{12})_w}$ the die swell increased by an amount less than or equal to the previous increase. The HDPE MI = 0.02 and HDPE MI = 0.1 showed the highest die swell in the range of $\frac{N_1 w}{(\tau_{12})_w}$ shown, while the PP showed the least die swell. There would appear in Figure 40 a slight tendency of the polymer melts to group themselves. The PS and PP appear close together, as do the LDPE and HDPE MI = 5, and the HDPE MI = 0.1 and HDPE MI = 0.02.

Isothermal Swell. The die swell observed isothermally as a function of $\frac{N_1 w}{(\tau_{12})_w}$ is shown in Figure 41. The six polymer melts show monotonically increasing die swell with increasing $\frac{N_1 w}{(\tau_{12})_w}$. The LDPE shows similar results to the other polymers, because at this low range of $\frac{N_1 w}{(\tau_{12})_w}$ values, the character of the curve is similar to that of the other polymers and has not yet started to change in character. The curves appear spread out, similar to those of the annealed extrudates and not as compacted as the curves for frozen extrudates and photographic data. There appears to be a tendency for the polymers to group themselves. The polethylenes locate in a different area of the plot than the PS and PP. The HDPE MI = 0.1 showed the largest amount of die swell over the range of $\frac{N_1 w}{(\tau_{12})_w}$ values shown, while the PS and PP showed the least die swell.

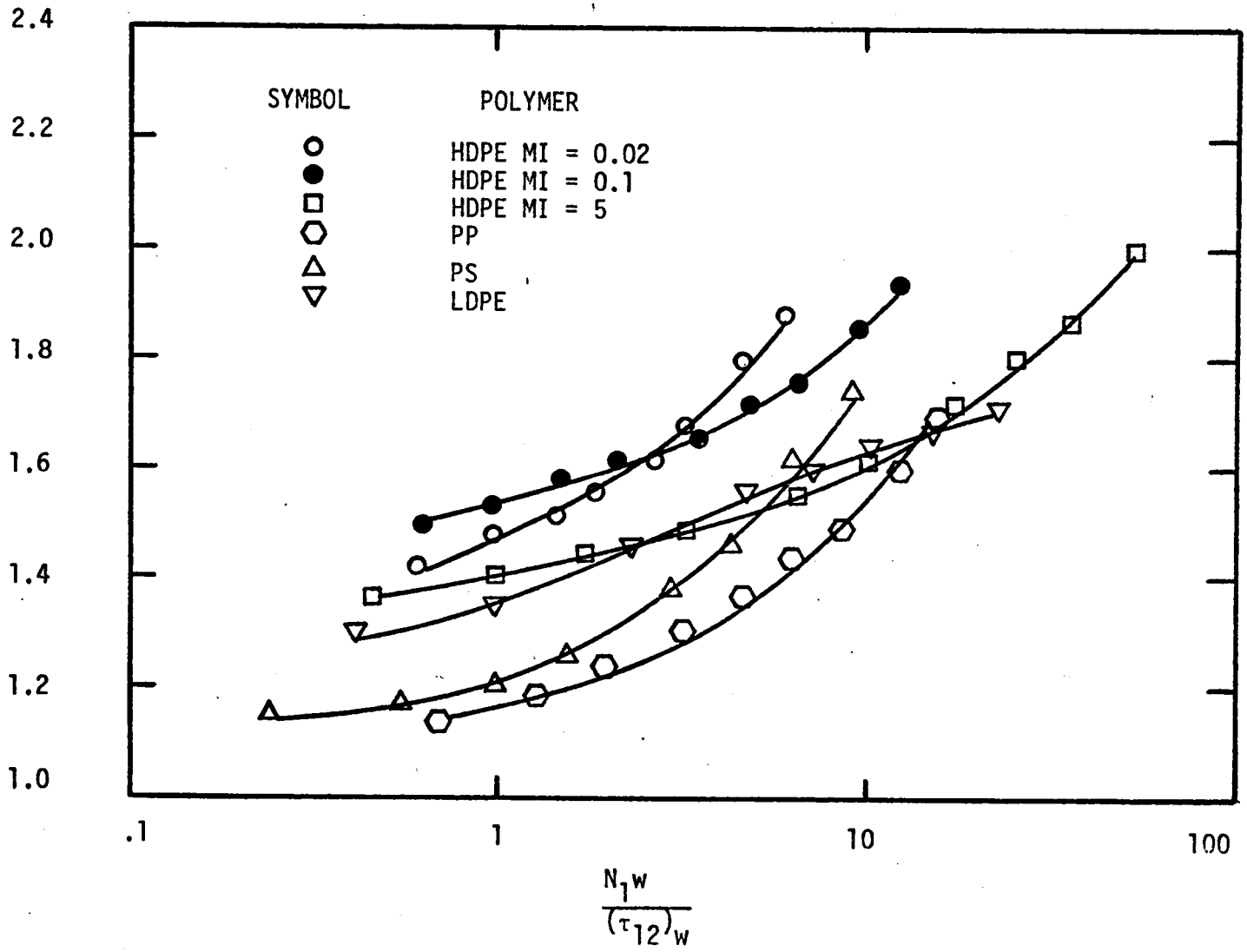

Figure 40. Die Swell of Annealed Extrdudates as a Function of $\frac{N_1 w}{(\tau_{12})_w}$ for Six Polymer Melts, L/D = 48

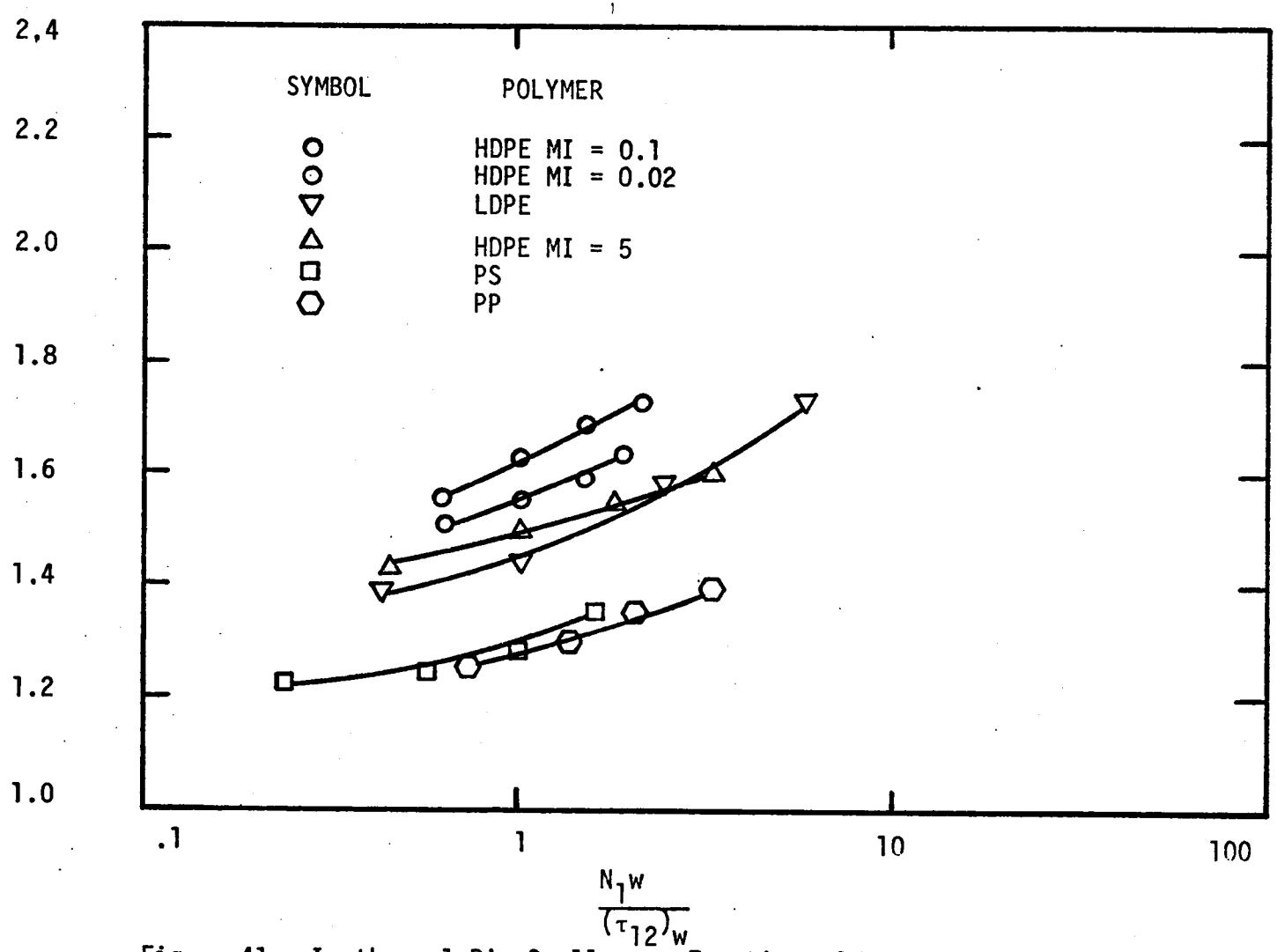

Figure 41. Isothermal Die Swell as a Function of $\frac{N_1 w}{(\tau_{12})_w}$ for Six Polymer Melts, L/D = 48

General Observations. The die swell for frozen and pictorial data as a function of $\frac{N_1 w}{(\tau_{12})_w}$ fall more closely together than the curves of die swell for the annealed and isothermal data. The isothermal data shows the largest swell, at a constant $\frac{N_1 w}{(\tau_{12})_w}$ while the frozen data showed the least swell. The data for the frozen extrudates at low $\frac{N_1 w}{(\tau_{12})_w}$ values is generally close together, however, at high values of $\frac{N_1 w}{(\tau_{12})_w}$ the curves spread apart. The annealed data and isothermal data comparing each melt are spread quite far apart. There is a tendency for the polymers to group themselves, one group being PS and PP and the other being the polyethylenes. The polymer melts in each group show similar magnitudes of die swell at the same $\frac{N_1 w}{(\tau_{12})_w}$ values.

A problem in the interpretation of this data is the presumption of the constancy of J_e or G which has been used to extrapolate the normal stress data to higher shear rates.

D. BEHAVIOR OF "FAMILIES" AND COMPARISON WITH LITERATURE

Commercial Polystyrene

Commercial polystyrenes are made in a similar manner, and have similar molecular weight distribution, branching and should have similar functional shapes. It is only rational to compare the experimental polystyrene data with literature values for commercial polystyrene melts.

The die swell of two commercial polystyrenes is compared in

Figure 42 as a function of shear rate. These polymers include the PS used in this work and that used in the work of Graessley, et.al. (29). The die swell of these extrudates was measured using micrometers and consists only of frozen extrudate data. The PS used in this work had a number average molecular weight, M_n, of 78,000 and a molecular weight distribution, $\frac{M_w}{M_n}$, of 3.1. The polystyrene used by Graessley was Dow Styron with an M_n of 220,000 and $\frac{M_w}{M_n} = 3.1$. From Figure 42 we can see that the PS of $M_n = 220,000$ shows slightly higher die swell. Compared to Figure 20, the plot of die swell for all six polymer melts as a function of shear rate, this would appear to show that the data for commercial polystyrene extruded through long L/D capillaries, is relatively consistent and less scattered than the data for the polymers investigated in this study.

The die swell of five commercial polystyrenes as a function of shear stress is shown in Figure 43. The polystyrenes included in this plot include those in Figure 42 and also a Dow Styron polystyrene used by Graessley, et.al. with $M_n = 261,000$ and $\frac{M_w}{M_n} = 2.5$, a polystyrene blend used by Vlachopoulos (73) which had $M_w = 212,000$ and $\frac{M_w}{M_n} = 2.88$ and a Cadillac Plastics polystyrene used by Lee (39) with an unknown M_n and $\frac{M_w}{M_n}$, but had a shear viscosity of approximately 10^7 poise at low shear rates. This was roughtly 100 times larger than that of the polystyrene used in this work, 10^5 poise, at low shear rates. Vlachopoulos' data was taken at 170°C, Lee's data at 160°C and Graessley's, et.al. at 180°C. Lee and Vlachopoulos used dies with L/D ratios of approximately 20, which is about half the L/D

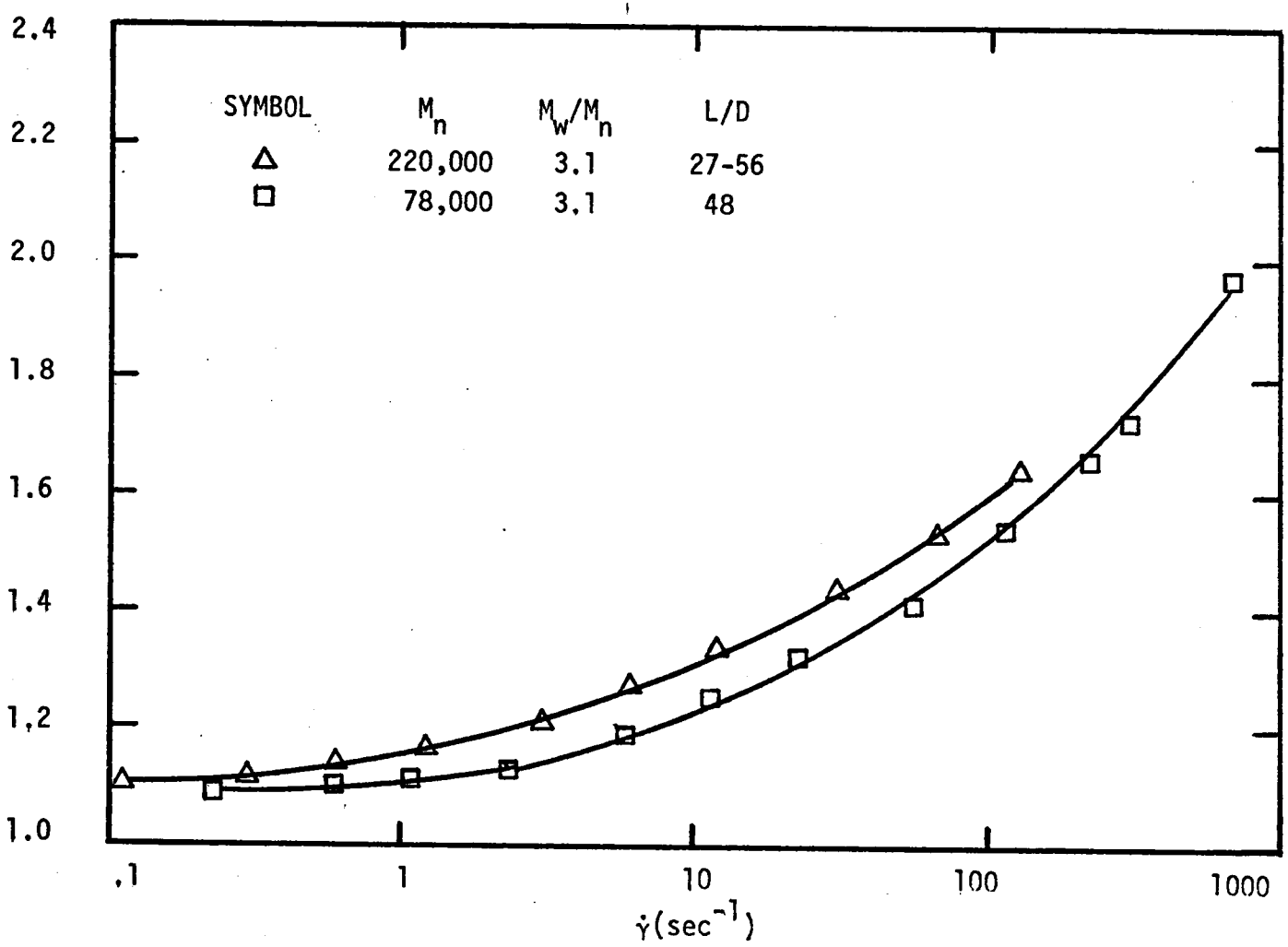

Figure 42. Comparison of Experimental and Literature Data Values of Die Swell for Frozen Commercial PS Extrudates as a Function of Shear Rate

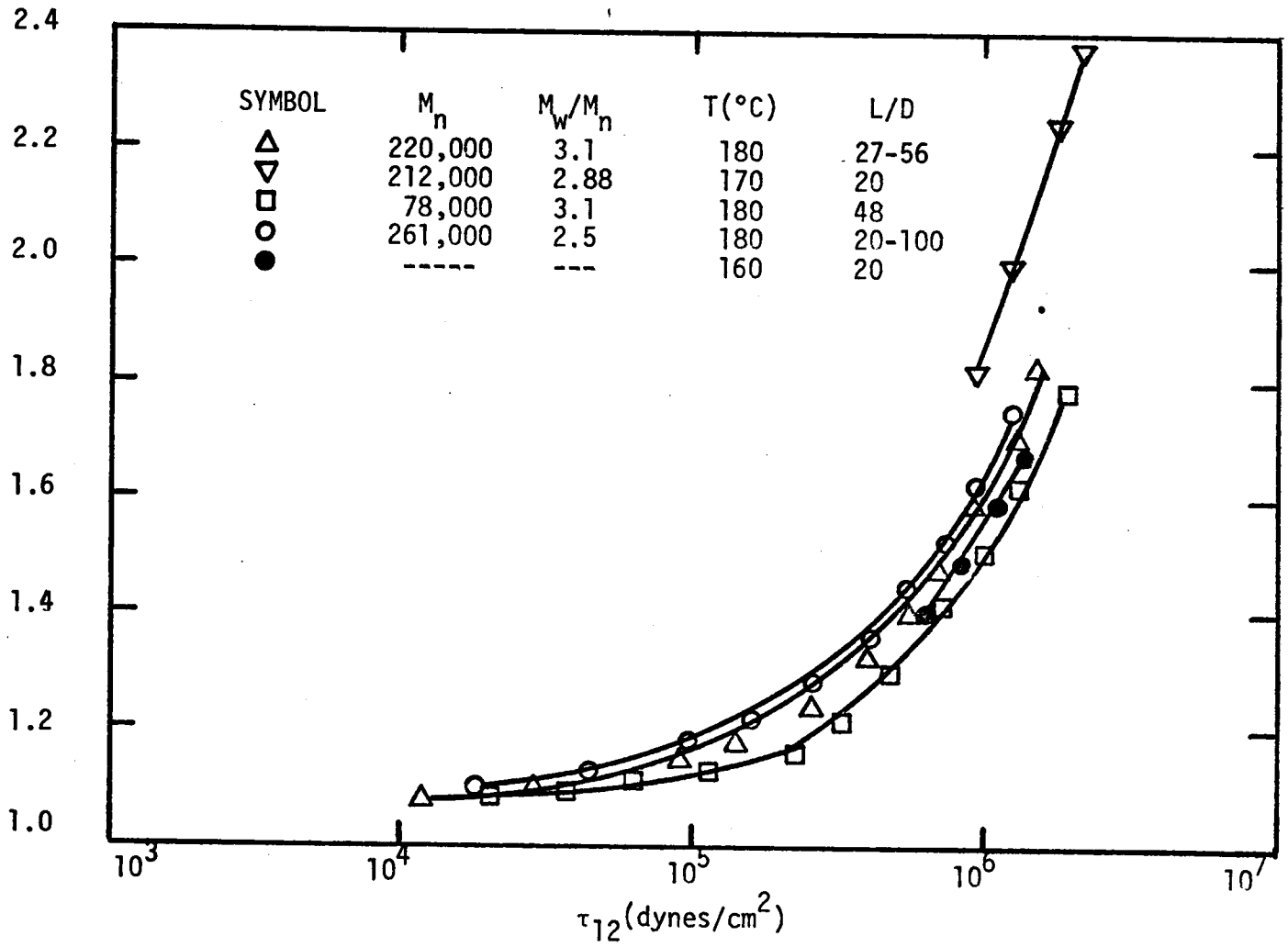

Figure 43. Comparison of Experimental and Literature Values of Frozen Commercial PS Die Swell as a Function of Shear Stress

ratio of those used in this work and by Graessley, et.al. There is a slight L/D effect on die swell from short L/D dies, however, for polystyrene this effect seems to be small for L/D's 20 and greater. Figure 43 shows that the die swell plotted as a function of shear stress for commercial polystyrenes is very consistent. All of the curves lie in close proximity to each other. The die swell of the polystyrene family is very close for each member, indeed, closer than the other polymer melts studied. Figure 44 shows the die swell of annealed polystyrene as a function of shear stress. The data includes PS used in this study and the polystyrene of M_n = 261,000 and $\frac{M_w}{M_n}$ = 2.5 used by Graessley, et.al. His annealed data shows a large similarity to the annealed data shown in this work.

Figure 45 shows die swell as a function of $\frac{N_1 w}{(\tau_{12})_w}$ for commercial polystyrene. This contains the data of Lee, Graessley, et.al., M_w = 220,000 and $\frac{M_w}{M_n}$ = 3.1 and also the data obtained in this work. These curves fall in close proximity to each other. The data for the commercial polystyrene die swell as a function of $\frac{N_1 w}{(\tau_{12})_w}$ appears to agree quite well. This PS data agrees much better with data from the same family of polymers than with the five different polymer melts. Literature data, however, is limited.

Comparison of Commercial Polystyrenes and Narrow Distribution Polystyrenes

A plot of the die swell as a function of shear rate for narrow M.W. distribution polystyrene is shown in Figure 46. The narrow M.W. polystryene is a Pressure Chemical Company polystyrene used by

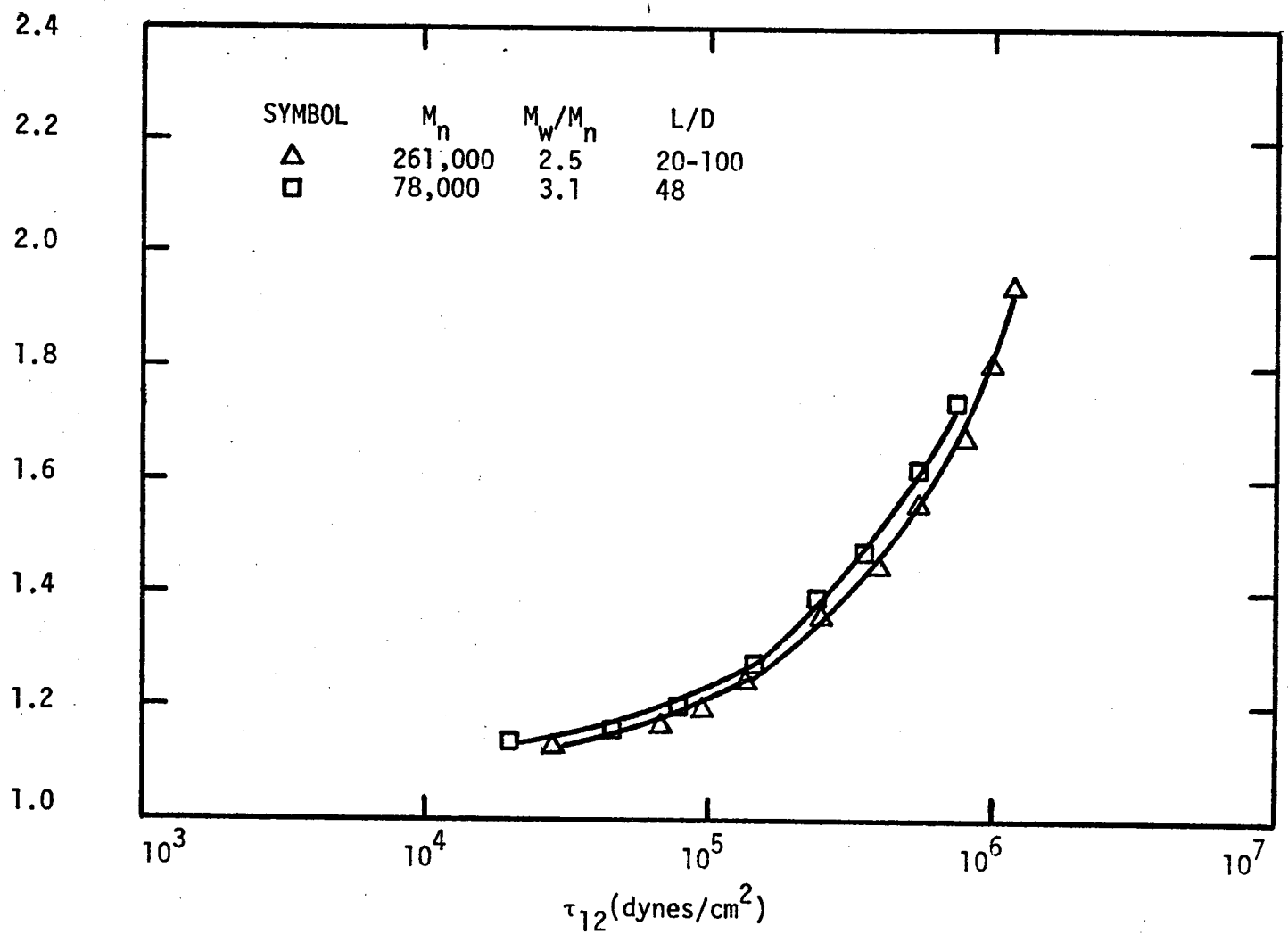

Figure 44. Comparison of Experimental and Literature Values of Annealed Commercial PS Die Swell as a Function of Shear Stress

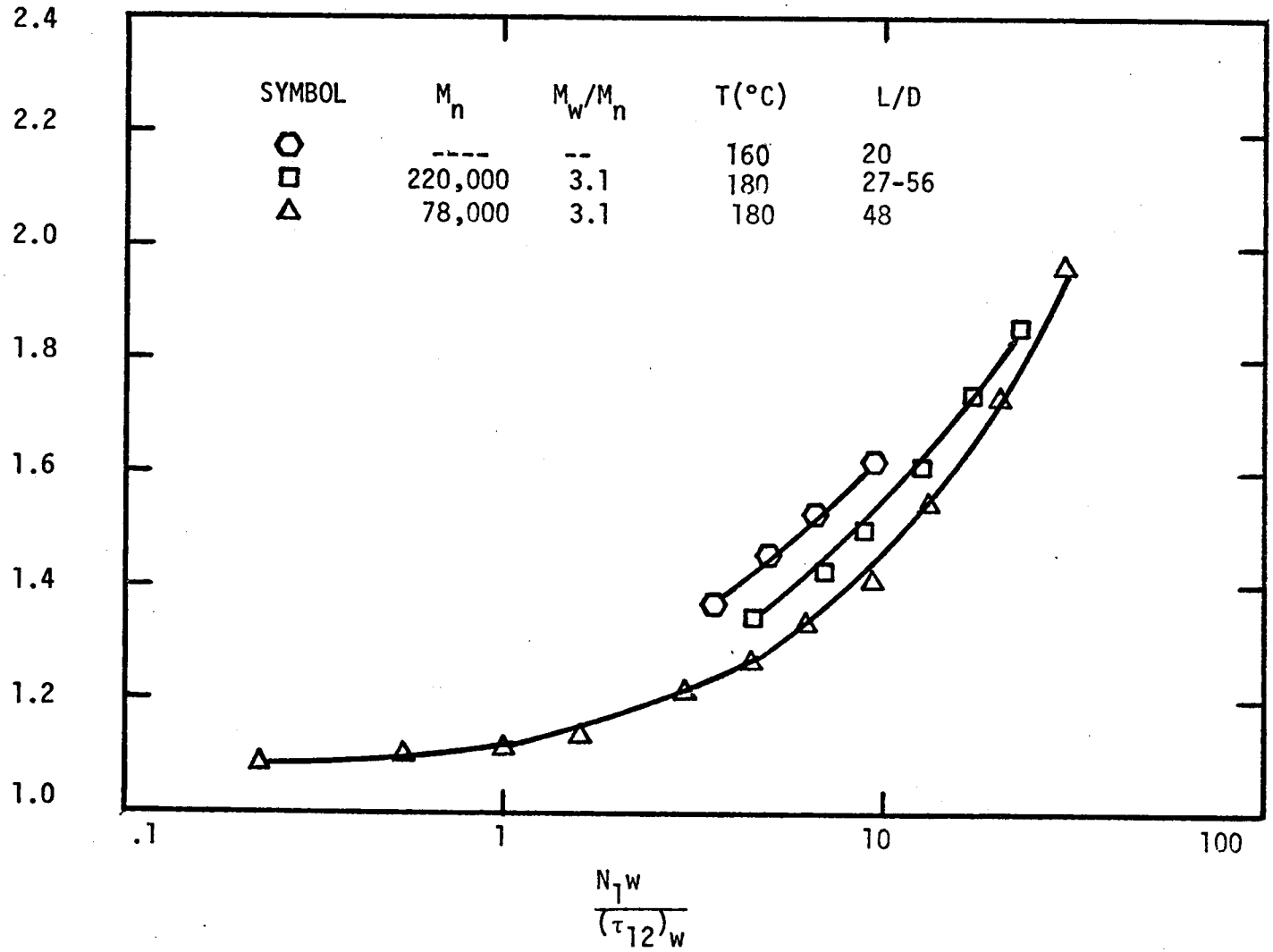

Figure 45. Comparison of Experimental and Literature Values of Frozen Commercial PS Die Swell as a Function of $\frac{N_1 w}{(\tau_{12})_w}$

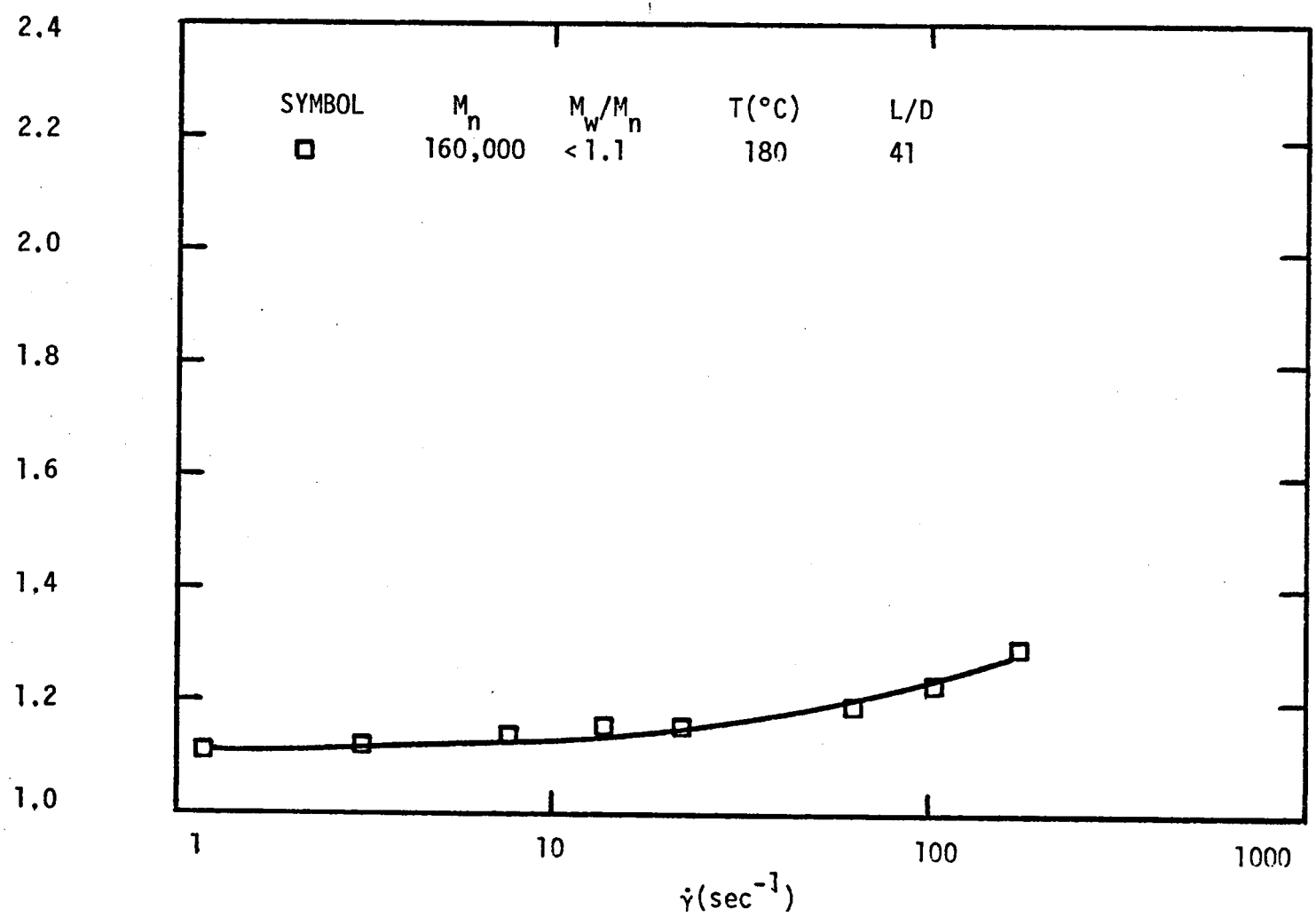

Figure 46. Literature Values of Frozen Die Swell as a Function of Shear Rate for Narrow Molecular Weight Distribution PS

Graessley, et.al. (29), with M_n = 160,000 and $\frac{M_w}{M_n}$ = < 1.1. Comparison of this with commercial polystyrenes shows that the magnitude of the die swell is less at comparable shear rates. The narrow M.W. distribution polystyrene displays an almost constant value of die swell over a large range of shear rates.

Figure 47 shows a comparison of the die swell as a function of shear stress for narrow M.W. distribution polystyrenes. Included are four narrow M.W. distribution polystyrenes, the one previously mentioned, another Pressure Chemical Company polystyrene used by Graessley, et.al. with M_n = 96,000 and $\frac{M_w}{M_n}$ = < 1.1. The other two are taken from the data of Vlachopoulos (73) and consist of Pressure Chemical Company polystyrenes with M_w = 670,000 and $\frac{M_w}{M_n}$ = < 1.20 and M_w = 1,800,000 and $\frac{M_w}{M_n}$ = < 1.20. The best comparison is with the work of Graessley, et.al. since his work was done at the same temperature as that used in the present work, 180°C. Vlachopoulos' data was taken at 230°C. The narrow M.W. distribution polystyrenes show an almost constant value of die swell over the most of the range of shear stresses and are located far away from the commercial polystyrene data.

The narrow M.W. distribution polystyrenes show little agreement with commercial data when plotted against shear rate or shear stress. The data of the six different polymer melts investigated shows as much agreement as the data for commercial polystyrenes and narrow M.W. distribution polystyrenes.

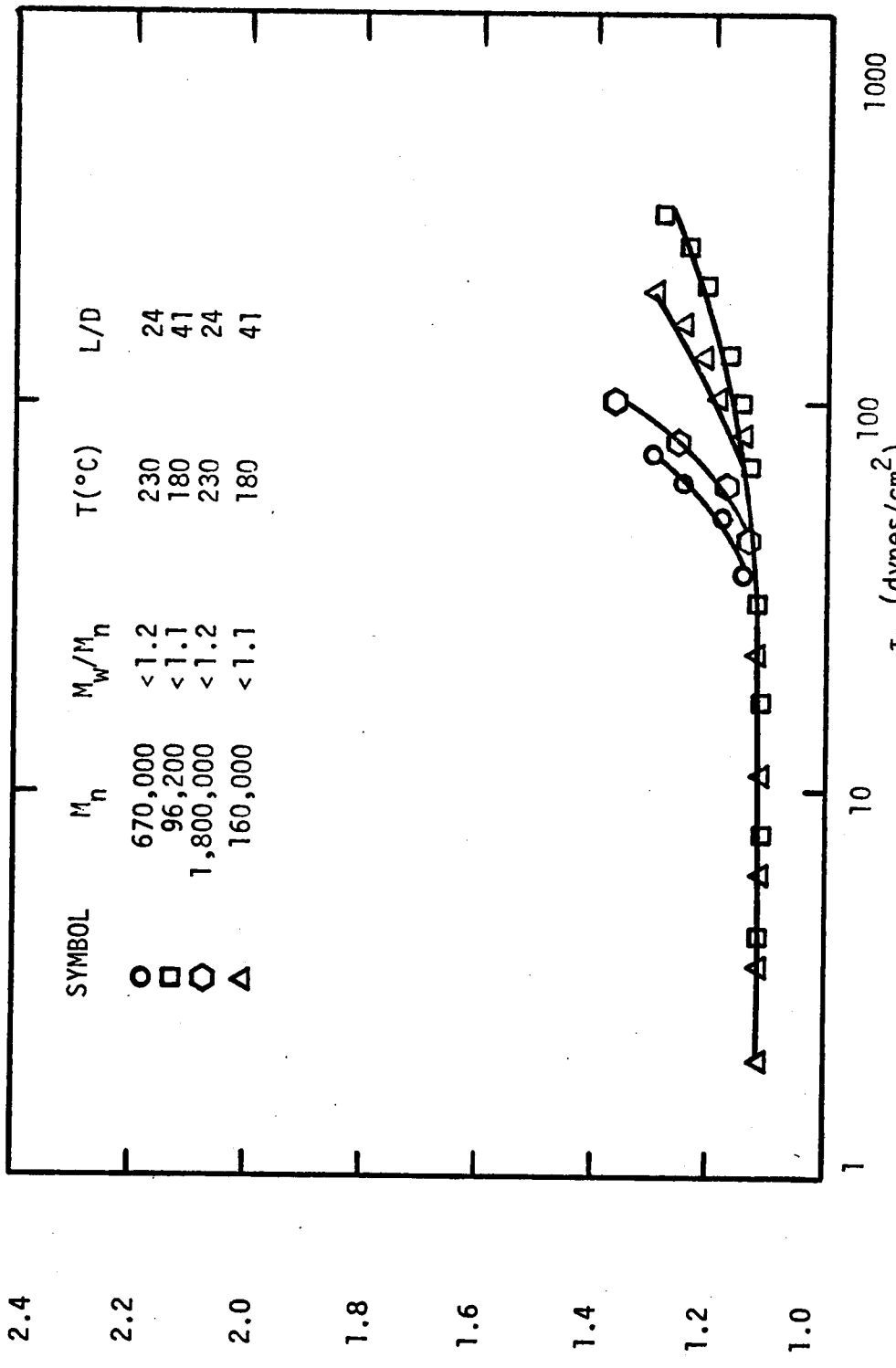

Figure 47. Literature Values of Frozen Die Swell as a Function of Shear Stress for Narrow Molecular Weight Distribution PS

High Density Polyethylene

The die swell of high density polyethylene as a function of shear rate is shown in Figure 48. Shown are the experimental values and literature values. The literature values consist of an HDPE MI = 0.2 and a HDPE of unknown melt index used by Mendelson (44, 45) and an HDPE MI = 0.73 used by Rogers (59). The extrusion temperatures ranged from 170°C to 200°C and large L/D dies. This consists only of frozen extrudate data. The number of die swell curves presented for long L/D dies is somewhat limited. The curves shown in Figure 48 appear similar in shape and only the data for HDPE MI = 0.2 differs radically from the other data. This data for HDPE's seems more spread out than just the data for the six polymer melts used in this work, as shown in Figure 20. Figure 49 shows a comparison of die swell for annealed HDPE as a function of shear rate. Also shown in Mendelson's HDPE MI = unknown. This appears to show reasonable agreement with our own data. Only one literature curve is presented, because annealing work is limited and the major portion of this is limited to very short L/D dies.

The die swell as a function of shear stress is shown in Figure 50 for frozen extrudates. Included are the HDPE's used in this study, the two HDPE's used by Mendelson which have been previously mentioned and a HDPE of unknown melt index used by Lee (39), with a viscosity comparable to that of our own HDPE MI = 0.02. Again, only the data of HDPE MI = 0.2 is radically different from the other data. This data is spread out more than the data comparing just the six polymer

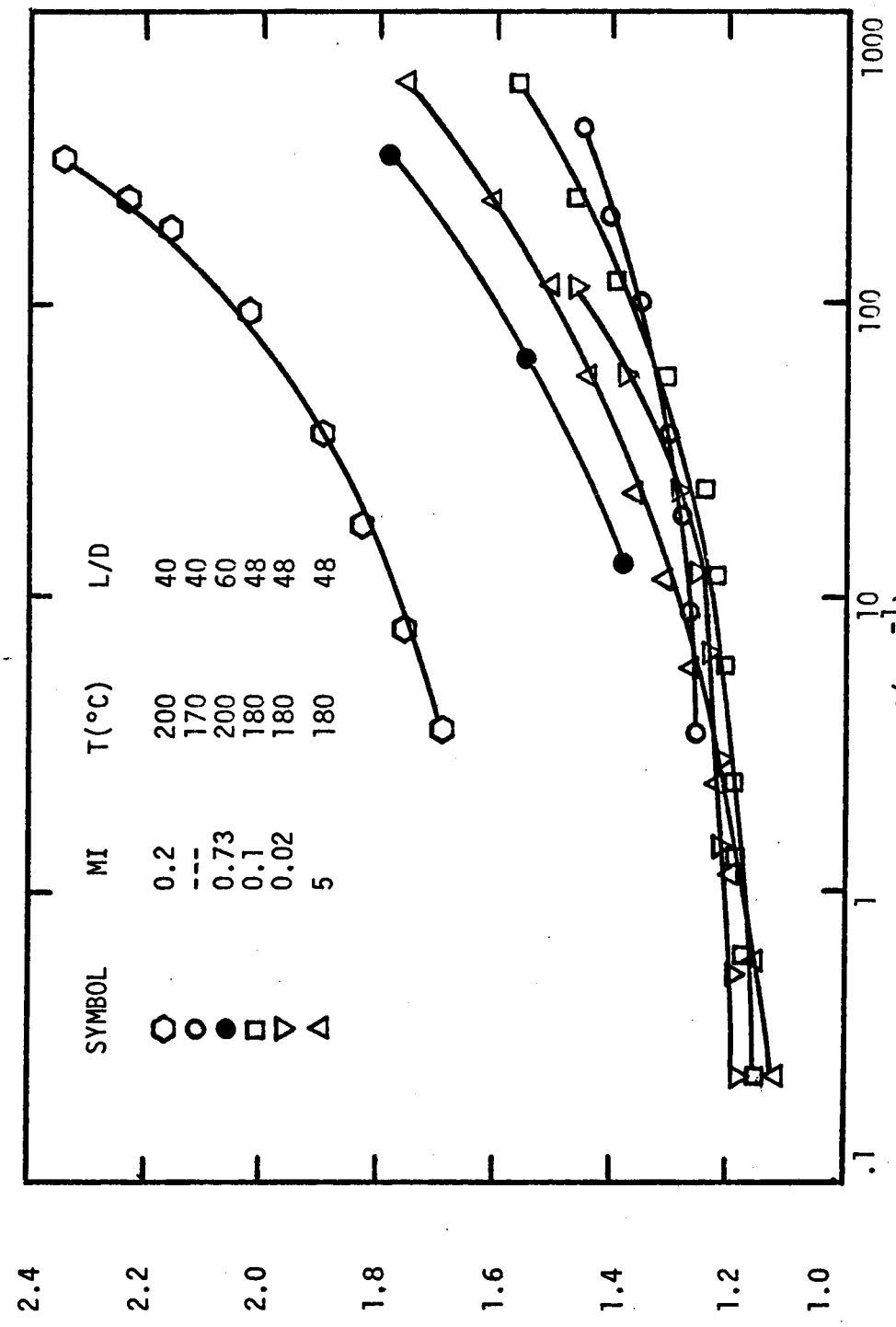

Figure 48. Comparison of Experimental and Literature Values of Frozen Die Swell as a Function of Shear Rate for HDPE

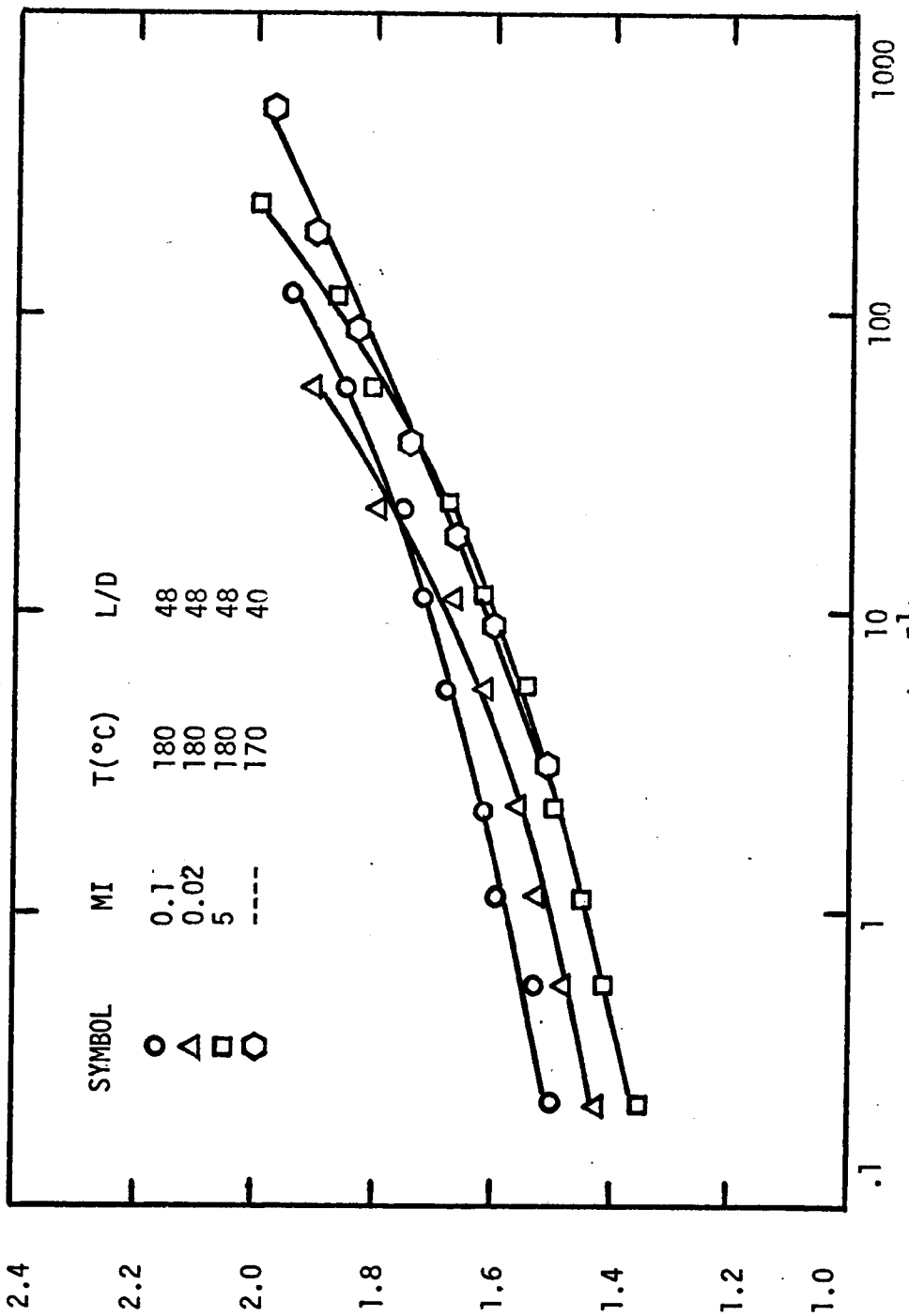

Figure 49. Comparison of Experimental and Literature Values of Annealed Die Swell for HDPE's as a Function of Shear Rate

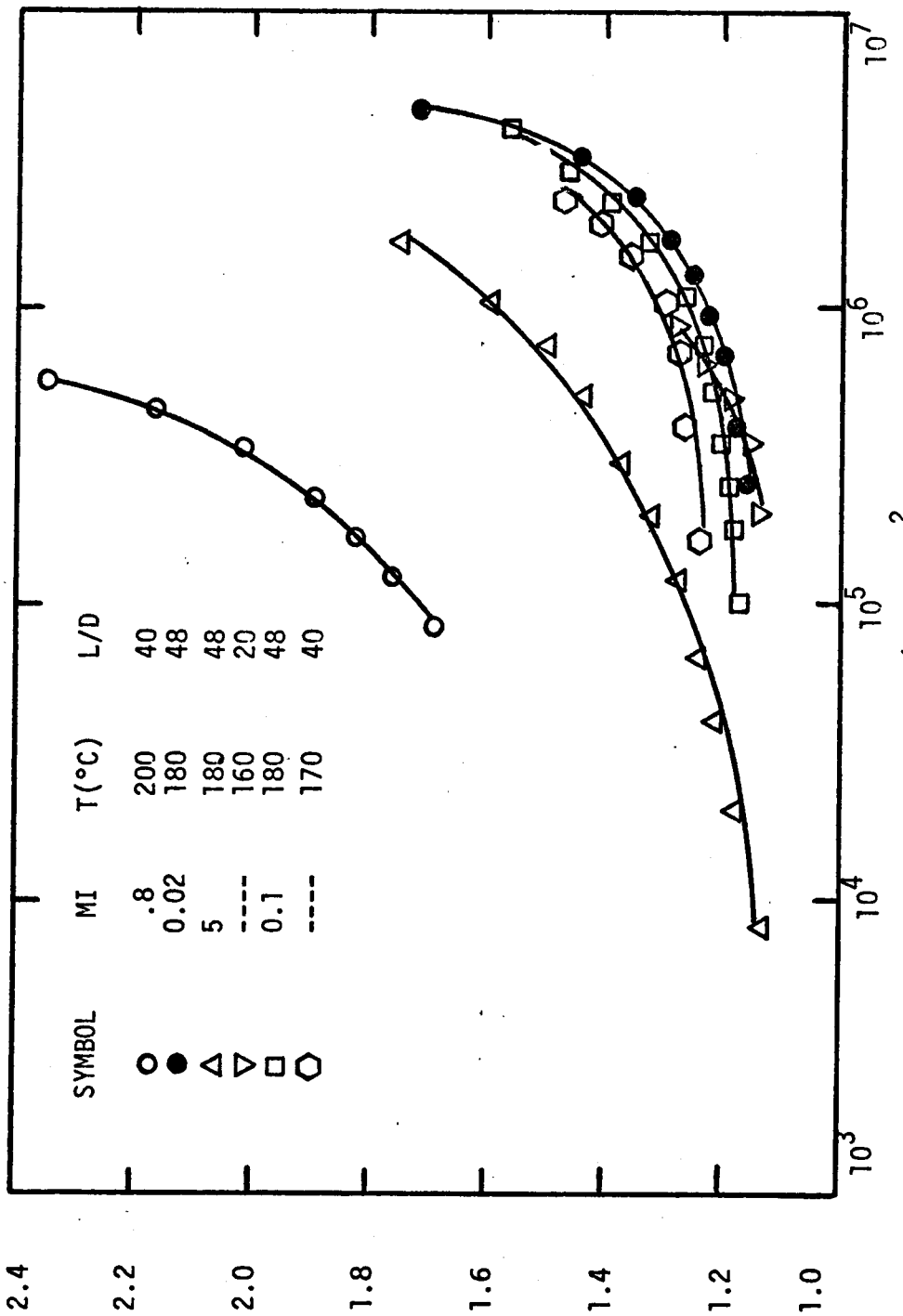

Figure 50. Comparison of Experimental and Literature Values of Frozen Die Swell as a Function of Shear Stress for HDPE

melts studied.

Figure 51 compares the die swell as a function of $\frac{N_1 w}{(\tau_{12})_w}$ for experimental and literature values. Shown are the polymers discussed in the previous paragraph. The data is quite spread out. The plot of $\frac{N_1 w}{(\tau_{12})_w}$ versus die swell for the six polymer melts studied show closer agreement than just comparing HDPE's.

High and Low Density Polyethylene

The die swell of high and low density polyethylenes as a function of shear rate are shown in Figure 52. Included are the data of Mendelson and Rogers previously discussed for HDPE, LDPE melt index unknown used by Mendelson (45) and experimental data for LDPE and HDPE's. There is much scatter between the curves, however, the two LDPE curves agree reasonably well. The data for the six polymer melts shows better agreement when compared than does the data for this family of polymers.

The die swell of annealed LDPE is shown as a function of shear rate in Figure 53. This consists of experimental data and data compiled by Mendelson for the LDPE mentioned previously. The swell in both cases was roughtly the same magnitude.

Figure 54 shows the die swell of HDPE's and LDPE's as a function of shear stress. Included are experimental data of the HDPE's and LDPE's used in this work, Mendelson's HDPE and LDPE data as previously discussed and Lee's (39) HDPE data discussed in the previous section. The LDPE's agree quite well, along with HDPE MI = 5, the rest of the data is scattered. These melts show less agreement than the data shown

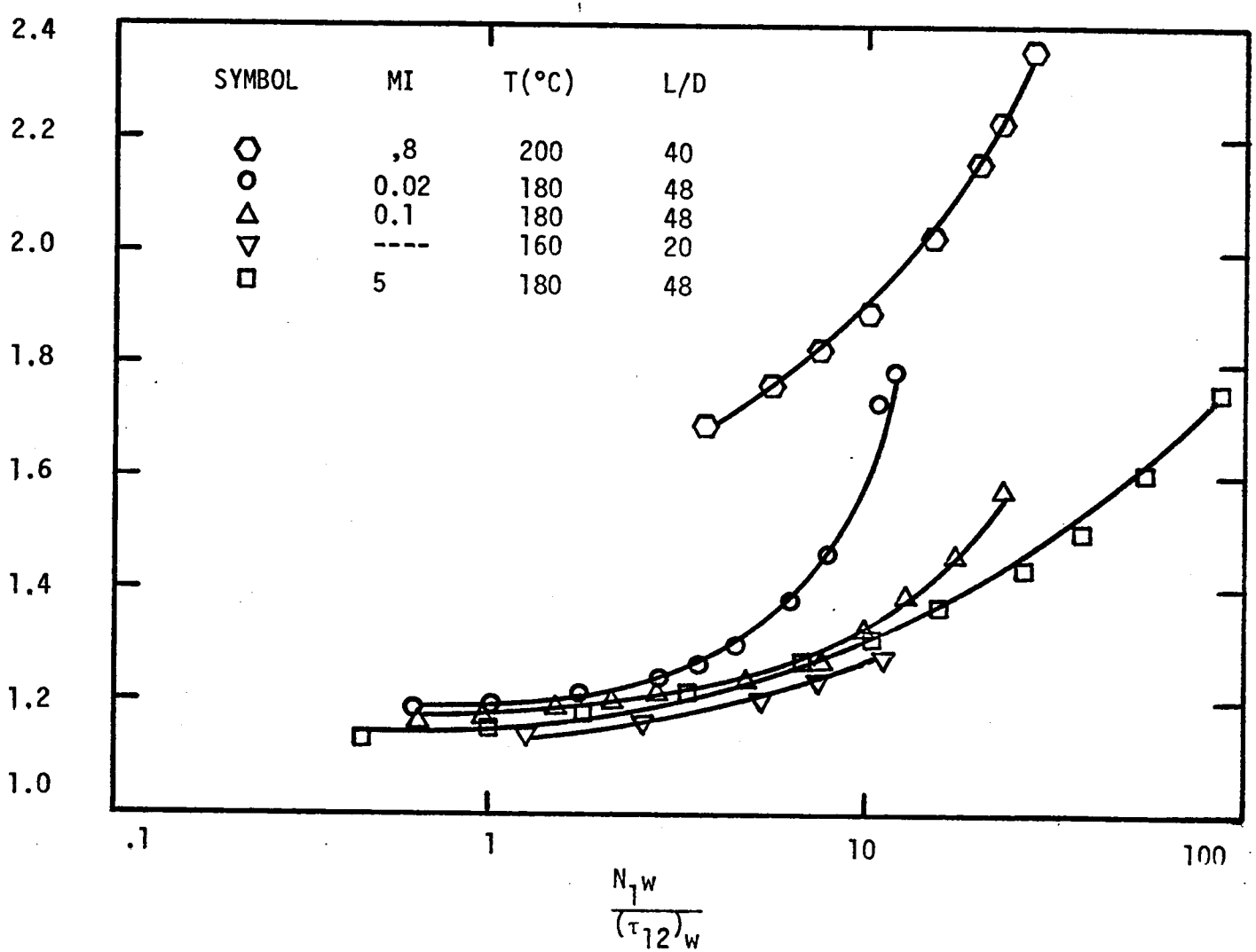

Figure 51. Comparison of Experimental and Literature Values of Frozen Die Swell as a Function of $\frac{N_1 w}{(\tau_{12})_w}$ for HDPE

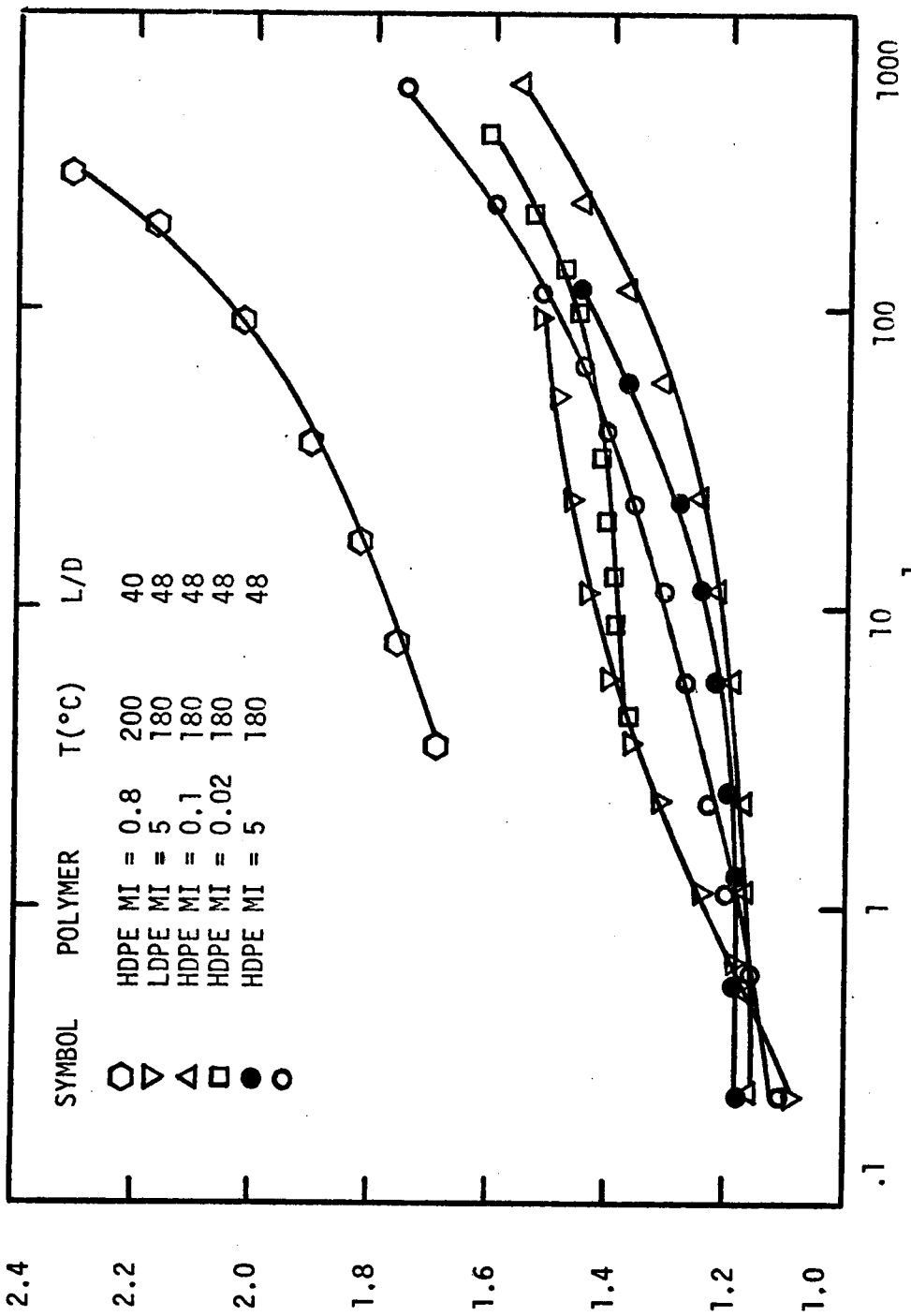

Figure 52. Comparison of Experimental and Literature Values of Frozen Die Swell as a Function of Shear Rate for HDPE and LDPE

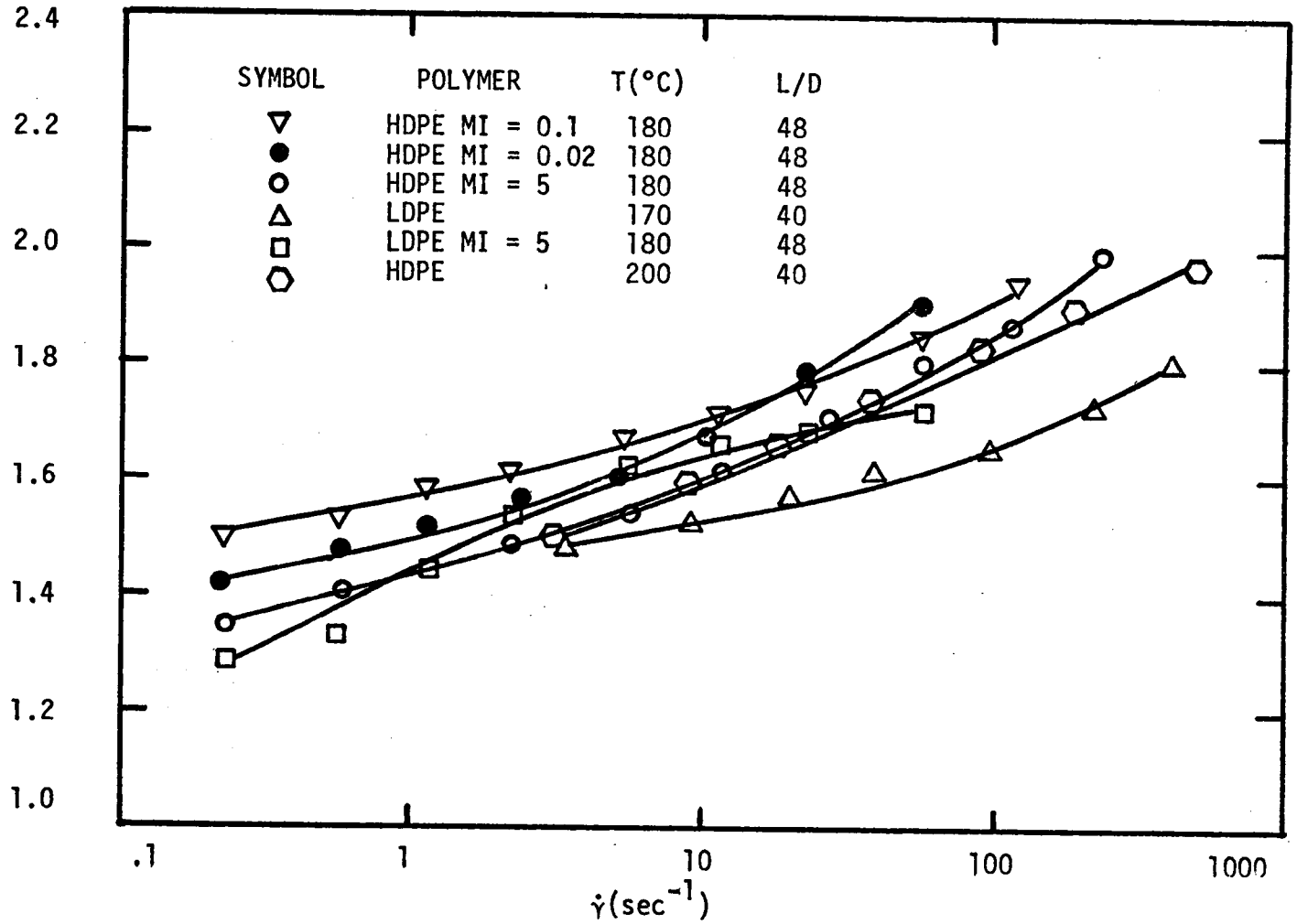

Figure 53. Comparison of Experimental and Literature Values of Annealed Die Swell as a Function of Shear Rate for HDPE and LDPE

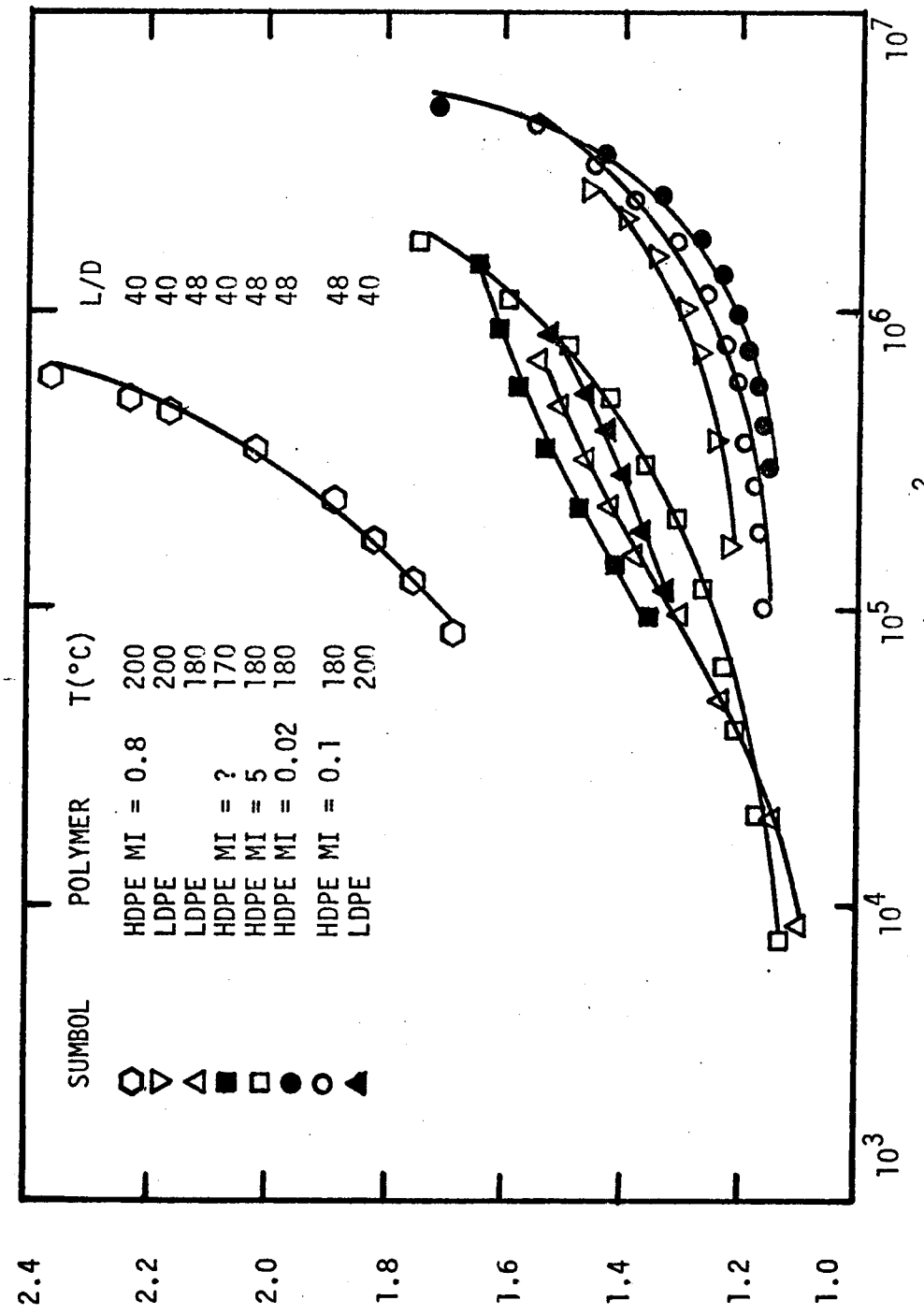

Figure 54. Comparison of Experimental and Literature Values of Frozen Die Swell as a Function of Shear Stress for HDPE and LDPE

for the six polymer melts used in this work.

Figure 55 shows LDPE and HDPE data for the swell as a function of $\frac{N_1 w}{(\tau_{12})_w}$. Shown are the HDPE MI = 0.2 of Mendelson, Lee's HDPE and experimental results. Again there is much scatter between the data and there is less agreement for melts of this general family than for the combination of melts studied.

E. COMPARISON WITH VARIOUS THEORIES

There have been several theories of die swell. These consist of the theories set forth by Tanner (66), Graessley (29) and Bagley (2). The experimental data for frozen die swell is shown as a function of $\frac{N_1 w}{(\tau_{12})_w}$ in Figure 56 compared to predictions of die swell from Graessley, Bagley, Tanner and Equation 53 in this paper. The HDPE MI = 0.02 and the PS appear to agree reasonably well with Tanner's prediction. The other polymer melts show very little agreement with any of the predictions. Tanner, however, assumed isothermal flow in his analysis and these data are not nearly isothermal, containing frozen in stresses.

Figure 57 shows the die swell measured from photographs compared with theory. Most of the polymers agree fairly well with Tanner's analysis, except for the HDPE MI = 5 which is far from the theoretical curves, especially at high values of $\frac{N_1 w}{(\tau_{12})_w}$. The LDPE shows a different character than the theoretical curves, but falls in the same general area as the theoretical curves. Thus, it agrees in general placement of the data points, if not in the shape of the

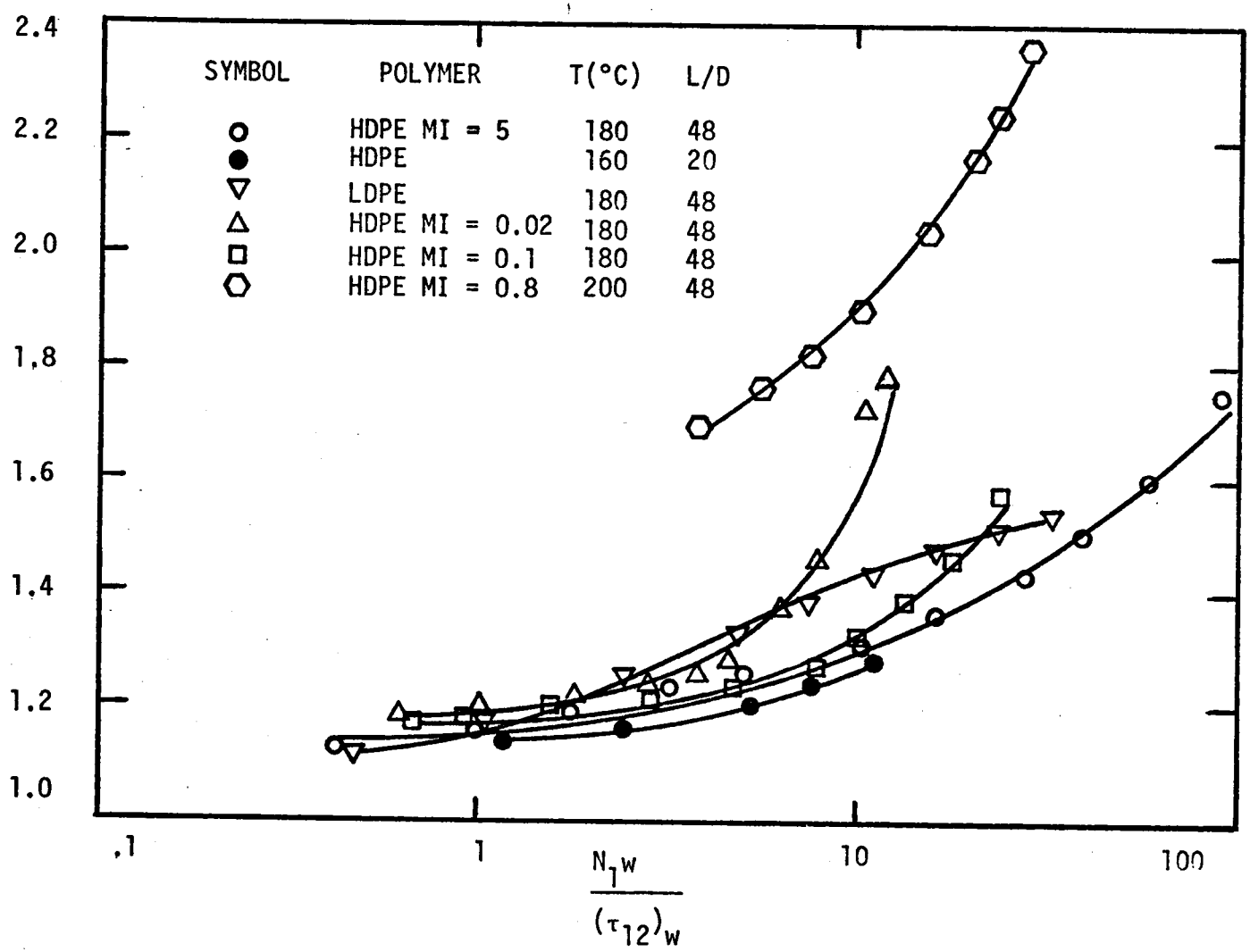

Figure 55. Comparison of Experimental and Literature Values of Frozen Die Swell as a Function of $\frac{N_1 w}{(\tau_{12})_w}$ for HDPE and LDPE

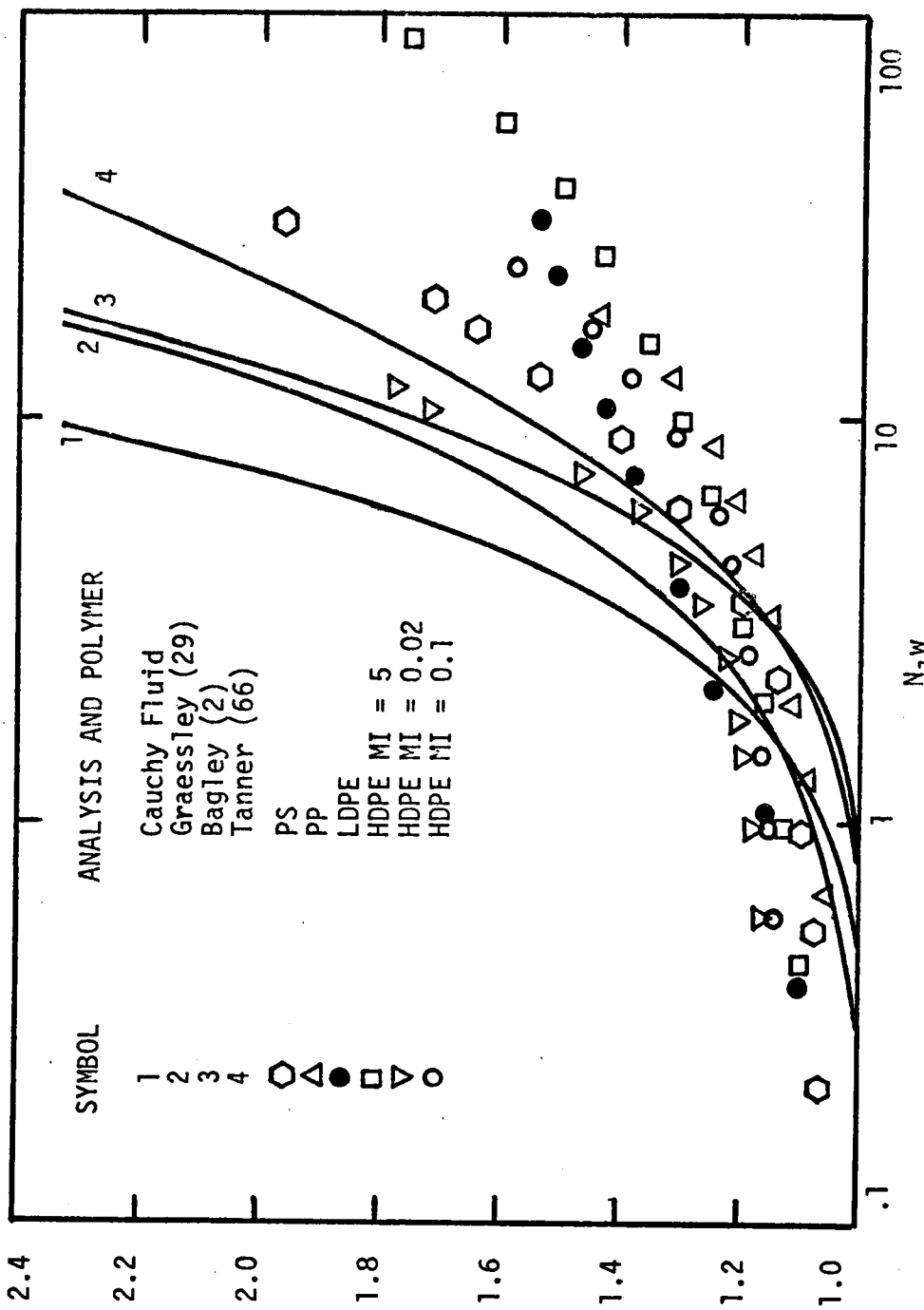

Figure 56. Comaprison of Experimental Frozen Die Swell Measurements with Predictions

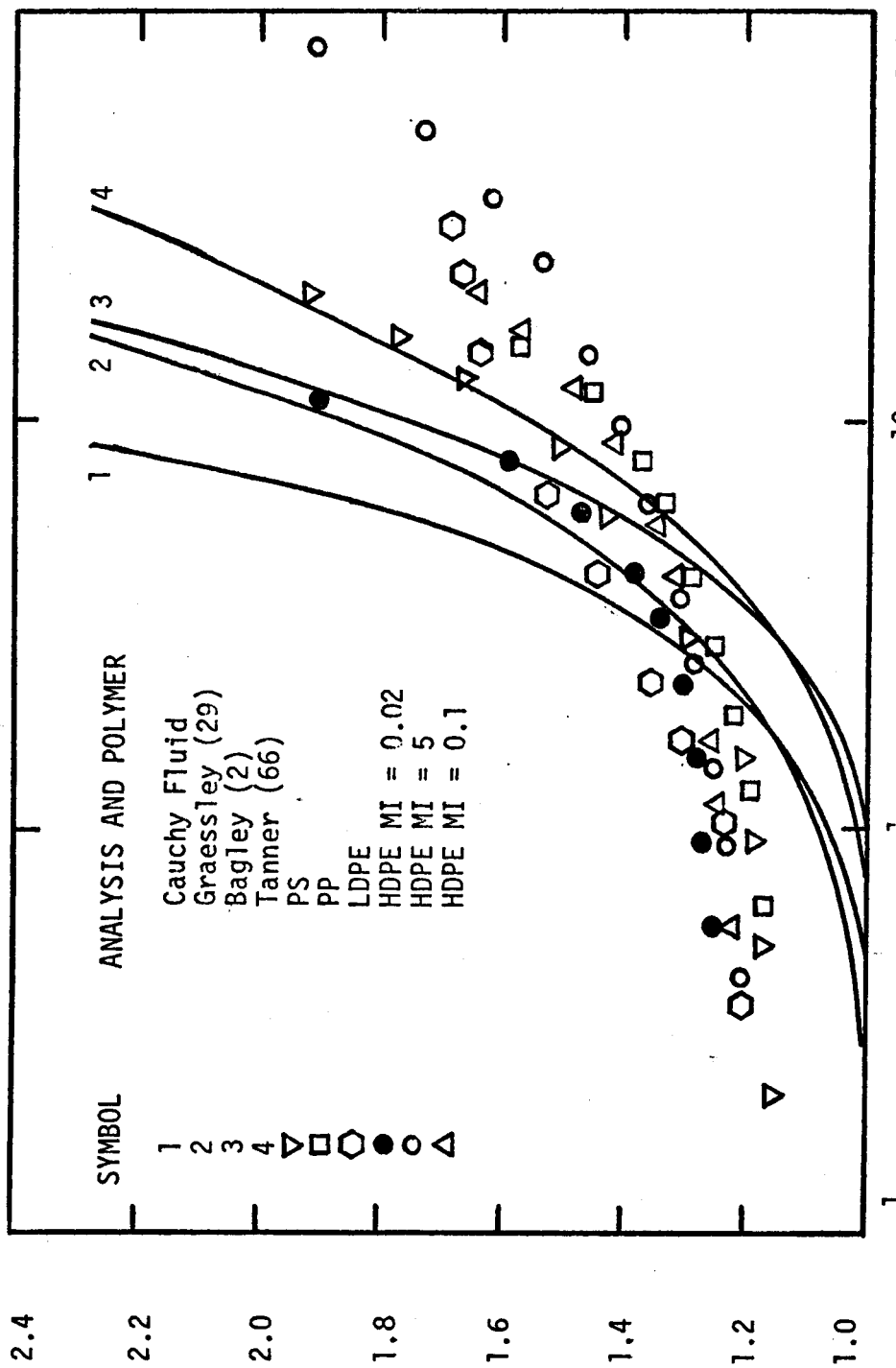

Figure 57. Comparison of Experimental Die Swell Measured from Photographs with Predictions

curve itself.

The die swell of the annealed extrudates compared with theory are shown in Figure 58. The annealing was essentially done to release frozen in stresses in the cooled extrudates. This comparison should then agree more closely with theory than either the frozen or pictorial data. The experimental die swell at low $\frac{N_1 w}{(\tau_{12})_w}$ is well above the predictions except for the PS and PP. The PS falls generally between Graessley's and Tanner's predictions. The PP data generally follows Tanner's predictions. The HDPE MI = 0.02 and HDPE MI = 0.1 data show a large deviation from all predictions at low values of $\frac{N_1 w}{(\tau_{12})_w}$, but at higher values of $\frac{N_1 w}{(\tau_{12})_w}$ fall between the theoretical predictions of Equation 53 and Tanner. Data points for LDPE and HDPE MI = 5 fall between the theoretical predictions only in a small interval of $\frac{N_1 w}{(\tau_{12})_w}$ from two to fifteen and differ significantly from predictions at high values of $\frac{N_1 w}{(\tau_{12})_w}$.

The isothermal die swell should give the best correlation with predictions, since isothermal flow was an assumption. This data is shown as a function of $\frac{N_1 w}{(\tau_{12})_w}$ in Figure 59. The die swell is well above that predicted. Equation 53, however, shows the closest agreement to the experimental data. Tanner's prediction differs by the largest amount.

Comparing all polyethylene data to predictions, for frozen extrudates only, we observe that only two of the HDPE's agree with predictions as seen in Figure 60. These are the HDPE MI = 0.02 and Mendelson's HDPE MI = .8. The curves for these two polymers lie between

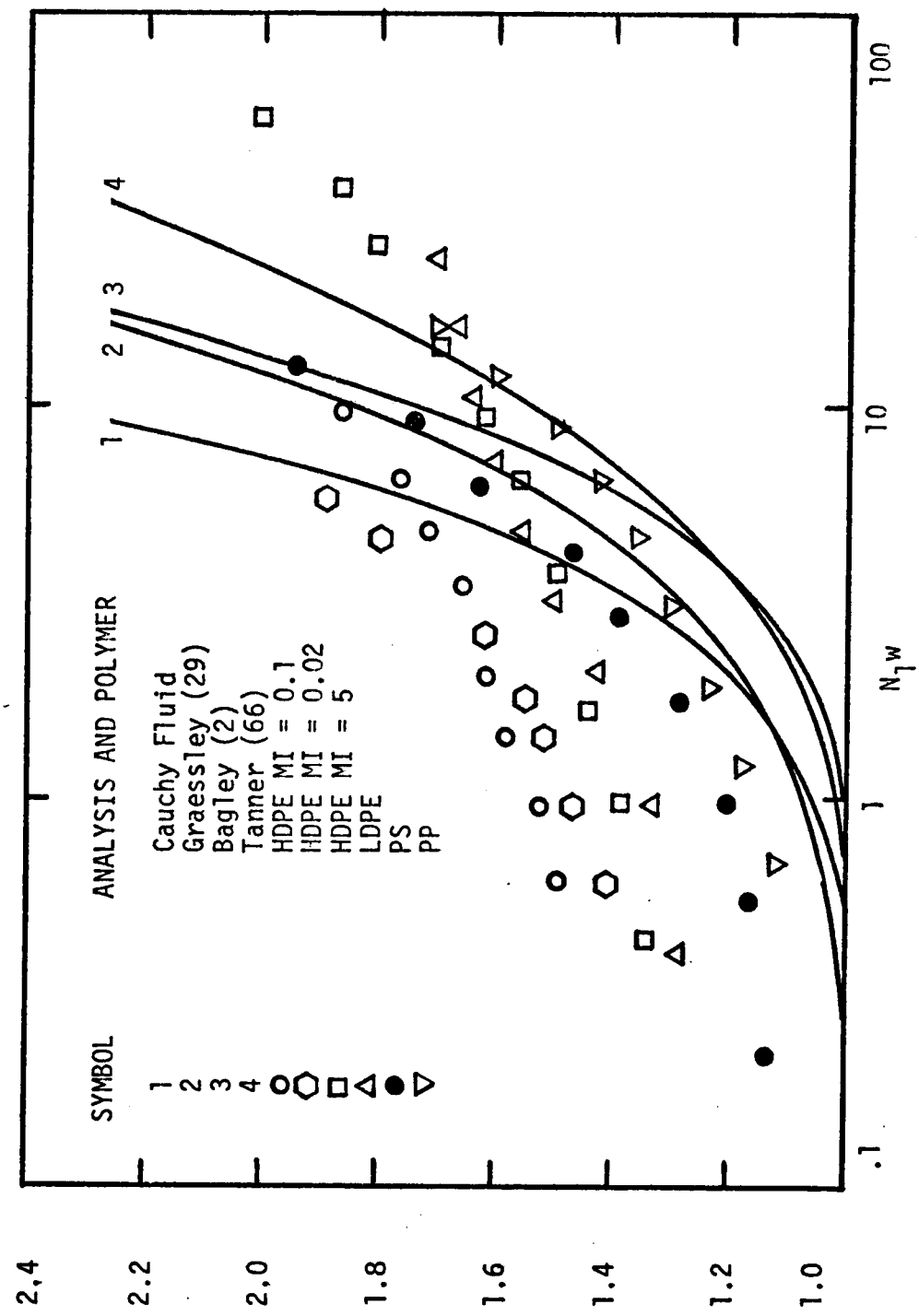

Figure 58. Comparison of Experimental Die Swell of Annealed Extrudates with Predictions

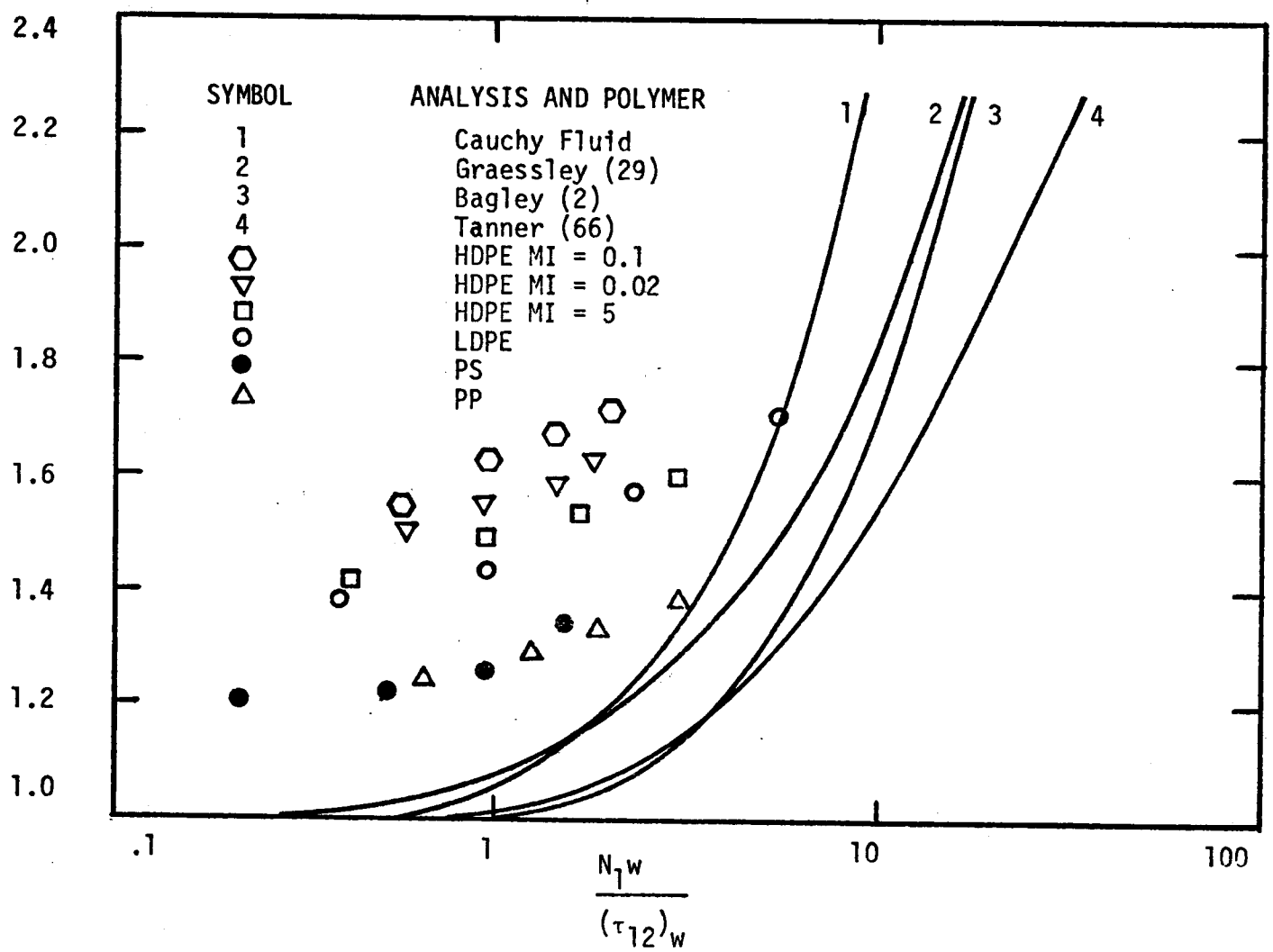

Figure 59. Comparison of Experimental Isothermal Die Swell with Predictions

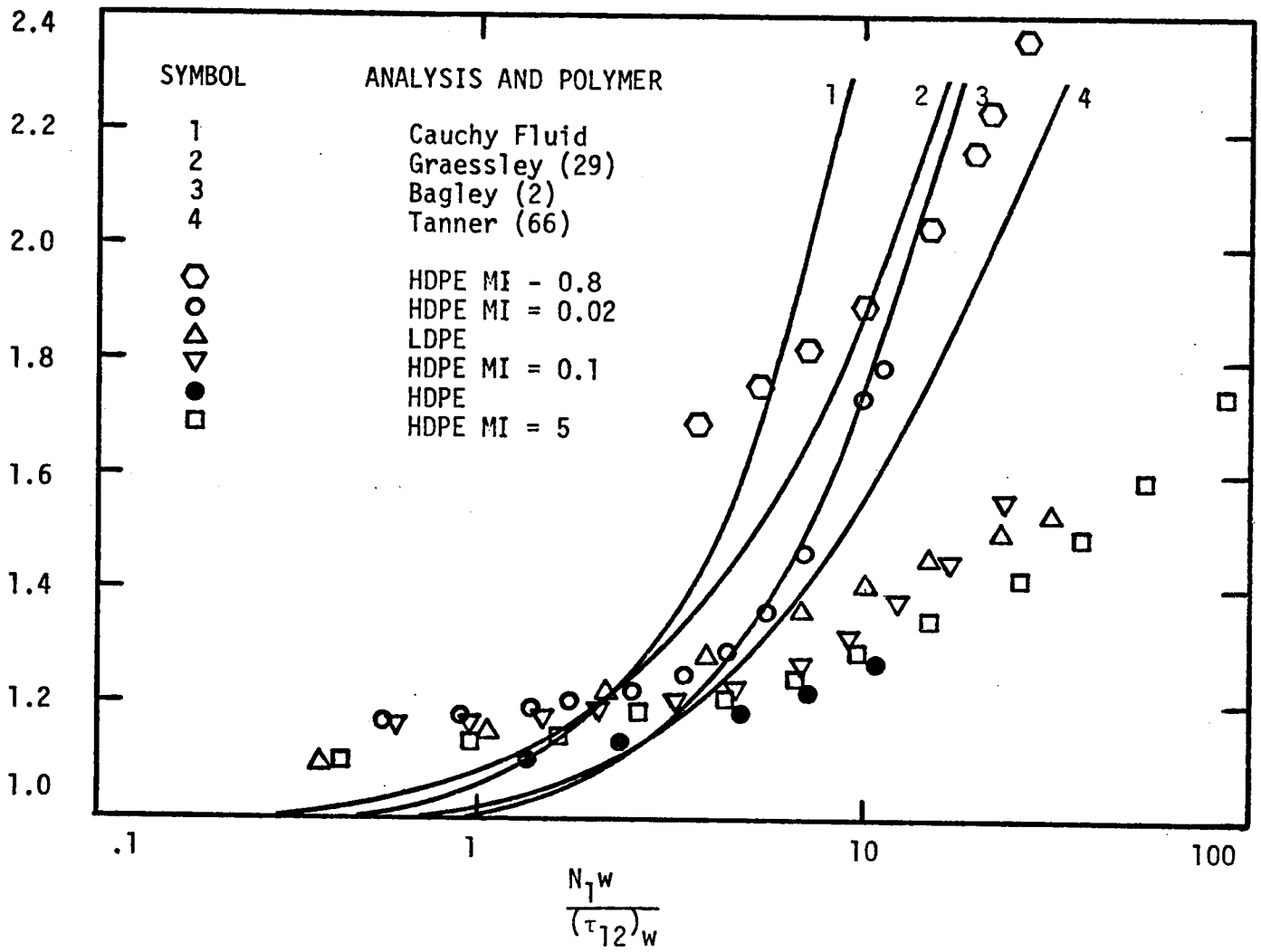

Figure 60. Comparison of Experimental and Literature Values of Frozen HDPE and LDPE Die Swell with Predictions

the predictions of Equation 53 and Tanner. The other polymers lie outside of these predictions at values of $\frac{N_1 w}{(\tau_{12})_w}$ exceeding five.

Figure 61 shows a comparison of PS and PP data for long L/D dies. Included is literature data discussed in the previous section. The curves for the frozen extrudates follow Tanner's theoretical curves. We observe that the PS with highest viscosity falls between Equation 53 and Tanner's predictions. The lowest viscosity PS follows Tanner's curve and lies just outside the area bounded by Equation 53 and Tanner's curves. The intermediate viscosity PS lies between the other two. The PP curve has generally the same shape as the PS curves. The PP curve lies primarily outside of area bounded by Equation 53 and Tanner's curves, except at low values of $\frac{N_1 w}{(\tau_{12})_w}$.

It would appear that the PS and PP data fit theoretical predictions much better than HDPE and LDPE data.

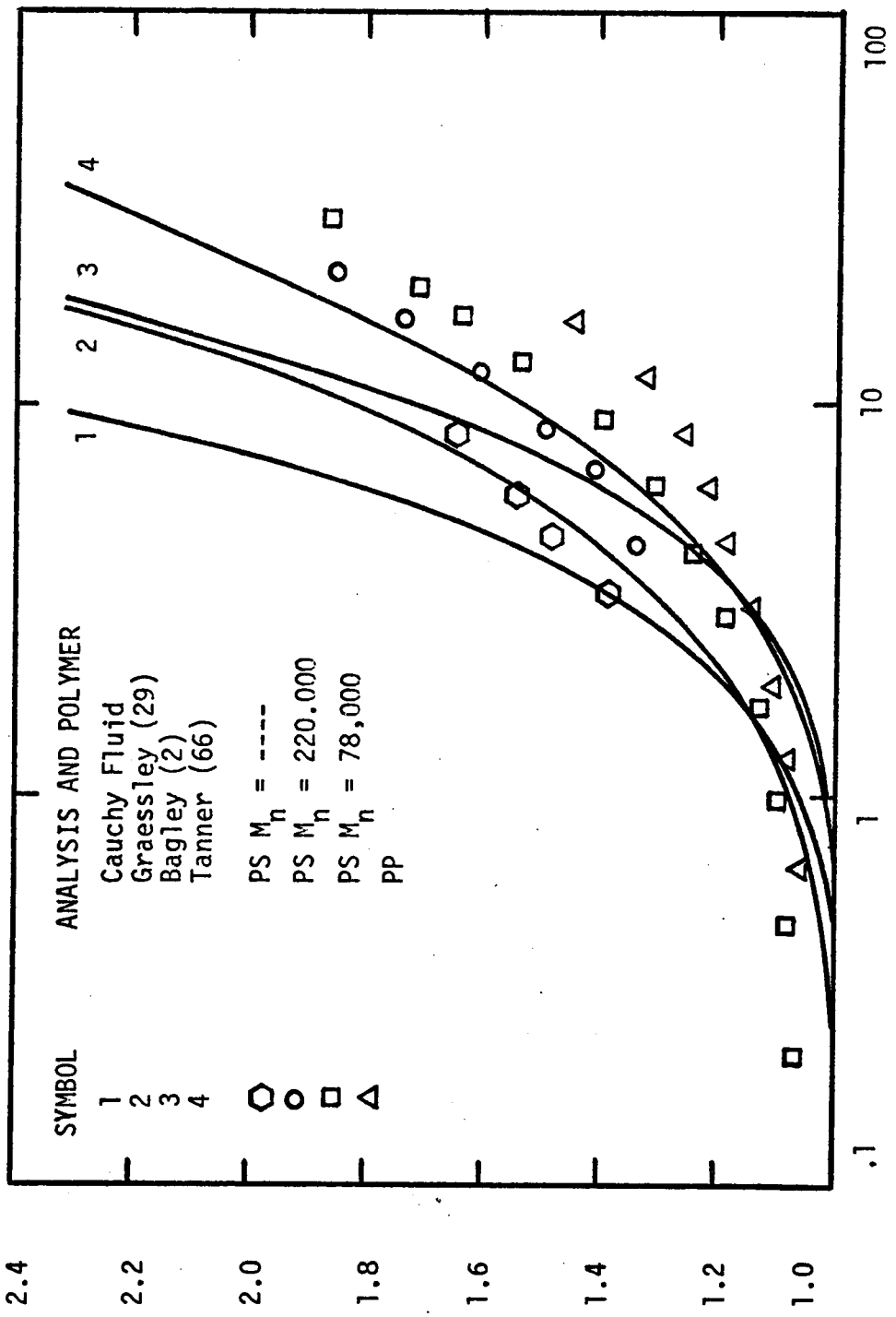

Figure 61. Comparison of Experimental and Literature Values of Frozen Die Swell of PS and PP with Predictions

CHAPTER VI

DIE SWELL UNDER APPLIED TENSION

A. INTRODUCTION

In the melt spinning of fibers, molten polymers exit from a die and are drawn down by applied forces. The normal amount of die swell obtained in extrusion is decreased by the action of the applied forces. In this chapter, we will investigate the magnitude of this reduction and its dependence upon applied forces.

B. EQUIPMENT

The polymers were fed into a one-inch Modern Plastics Machinery screw extruder. The melt was then forced through screens into a metering pump and into a single hole capillary die. The die which was used had a diameter of 0.062 inches and an L/D ratio of ten. The take-up device was driven by a 0-4000 RPM motor controlled by a Heller motor controller. The fiber was wound on a spool-type take up.

The pump block head containing the metering pump and the spinneret was maintained at the desired temperature using a three mode controller.

Fiber tensions were measured with a Rothschild tensiometer using a 0-10 gram range measuring head. In using this device one is limited by the size of the fiber on which the tension can be measured.

C. PROCEDURE

Three polymers were chosen to be melt spun. These consisted of PP, HDPE MI = 5 and HDPE MI = 0.1. Nine experimental runs were made. The flow rate was held constant and the tension on the fiber was varied by increasing the take-up speed. The temperature used was 180°C.

For a given run, photographs were taken of the fiber as it emerged from the spinneret. The mass flow rate was determined for the run by dividing the weight of the fiber produced by the time to produce it for each run. The tension for that take-up velocity was measured using the tensiometer readings and then time averaging them when the readings varied. During some take-up times the tension was constant and time averaging was not necessary.

A 35mm camera with fine grain film was used to take the photographs with an enlargement varying from 1/1 to 2/1 depending upon the experiment. The negatives were "blown up" on a grid screen using a slide projector and the diameter of the fiber was measured. The diameter of the fiber was measured at a point approximately 0.2 inches below the spinneret. The diameter of the fiber at this point appeared to be the maximum. Enlargement on the grid screen was 50/1 to 100/1 depending upon the run.

D. RESULTS

The HDPE MI = 0.1 appeared to be unspinable at this temperature. The fiber was observed to break at even the slightest tension and

slowest take-up velocities, shown in Figure 62.

The PP fiber was spinable at 180°C and the die swell was observed to decrease rapidly as tension was first applied and then to decrease more slowly as more tension was applied. The tension was observed to reach almost a plateau. The tension increased as the take-up velocity increased for a period but then appeared to almost level off. At this point large increases in take-up velocity showed little change in tension. The die swell as a function of fiber tension is also shown in Figure 62.

The HDPE MI = 5 was observed to have decreasing die swell at increasing tensions. The die swell was observed to decrease abruptly as tension was first applied, but after the tension reached 0.75 grams, large increases in tension produced only small changes in the die swell. This is analogous to what was observed for PP. The tension was also observed to increase with take-up velocity to a point, and then large changes in take-up velocity produced only small changes in tension. This is similar to observations for PP. The behavior of the die swell as a function of tension is shown in Figure 62.

Figure 62 also shows a comparison of the die swell of the three polymers as a function of tension. The HDPE MI = 0.1 shows the highest die swell at zero tension, but as the tension increased the fiber broke. The HDPE MI = 5 shows die swell in the range of 1.5-1.6 at zero tension. As the tension increased, the die swell decreased. The PP showed the least die swell at zero tension, being approximately 1.5. The PP die swell is consistently lower than that of the polyethylene. Figure 63 shows the die swell as a function of take-up

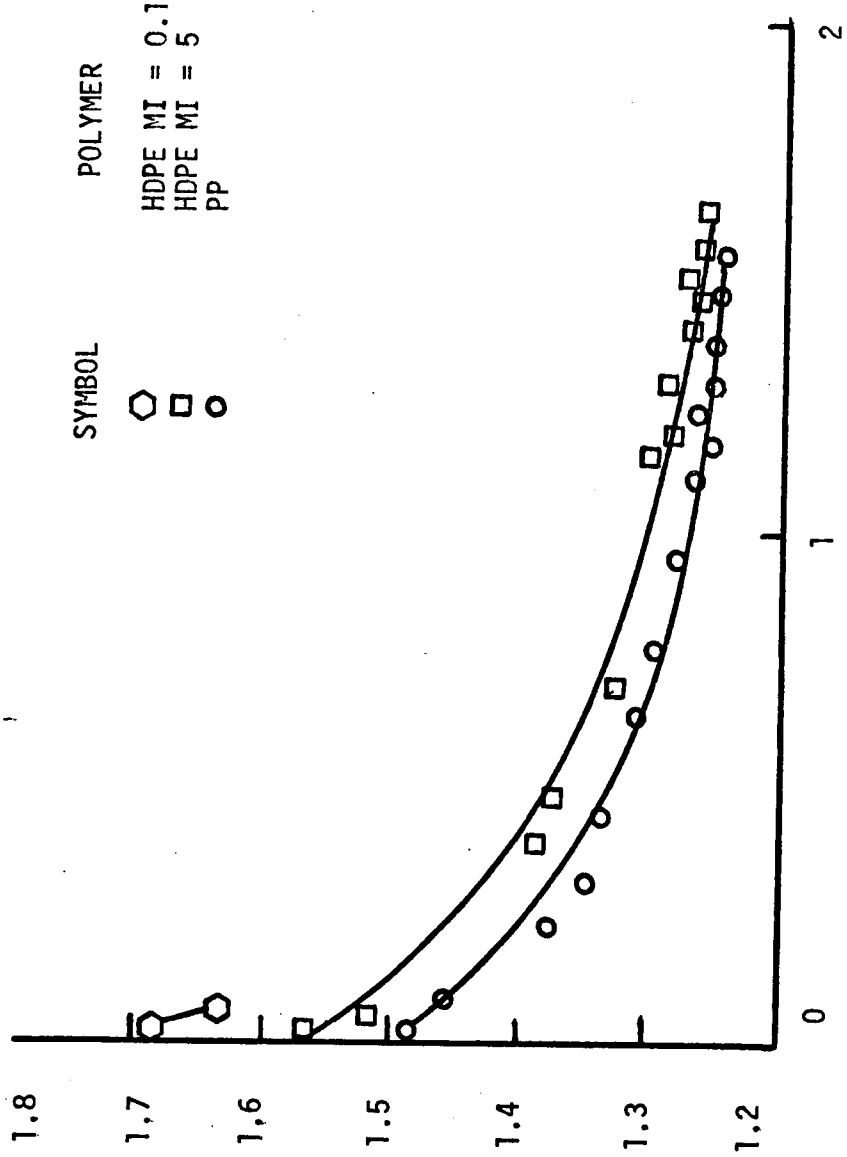

Figure 62. Die Swell as a Function of Tension

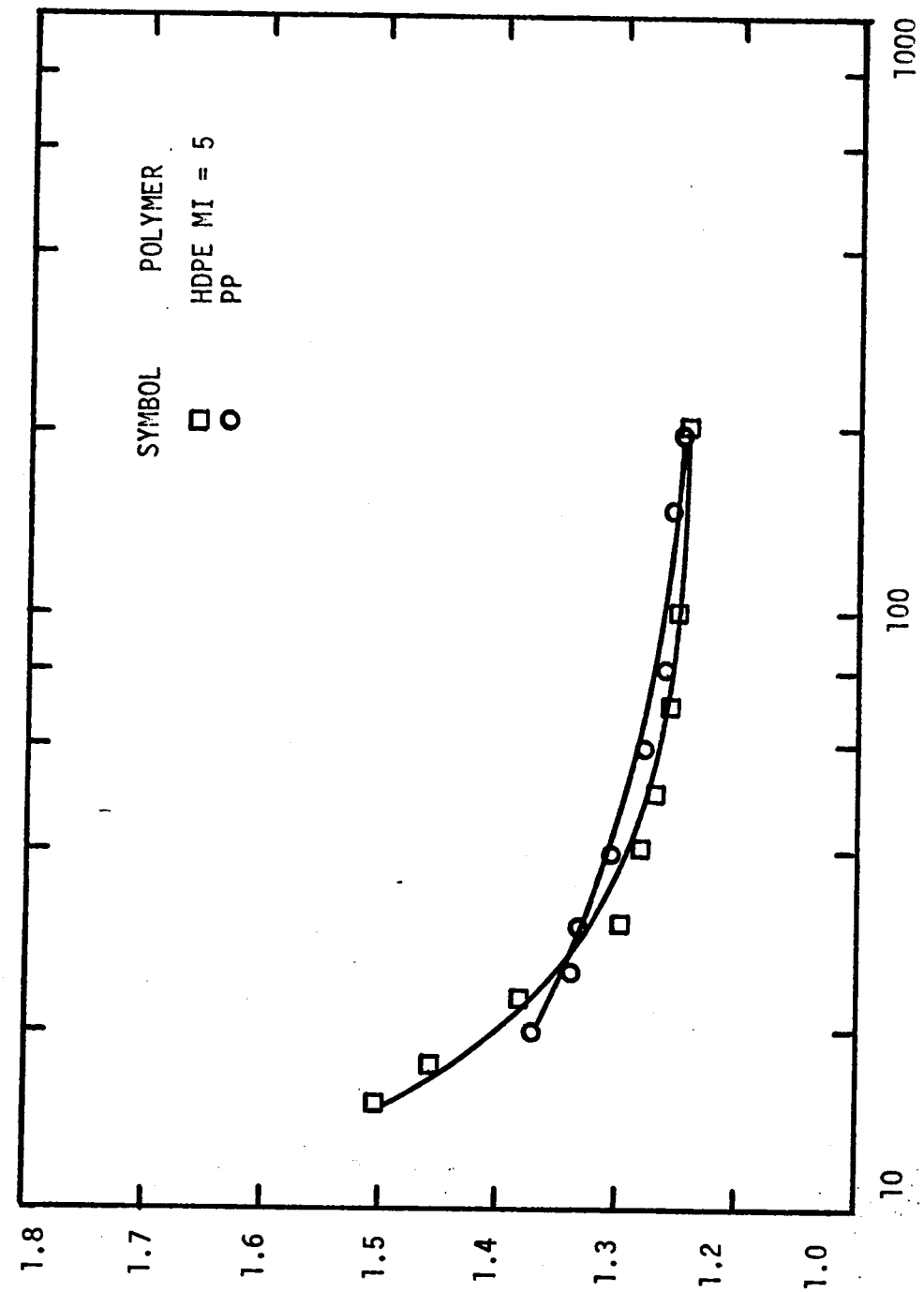

Figure 63. Die Swell as a Function of Take-up Velocity

velocity. This shows that the HDPE MI = 5 has a greater fiber tension at a given take-up velocity than the PP.

Figure 64 shows the die swell as a function of stress. The HDPE MI = 5 shows a higher die swell than the PP over the range of stresses observed.

The die swell at zero tension measured from the extruder data can be compared to die swell data taken from short L/D dies using the Instron capillary rheometer. The only reasonable comparison would be from photographic data. The flow rate in the extruder corresponded roughly to a shear rate of 10 sec^{-1}. At this shear rate the die swell data taken from the Instron capillary rheometer and that from the extruder are very nearly the same. There is less than five percent difference in the die swell measurements from both apparatuses.

E. INTERPRETATION

We can attempt to analyze this swell in a manner similar to Tanner's analysis (66). Tanner assumed a tension free jet such that

$$2\pi \int_0^R \tau_{zz}\, r\, dr = 0 \qquad (54)$$

It is supposed that the residual stresses τ_{zz} relax away or are dissipated through a slow viscoelastic flow after emergence from the die. For a fiber under tension, this would be

$$2\pi \int_0^R \tau_{zz}\, r dr = S \qquad (55)$$

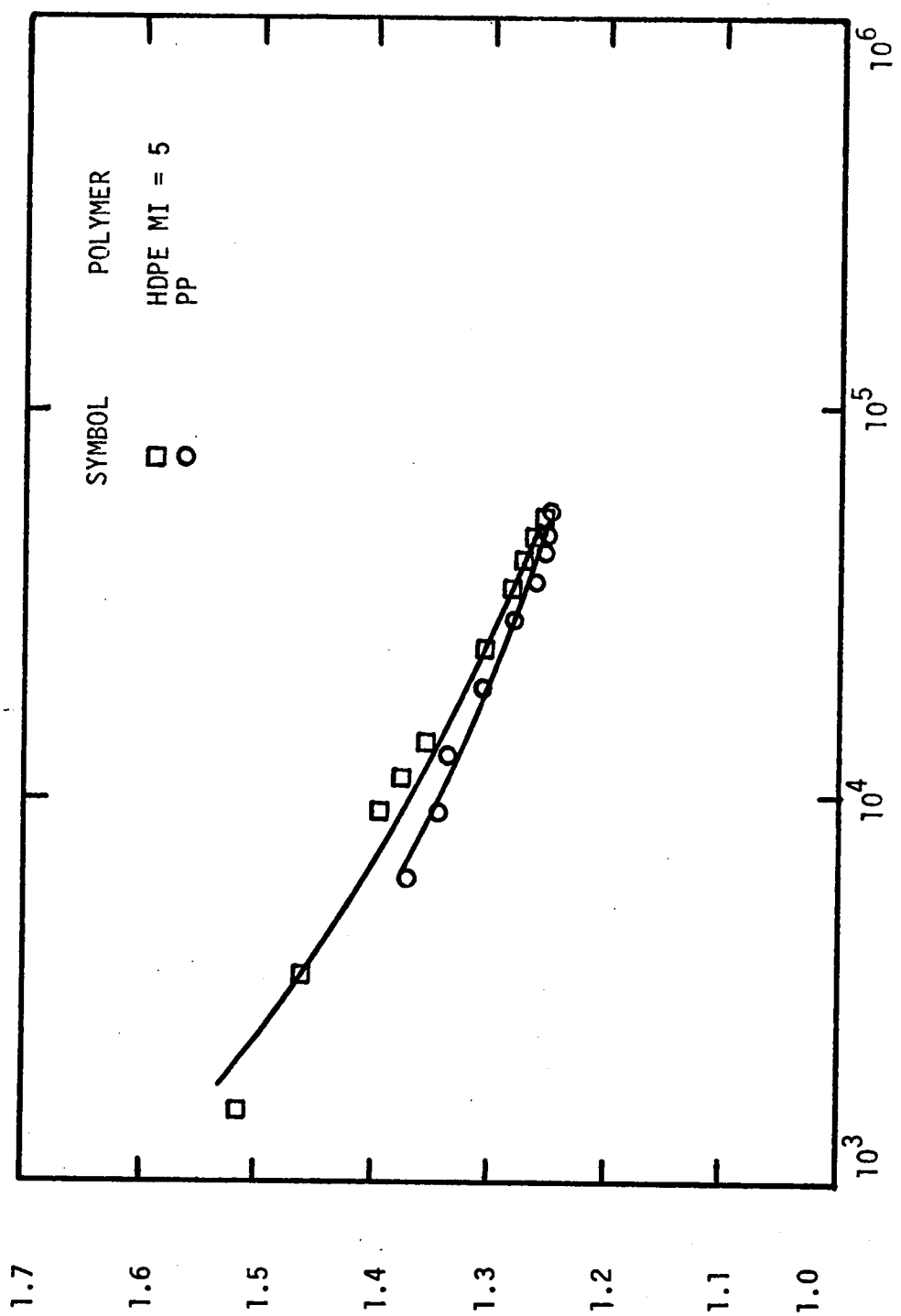

Figure 64. Die Swell as a Function of Stress

where S is the tension on the fiber. Thus, following Tanner's analysis,

$$N_1 + G - \tau_{zz}/\alpha^4 = H^* \left[\frac{1}{\alpha^4} + f'^2 \right] \tag{55}$$

Since $G = H^* \alpha^2$ and $H^* \alpha f' = \tau_{12}$, we can put Equation (55) in the form

$$N_1 + G - \tau_{zz}/\alpha^4 = G/\alpha^6 + \tau_{12}^2/G \tag{56}$$

Then, integrating over the cross section gives an equation for the radial expansion

$$\int_0^R (N_1 + G - \tau_{12}^2/G)\, 2\pi r dr = \frac{1}{\alpha^6} \int_0^R 2\pi r\, G\, dr$$

$$- \frac{1}{\alpha^4} \int_0^R \pi r \bar{\tau}_{zz}\, dr \tag{57}$$

or,

$$\left[1 + \frac{1}{2} \frac{N_1}{\tau_{12}}\right] = \left(\frac{D_j}{D}\right)^6 + \left(\frac{D_j}{D}\right)^4 \frac{\bar{\tau}_{zz}}{G} \tag{58}$$

Rearranging, and remembering $\left[1 + \frac{1}{2} \frac{N_1}{\tau_{12}}\right] = \left[\frac{D_j}{D}\right]^6_{\tau_{zz}} = 0$

$$\left[\frac{D_j}{D}\right]^6_{\tau_{zz}=0} = \left[\frac{D_j}{D}\right]^6 + \left[\frac{D_j}{D}\right]^4 \frac{\bar{\tau}_{zz}}{G} \tag{59}$$

$$\left[\frac{D_{\tau_{zz}}}{D_o}\right]^6 = 1 - \left[\frac{D^2}{D_o^6} \frac{D^4_{\tau_{zz}}}{}\right] \left[\frac{\bar{\tau}_{zz}}{G}\right] \tag{60}$$

where D_o is the diameter of the jet at zero tension. This is plotted in Figure 65 with $\frac{D\tau_{zz}}{D_o}$ as a function of $[\frac{D^2D^4\tau_{zz}}{D_o^2}]\,[\bar{\tau}_{zz}]$. The PP curve appears to lie above that of the HDPE MI=5.

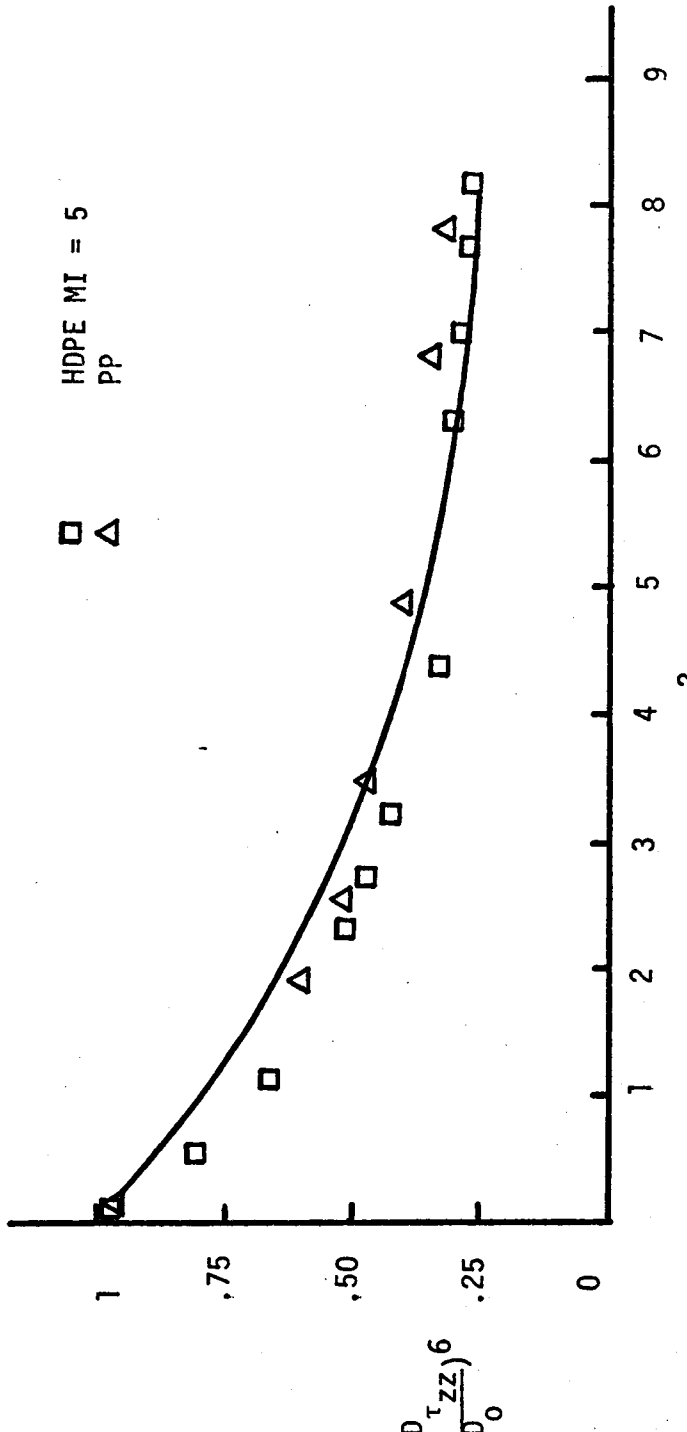

Figure 65. $\left[\frac{D_{\tau_{zz}}}{D_o}\right]^6$ as a Function of $\left[\frac{D_{\tau_{zz}}}{D_o^6}\ \tau_{zz}\right]$.

CHAPTER VII

CONCLUSIONS

(1) The first normal stress difference and the viscosity were measured using a Weissenberg rheogoniometer for six polymer melts at 180°C. In addition, the viscosity of the same melts was measured at a large shear rate range in the Instron capillary rheometer.

(2) The die swell of the six polymer melts was measured in four different ways: (a) from frozen extrudates, (b) from photographs of the emerging extrudate, (c) from extrudates annealed in a silicone oil bath, (4) from photographs of extrusion into a hot silicone oil bath, approaching isothermal extrusion. The data from the annealed and isothermal extrudates appeared to separate into two groups when plotted as a function of $\frac{N_1 w}{(\tau_{12})_w}$. These groups consisted of (1) PS and PP and (2) the HDPE's and LDPE. When compared to plots of frozen extrudate data, the annealed and isothermal data showed a larger magnitude of die swell and appeared to reorder itself because of the varying amount of residual stresses released.

(3) The predictions of die swell can vary depending upon the strain tensor used in the analysis. Calculations of unconstrained recovery using a Cauchy tensor predicts greater die swell because of greater recovery perpendicular to the shear direction, compared to calculations based upon the Finger tensor. The analyses based upon unconstrained recovery predicts different results if we assume

varying τ_{12} and recovery with position and integrate die swell across the radius, as opposed to assuming constant recovery and letting the residual axial stresses vary across the radius of the jet. Different theories of die swell due to Bagley and Graessley are also considered.

The predictions of Tanner are much lower than observed data for isothermal and annealed extrudates in the case of HDPE's and LDPE. The annealed PS and PP data agree reasonably well with Tanner's predictions and appear to fall between predictions based on the Cauchy tensor and Finger tensor. The isothermal data for the HDPE's and LDPE is well above all predictions.

(4) The die swell of polymer melts under tension was measured photographically. Initially applied tension had a marked effect on the die swell, but as the tension was increased, the effect became smaller.

BIBLIOGRAPHY

BIBLIOGRAPHY

1. Acierno, D., J. N. Dalton, J. M. Rodriguez and J. L. White, J. Appl. Poly. Sci., 15, 2395 (1971).

2. Bagley, E. G. and H. J. Duffey, Trans. Soc. Rheol., 14, 545 (1970).

3. Bagley, E. B., S. H. Storey and D. C. West, J. Appl. Poly. Sci,

4. Ballenger, T. F., M.S. Thesis in Chemical Engineering, The University of Tennessee, March 1971.

5. Ballenger, T. F., I. J. Chen, J. W. Crowder, G. E. Hagler, D. C. Bogue and J. L. White, Trans. Soc. Rheol., 15, 195 (1971).

6. Ballenger, T. F. and J. L. White, J. Appl. Poly. Sci, 15, 1949 (1971).

7. Barus, C., Am. J. of Sci., 45, 88 (1893).

8. Bernstein, B., E. A. Kearsley and L. J. Zapas, Trans. Soc. Rheol., 7, 391 (1963).

9. Bialas, G. A. and J. L. White, Rubber Chem. and Tech., 43, 675 (1969).

10. Bialas, G. A. and J. L. White, Rubber Chem. and Tech., 42, 682 (1969).

11. Bird, R. B. and P. J. Carreau, Chem. Eng. Sci., 23, 427 (1968).

12. Bogue, D. C. and J. L. White, Engineering Analysis of Non-Newtonian Fluids, NATO Agardograph, 144 (1970).

13. Boltzman, L., Sitzgsber Akad. Wisss. Wien., 70, 275 (1874).

14. Chen, I. J., Ph.D. dissertation, University of Tennessee, June 1971.

15. Chen, I. J. and D. C. Bogue, Trans. Soc. Rheol., 16:1, 59 (1972).

16. Chen, I. J., G. E. Hagler, L. E. Abbott, D. C. Bogue and J. L. White, Trans. Soc. Rheol., 16, 473 (1972).

17. Coleman, B. D. and H. Markovitz, J. Appl. Phys., 35, 1 (1964).

18. Coleman, B. D. and W. Noll, Arch. Rat. Mech. Anal, 6, 355 (1960).

19. Cooper, W. M. and W. F. O. Pollett, J. Appl. Polym. Sci., 13, 2313 (1969).

20. Dalton, J. N., M.S. Thesis in Chemical Engineering, The University of Tennessee, August 1971.

21. Dee, H. B., M.S. Thesis in Chemical Engineering, The University of Tennessee, December 1973.

22. deWitt, T. W., J. Appl. Phys., 26, 889 (1955).

23. Dharod, K. C., M.S. Thesis in Chemical Engineering, The University of Tennessee, August 1973.

24. Dillon, J. and Johnston, J. Appl. Phys., 4, 225 (1933).

25. Duda, J. L. and J. S. Vrentas, Chem. Eng. Sci, 22, 857 (1967).

26. Eckert, R. E., J. Appl. Polym. Sci., 7, 1715 (1963).

27. Freeman, S. M. and K. Weissenberg, Nature, 161, 324 (1948).

28. Gavis, J. and M. Modan, Phys. Fluids, 10, 487 (1967).

29. Graessley, W. W., S. D. Glasscock and R. L. Crawley, Trans. Soc. Rheol., 14, 519 (1970).

30. Green, A. E. and R. S. Rivlin, Arch. Rat. Mech. Anal., 1, 1 (1957).

31. Goren, S. L. and S. Wronski, J. Fluid Mech, 25, 185 (1966).

32. Han, C. D., J. Appl. Poly. Sci, 17, 1298 (1973).

33. Han, C. D. and M. Charles, Trans. Soc. Rheol., 14, 213 (1970).

34. Han, C. D., M. Charles and W. Phillipoff, Trans. Soc. Rheol., 14, 393 (1970).

35. Han, C. D., T. C. Yu and K. V. Kim, J. Appl. Polym. Sci., 15, 2567 (1971).

36. Harmon, J., J. Franklin Inst., 259, 519 (1955).

37. Hencky, H., ZAMM, 4, 323 (1924).

38. King, R. G., Rheol. Acta., 5, 35 (1966).

39. Lee, B. L., Ph.D. Dissertation, The University of Tennessee, August 1974.

40. Lodge, A. S., Trans. Faraday Soc., 52, 120 (1956).

41. Lodge, A. S., Elastic Liquids, Academic Press, New York, 1964, p. 131.

42. Maxwell, J. C., Phil. Trans. Roy. Soc., A157, 49 (1867).

43. McLuckie, C. and M. G. Rogers, J. Appl. Polym Sci., 13, 1049 (1969).

44. Mendelson, R. A. and F. L. Finger, J. Poly. Sci, Part C., 35, 177 (1971).

45. Mendelson, R. A. and F. L. Finger, J. Appl. Polym. Sci., 17, 797 (1973).

46. Metzner, A. B., Trans. Soc. Rheol, 13, 467 (1969).

47. Metzner, A. B., E. L. Carley and I. K. Park, Mod. Plastics, 37, November 11, 133 (1960).

48. Metzner, A. B., W. T. Houghton, R. E. Hurd and C. C. Wolfe, Second Order Effects in Elasticity, Plasticity and Fluid Dynamics, Pergammon (1962).

49. Metzner, A. B., W. T. Houghton, R. A. Sailor and J. L. White, Trans. Soc. Rheol., 5, 133 (1961).

50. Middleman, S., IEC Fund., 3, 118 (1964).

51. Middleman, S., The Flow of High Polymers, Wiley, New York (1968).

52. Middleman, S. and J. Gavis, Phys. Fluids, 4, 355 (1961).

53. Nakajima, N. and M. Shida, Trans. Soc. Rheol., 10, 299 (1966).

54. Noll, W., Arch. Rat. Mech. Anal., 2, 197 (1958).

55. Oldroyd, J. G., Quart. J. Mech. Appl. Math., 4, 271 (1951).

56. Oldroyd, J. G., Proc. Roy. Soc., A245, 278 (1958).

57. Oyanogi, Y. and Y. Yamaguchi, J. Soc. Mat. Sci. Japan, 20, 659 (1971).

58. Pearson, J. R. A., Plastics and Polymers, August (1969).

59. Rogers, M. G., J. Appl. Polym. Sci., 14, 1679 (1970).

60. Sakamoto, K. and R. S. Porter, J. Polym. Sci. B, 8, 177 (1970).

61. Schroff, R. N. and M. Shida, J. Polym. Sci, A-2, 8, 1917 (1970).

62. Spencer, R. S. and R. E. Dillon, J. Colloid Sci., 3, 163 (1948).

63. Spencer, R. S. and R. E. Dillon, J. Colloid Sci., 4, 241 (1949).

64. Spriggs, T. W. and R. B. Bird, Ind. Eng. Chem. Fund., 4, 182 (1964).

65. Spriggs, T. W. and R. B. Bird, Chem. Engr. Sci., 20, 931 (1965).

66. Tanner, R. I., J. Polym. Sci., A-2, 8, 2067 (1970).

67. Tanner, R. I., Appl. Polym. Symp., 20, 201 (1973).

68. Tordella, J. P., J. Appl. Phys., 27, 454 (1956).

69. Tordella, J. P., Trans. Soc. Rheol., 1, 203 (1957).

70. Tordella, J. P., J. Appl. Polym. Sci., 7, 215 (1963).

71. Treloar, L. R. G., The Physics of Rubber Elasticity, Oxford University Press (1958).

72. Van Wazer, J. R., J. W. Lyons, K. Y. Kim and R. E. Colwell, Handbook of Viscosity and Flow Measurements, Interscience, New York (1963).

73. Vlachopoulos, J., M. Horie and S. Lidorikis, Trans. Soc. Rheol., 16, 669 (1972).

74. White, J. L., J. Appl. Polym. Sci., 8, 2339 (1964).

75. White, J. L., Rubber Chem. and Tech., 42, 691 (1969).

76. White, J. L., Appl. Polym. Symp., 20, 155 (1973).

77. White, J. L., "Notes on Elastic Recovery and Die Swell," The University of Tennessee (1973).

78. White, J. L., Personal Interview, April 1974.

79. White, J. L. and J. Crowder, "Polymer Science and Engineering Report #13, The University of Tennessee (1973).

80. White, J. L. and A. B. Metzner, J. Appl. Polym. Sci., 7, 1867 (1963).

81. White, J. L., D. G. Salladay, D. O. Quissenberry and D. L. McLean, J. Appl. Polym. Sci., 16, 2811 (1972).

82. White, J. L., R. C. Ufford, K. C. Dharod and R. L. Price, J. Appl. Polym. Sci., 16, 1313 (1972).

83. Williams, M. C. and R. B. Bird, AIChE J., 12, 1064 (1966).

84. Zapas, L. J. and T. Craft, J. Res. Nat. Bur. Stand., 68B, 451, (1965).

85. Zaremba, S., Bull. Acak. Sci., Cracovie, 594 (1903).

APPENDIX

APPENDIX A

NORMAL STRESS DATA

In this appendix the normal stress data obtained from the rheogoniometer is presented.

HDPE MI = 5

$\dot{\gamma}$	N_1
.0133	3.0×10^2
.0133	4.7×10^2
.042	1.3×10^2
.042	1.9×10^3
.042	1.8×10^3
.042	1.8×10^3
.133	6.0×10^3
.133	6.3×10^3
.133	5.7×10^3
.133	6.6×10^3
.261	1.3×10^4
.261	1.3×10^4
.261	1.4×10^4
.261	1.4×10^4
.420	2.1×10^4
.420	2.0×10^4
.420	2.7×10^4
.420	1.9×10^4
.666	3.6×10^4
.666	3.5×10^4
.666	3.8×10^4
.666	3.6×10^4
1.330	7.7×10^4
1.330	7.9×10^4
1.330	8.0×10^4

HDPE MI = 0.1

$\dot{\gamma}$	N_1
.0133	1.5×10^3
.0133	7.2×10^3
.042	8.7×10^3
.042	9.1×10^3
.042	1.3×10^4
.042	8.6×10^4
.133	3.7×10^4
.133	3.1×10^4
.133	3.0×10^4
.133	3.0×10^4
.261	6.4×10^4
.261	6.4×10^4
.261	6.4×10^4
.261	6.7×10^4
.420	1.1×10^5
.420	1.8×10^5
.420	1.2×10^5
.420	1.2×10^5
.666	2.0×10^5
.666	2.0×10^5
.666	1.9×10^5
.666	1.8×10^5
1.33	4.1×10^5
1.33	4.0×10^5
1.33	4.0×10^5

HDPE MI = 0.02

$\dot{\gamma}$	N_1
.0133	1.0×10^4
.0133	5.3×10^3
.042	2.1×10^4
.042	2.7×10^4
.042	2.6×10^4
.042	2.3×10^4
.133	5.1×10^4
.133	5.8×10^4
.133	6.1×10^4
.133	6.3×10^4
.261	1.2×10^5
.261	1.2×10^5
.261	1.2×10^5
.261	1.2×10^5
.420	2.1×10^5
.420	3.0×10^5
.420	2.5×10^5
.420	2.4×10^5
.666	3.1×10^5
.666	3.2×10^5
.666	3.2×10^5
.666	3.2×10^5
1.33	4.7×10^5
1.33	5.0×10^5
1.33	4.9×10^5
1.33	5.0×10^5

LDPE

$\dot{\gamma}$	N_1
.0133	6.1×10^2
.0133	7.3×10^2
.042	3.7×10^3
.042	2.8×10^3
.042	3.3×10^3
.042	2.6×10^3
.133	8.4×10^3
.133	8.9×10^3
.133	1.1×10^4
.133	1.0×10^4
.261	1.6×10^4
.261	1.7×10^4
.261	2.3×10^4
.261	2.0×10^4
.420	3.1×10^4
.420	2.7×10^4
.420	3.0×10^4
.420	3.2×10^4
.666	5.0×10^4
.666	5.1×10^4
.666	5.4×10^4
.666	4.0×10^4
1.33	1.2×10^5
1.33	1.1×10^5
1.33	9.3×10^4
1.33	1.0×10^5

PS

$\dot{\gamma}$	N_1
.0133	7.9×10^2
.0133	1.0×10^3
.042	3.9×10^3
.042	4.6×10^3
.042	4.1×10^3
.042	7.0×10^3
.133	1.1×10^4
.133	1.9×10^4
.133	1.2×10^4
.133	1.7×10^4
.261	3.2×10^4
.261	3.5×10^4
.261	3.0×10^4
.261	3.4×10^4
.420	5.3×10^4
.420	6.1×10^4
.420	6.1×10^4
.420	6.0×10^4
.666	8.5×10^4
.666	8.5×10^4
.666	8.6×10^4
.666	9.0×10^4
1.33	1.8×10^5
1.33	1.8×10^5
1.33	1.8×10^5
1.33	1.7×10^5

PP

$\dot{\gamma}$	N_1
.0133	6.7×10^3
.0133	9.2×10^2
.042	6.7×10^3
.042	6.3×10^3
.042	1.1×10^4
.042	8.0×10^3
.133	1.9×10^4
.133	1.3×10^4
.133	3.1×10^4
.133	2.8×10^4
.261	2.9×10^4
.261	5.0×10^4
.261	4.3×10^4
.261	2.0×10^4
.420	6.4×10^4
.420	7.2×10^4
.420	7.7×10^4
.420	7.0×10^4
.666	1.0×10^5
.666	1.2×10^5
.666	1.2×10^5
.666	1.2×10^5
1.33	2.2×10^5
1.33	2.3×10^5
1.33	2.2×10^5
1.33	2.2×10^5

POLYMER	ONSET OF SCREW OR HELIX DISTORTION		ONSET OF GROSS DISTORTION
	$\dot{\gamma}$ (sec^{-1})	τ ($dynes/cm^2$)	$\dot{\gamma}$(sec^{-1})
HDPE MI = 0.1	666	4.0×10^6	1450
HDPE MI = 0.02	666	4.5×10^6	1450
PP	72	1.1×10^6	333
PS	666	2.4×10^6	3330
LDPE	133	1.0×10^6	3330
HDPE Mi = 5	7260	4.0×10^6	----

VITA

Joseph Roman was born on January 23, 1950 in Scranton, Pennsylvania. He is the son of Mr. and Mrs. Joseph Roman.

The author obtained his elementary and secondary education in the scranton public school system, graduating from high school in 1967. He attended Keystone Junior College and graduated in 1969, transferred to the University of Tennessee and received his Bachelor of Science degree in Chemical Engineering in 1971.